Development of 3D cancer models and targeted fluorescent gold nanoclusters

By

Ashkan Kamali Dashtarzheneh

Thesis submitted for the degree of Doctor of Philosophy (PhD)

Department of Surgery and Interventional Science
University College London

2017

I confirm that I have accomplished and written all the work explained in this thesis. This work is original, any parts that have been shown as part of teamwork are clearly indicated, and all external references are clearly cited.

Ashkan Kamali Dashtarzheneh

Abstract

The aim of this thesis was to study and develop suitable natural binary hydrogels to generate and isolate 3D spheroids from cancer cell lines (HT29 & MCF7) initially grown on 2D surfaces. The isolated spheroids were then used for fluorescent gold nanocluster (AuNCs) targeting studies.

The major novel findings of this work are:

1. The low melting temperature agar in combination with either collagen or egg albumen were slow in generating spheroids and at times inhibited their formation. Isolating any formed spheroids from the preparation was difficult with disruption and loss of the cluster formation. This combination format was found to be unsuitable in the study.

2. The natural macromolecule based carboxymethyl cellulose in combination with gelatine as a gel, gave the ideal outcome in generating spheroids in a short time. Its porous structure can be fine-tuned by varying the composition ratio of CMC and gelatine and autoclaving the mixture at 121°C. The swelling capacity and gelling properties of the CMC+gelatine mixture was ideal for generating cancer cell spheroids and harvesting by low centrifugation without destroying the clusters.

3. Spheroids greater than 200μm in diameter displayed hypoxic environment at the core detected using hypoxic fluorescent probes.

4. A novel specific cancer marker calreticulin was detected at increased levels on the surface membranes of spheroids using fluorescent gold nanoclusters conjugated to anti-calreticulin antibodies.

5. Specificity of anti-calreticulin antibodies via translocation for surface calreticulin was established by testing in a 3D co-culture of preformed endothelial cells (HUVECs) on membrane inserts with harvested fixed spheroids at the basolateral surface.

6. The obtained results suggest that the porous natural polymer carboxymethyl cellulose in combination with gelatine shows great promise in generating harvestable cancer cell spheroids reminiscent of tumours *in vivo* at low cost, high efficiency and robustness.

Table of Contents

ACKNOWLEDGMENTS

Firstly, I would like to express my truthful appreciation to my advisors Prof. Marilena Loizidou and Dr. Bala S Ramesh for the continuous support throughout my Ph.D. study and related research, for their motivation, patience, and vast knowledge. Their guidance assisted me in all the time of research and writing of this thesis. I could not have imagined having better advisors and mentor for my Ph.D. study.

I also would like to thank my Ph.D. colleagues for their encouragement and hints, which incented me to widen my research from different perspectives. I also would like to thank all my friends who supported me in writing, and incented me to strive towards my goal.

At the end, I would like to express appreciation to my family. Words cannot describe how grateful I am to my mother and father for all the sacrifices that they have made on my behalf. Without their precious support, it would not be possible to accomplish this research.

ABBREVIATIONS:

2D	Two-dimensional
3D	Three-dimensional
A/E	Agar/Egg white
A/C	Agar/Collagen
CMC	Carboxymethylcellulose
CRC	Colorectal Cancer
DMEM	Dulbecco's Modified Eagles' Medium
EGFR	Epidermal growth factor receptor
FGF	Fibroblast growth factor
HIF	Hypoxia inducible factor
NP	Nanoparticles
TEM	Transmission Electron Microscope
QD	Quantum dot
HT29	Human colon adenocarcinoma cell line
MCF7	Michigan Cancer Foundation-7
HUVECs	Human umbilical vein endothelial cell line
RNA	Ribonucleic acid
mRNA	Messenger RNA
MMP9	Matrix metalloproteinase 9
VEGF	Vascular Endothelial Growth Factor
PTPRO	Protein tyrosine phosphate
QY	Quantum yield
FDA	Fluorescein diacetate
PI	Propidium iodide
CRT	Calreticulin
ER	Endoplasmic reticulum
AuNCs	Gold nanoclusters
AuNCs-Anti-CRT	Gold nanoclusters conjugated to anti-calreticulin
Anti-EGFR	Anti-epidermal growth factor receptor
TFO	Triplex-forming oligonucleotide

CHAPTER 1

Introduction

1. Introduction:

1.1.   Nanotechnology in cancer detection

Nanotechnology is science, engineering, and technology which involves manipulation of matter on a 'nano' scale (1 to 100 nanometers). The nanotechnology devices used for the medical application called nanomedicine. In nanomedicine the nanoscale materials, such as biocompatible nanoparticles and nanoclusters, used for diagnosis, delivery, sensing in a living organism. Cancer starts when tumour suppressor genes in healthy cells stop being expressed. This starts a cascade of events, usually involving a number of gene mutations which result in loss of proliferation control and the ability to metastasise. Cancer conventional detection is done by determination of the physical growth changes in the organ using X-rays and CT Scans and confirmed using biopsy and even through cell culture (1). These techniques come with some limitations, such as decreased sensitivity, and hence the detection is possible only after a substantial growth of the cancer cells. Cells are within the size range of 2-100 microns, and nanoparticles (NP) are within the nanoscale size. Hence, nanoparticles can pass through the cells and reach the DNA molecules. There is, therefore, a probability that a defect in the genes can be easily identified *in vitro* and eventually *in vivo* (2). Cancer detection using nanoparticles has shown its potentiality when the cancer is in the developing stage. The nanoparticles can travel through the body, detect cancer-linked molecular changes, image the changes, release a therapeutic agent and then track how efficient the intervention is (3).

1.2.   Growth conditions, cell morphology, and population in 2D and 3D cultures

Many potential approaches in cancer studies have been under research including diagnosis and therapeutics. However, most researchers have been using monolayer cell cultures, the 2D immobile system. These forms of culture are utilized in the pre-clinical drug testing and use artificial matrices such as

glass and plastic. The 2D monolayer cell culture systems, therefore, fail to mimic the actual environment *in vivo* and hence give results that differ considerably with what would be expected in the body (4). The process of clinical drug screening involves introducing the drug into a cell culture, followed by testing the drug *in vivo* using animals and then proceeding on to clinical trials. Only about 5% of the test drugs get through the clinical stage of screening (5). Considering that the clinical trial phase is the costliest stage of drug development, there is the need to find a remedy for these failures especially regarding the toxicity and effectiveness of candidate anti-cancer agents (6). The proliferation of cells in the conventional cell culture is usually on a flat surface. This setup gives the cells a chance for even growth and proliferation because of the equal access of growth factors and nutrients from the culture medium. The necrotic cells and other wastes can be removed during the change of medium. The main characteristic of cells in the 2D monolayer is that they are flattened and usually more strained than they would appear in vivo. This difference in the orientation of the cells usually affects the cell processes including cell migration, multiplication, death, and expression of cellular products (7). Even with these characteristics in mind, most drug developers still use the conventional 2D cell culture systems to screen the drugs for cytotoxicity and effectiveness.

Unlike in the 2D cell culture systems, the 3D culture systems form a spheroid of cells, with some receiving less nutrition and oxygen than others (8). The interactions of the cells with each other and with the matrix in the 3D setup more accurately mimic *the in vivo* conditions of the cells, and hence the cell morphology and other cell processes match those in the body (9). Various cell growth stages such as growth and proliferation, apoptosis, necrosis, and hypoxia can be easily mimicked in the spheroids (10). The spheroid centre is covered by layers of cells that make it hard to access an equal amount of oxygen, growth factors and nutrients and hence making the cells at the core remain quiescent (11). The outer layers of the cell remain viable because they have access to nutrients and oxygen. These characteristics of the cells in a spheroid therefore closely mimic tumour cells in the body (12).
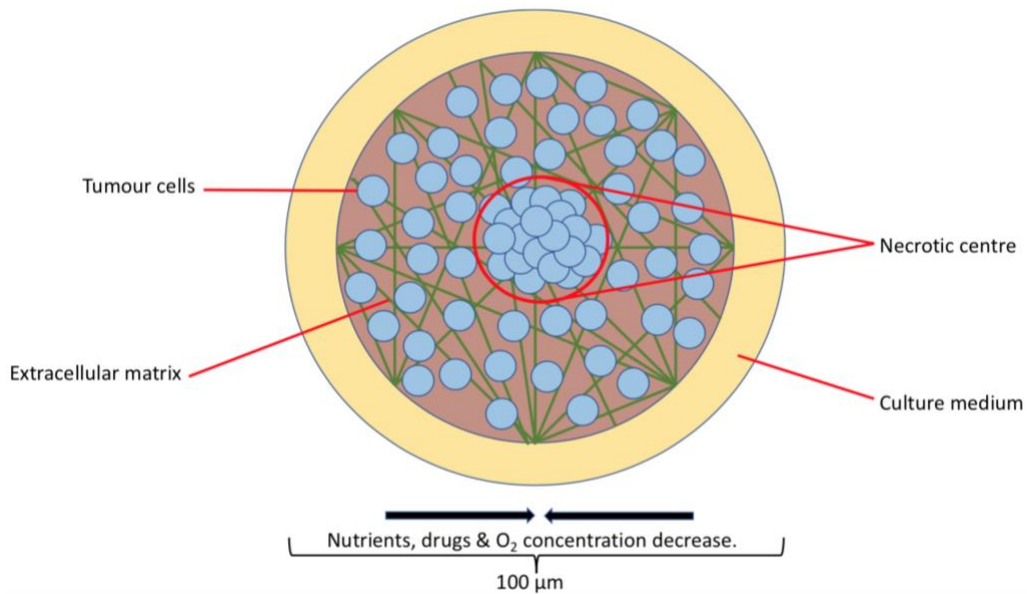
Figure 1.1: Spheroid structure

Likewise, the cellular processes in the 3D cell culture setup closely mimic the cell processes in the body (12). Taking cell proliferation as an example, the way it happens in the 2D is different from the cell proliferation in 3D. Some cells lines decline in the 3D setup while they continue growing in the 2D setup. Examples of such cells include colorectal cancer cell lines CRC. Other cells have been observed to multiply faster in the 3D setup than in the 2D cell culture systems such as breast cancer cells. The proliferation rate of the cell lines is also determined by the culture matrix in use (13). As much as some studies have shown that there is no significant difference between cells grown in the conventional cell culture system and the 3D setup, it is evident that the setup that closely mimics the in vivo scenario is the 3D culture system. Apart from the near identical mimic of the in vivo set up, 3D cultures also exhibit a reduced viability of cells and especially when the culture time is extended because of oxygen deficiency and nutrients and the accumulation of waste products at the spheroid core (14).

The physiological and the physical characteristics of the cells in a 3D culture also clearly show that cell processes such as gene expression, protein, and receptor expression differ from that of cells in a 2D cell culture system (15). For example, in 3D culture system of ovarian cancer cells mRNA expression levels of the cell surface receptors and the protease MMP9 had considerably increased compared to cells in 2D culture (201). The cancer cells grown in 2D

and 3D cultures show considerable differences in the way the proteins and other cell compositions are expressed, and in the normal cell processes including migration and invasion as well as proliferation and angiogenesis (16). for example, the migration of primary human foreskin fibroblasts on BME in 2D structure is very efficient while in 3D structure using same material they are completely unable to migrate (202). As mentioned above, the massive difference in the cellular activities between cells in 2D culture and the 3D culture is mostly because of the orientation of the cells and the unequal access of the nutrients and oxygen in the medium (17). Around 30% of the genes are expressed differently when cultured in the 2D and the 3D culture systems which is a massive difference when it comes to conducting crucial tests (18).

The genes responsible for limiting the proliferation and the growth of tissues are blocked in the 2D culture systems (19) as demonstrated in MCF10A breast cancer, a protein tyrosine phosphate, PTPRO had low to undetectable levels in 2D cultures, Downregulation of PTPRO by RNA interference inhibited the proliferation block during morphogenesis (203). When growing cells in culture, the detached cells from the tissue of origin makes them lose their characteristic and gain new characteristics after being cultured in 2D. When they are taken back to the 3D culture systems, they regain their normal characteristics such as morphology and proliferation (19). Of consideration when growing cells in a 3D culture is offering support for the translational and transcriptional processes that ensure that product profiles mimic the in vivo format (20).

As mentioned above, the cell to cell contact and the cell to matrix contact is important in the determination of how the cells will grow and how their products will be expressed in 3D cell culture systems. The 3D model almost mimics the exact environment of the cells unlike the 2D cell culture (21). The 3D cell cultures, therefore, give a more closely related response to drug tests as would happen in the body and hence should be preferred for drug tests over the 2D culture systems (22).

Research studies in cancer have shown that the cells and tumours in the 3D cell culture system tend to be more resistant to the cancer treatment drugs than

the 2D culture models. The activity and efficacy of the medicinal products in 3D culture is less than that in the 2D cultures (23). Drug interactions with the cells may require active interactions between cells and signalling from one product and cell to the other. This difference in the drug efficacy is therefore because of the difference in the cell to cell interactions, such as higher resistance to anti-cancer drugs in 3D cell cultures and signalling compared to 2D culture systems.

On top of that, the matrices involved also contributes to the way a cell makes its decisions on interacting with a drug (24) with one example showing that the presence of EGFR protein promotes drug resistance in a 3D model of breast cancer (204). The limited access to the cells in the core of the spheroid also contributes to cell survival as in cancer tumours and the reception of the drug into the cells (25). (Table 1.1)

Cellular behavior	2D	3D
Morphology	Sheet–like flat	Natural shape in spheroid
Proliferation	Regardless of cell types proliferation rate is faster than in vivo	Depends on cell types proliferation rate could be faster or slower compared to 2D
Exposure to drugs and nutrients	Cells exposed to drugs equally	Treatment agents may not be able to enter the spheroid core
Cell cycle	Mostly same cell cycle as equal exposure to nutrients	Spheroids contain proliferative, hypoxic and necrotic cells
Gene/protein expression	Different expression levels compared to in vivo models	More similar expression to vivo tissue origins
Drug sensitivity	Very effective treatment	Less effective treatment

Figure 1.2: The essential difference in cellular characteristics in 2D and 3D culture conditions (8).

1.3.   3D models scaffold

The formation of a 3D spheroid is determined by the matrix/scaffold in which the cells are grown. The cells are introduced into the medium which can be suspension medium and then allowed to attach to the polymerized 3D scaffold. The 3D matrices used in the 3D culture systems can either be synthetic or natural scaffold systems (26). Suitable 3D scaffolds must be used to mimic the spatial arrangement of cells in the body as well as provide the exact kind of support given to the cells in the body. Furthermore, the matrix must be cytocompatible to ensure that the cells grow and survive. The 3D cell culture

systems require the utilisation of suitable 3D scaffolds as in the body (27). These 3D scaffolds have been utilised in the processes of tissue engineering which requires complex cell interactions, and they have been adapted for the investigation of cell multiplication, development and the movement of cancer cells. This part of the introduction has been divided into two categories depending on the component of the scaffold: natural and synthetic scaffolds (28).

Some of the 3D matrices for cancer models contain organic gels as their main component which acts as a substrate for the tumour cell growth. The organic hydrogels are weaker in terms of mechanical support than those that are synthetically generated. However, they manage to replicate the natural environment of a tumour. One of the most common organic compositions of the natural hydrogels is collagen which effectively mimics the ECM-like environment in vitro, as this protein constitutes the bulk of the ECM (29). Another component is laminin which can be used as a replacement for or additive to collagen. The advantage of using laminin or collagen in the 3D matrix is that it allows maximum cell survival because of its natural characteristics. Collagen and laminin also provide binding sites for cells, needed for interactions which promote proliferation and movement, such as the RDG sequence in laminin which provides a binding site for adhesion proteins "cell adhesion molecules, CAMs" which anchor cells to the matrix (205). The disadvantage is that they provide a weak mechanical support for the 3D cell culture spheroids. Collagen hydrogels has an advantage in that as the cells proliferate, they remodel it and hence increase the contact required for cell-cell interactions and the alignment of cells required to mimic in vivo environment (30).

Reports show that some synthetic biological materials can mimic the features of the natural hydrogels while at the same time solve the support problem observed in the hydrogels to produce a more reliable 3D scaffold for cancer cells culture (31). On top of that, the synthetic matrices are biodegradable because they incorporate polymers such as polylactide, PGA, PLG, and PLGA. These polymers lead to the formation of different matrices such as mesh and fibres (32). They can, therefore, mimic the biological molecule structures

presented in the body. As mentioned above, these synthetic gels are more supportive mechanically, but they might have problems when it comes to cell adhesion to the polymers. In the bid to improve cell adhesion, the surfaces of the polymers are engineered (33). The process of mixing the scaffolds with some ECM compounds can also help increase the effectiveness of the synthetic scaffolds in cancer cell culture (34). The ability to engineer the scaffolds makes it easy to develop them into the preferred matrix without losing their ability to provide maximum mechanical support. The cell characteristics depend on the properties of the materials including their interaction with water and other external environments, the size of their pores and their chemistry (35). The process of engineering synthetic matrices to mimic in vivo structures of the tissues and organs is, therefore, not easy, but it is possible (36).

1.4.   Collagen

As mentioned above, collagen is one of the most utilised natural support systems for the 3D cell culture systems. Because collagen is the major component that makes up the connective tissue in the body, its ability to support the migration of the tumour cells in the external environment cannot be underestimated (37). Collagen gel is the most common to choose when it comes to more complex 3D assays because the protein stimulates the development of the endothelial cells which are important when it comes to the metastasis of the cancer cells (38). Collagen would be the most suitable support system for the 3D assays because cells proliferate unrestricted and its flexibility makes it easy to mimic the internal environment of the tumours (39).

The fact that a considerable amount of oxygen and nutrients can pass through the collagen model into the core of the spheroid makes the hypoxia level of the cells in the core reduced (40). A Collagen construct has considerably large pores that make it possible for drugs that are of high molecular weight to diffuse and travel into and out of the matrix and hence making it easy to access the core of the tumour (41). The sources of collagen are natural substances that have a high amount of the product such as the bovine skin, the placenta, and the rat tail. The fact that collagen can interact with receptors such as integrins makes it even suitable because it is bound to support gene expression

naturally. In this case, the target is the genes that determine the production of metalloproteinases, the factors that are responsible for the degeneration of the extracellular matrix and those that stimulate and the invasion of the tumour cells. (42).

1.5.　Egg white

Collagen and matrigel lack the ability to support a variety of cell interactions because they are designed to support only one type of cell. The egg white composition contained of protein, trace minerals, fatty material, vitamins, and glucose. The main three proteins included in the egg white composition that may potentially play a role in assisting the formation of cancer cells spheroids are Ovalbumin, Ovotransferrin and Ovomucoid. Since the development of the tumour incorporates the interactions between cancer cells and all the neighbouring cells, there is the need to find a matrix system that would support growth of the multicellular culture (43). Egg white is the best replacement when there is the need to synergise the growth of different types of cells all at once. The egg white can support the growth of cells from human, rat and mouse origin (43). This kind of matrix is essential when it comes to measuring the drug characteristics before and after angiogenesis. Apart from being effective, this method is also cost effective and yields reliable results for the assays (44).

1.6.　Crosslinked carboxymethylcellulose (CMC)

Crosslinked carboxymethylcellulose (CMC) is another reliable hydrogel that is degradable biologically, non-toxic and non-mutagenic (45). Its main component is cellulose that has been modified to improve its qualities. Cellulose is a polymer found in plants such as cotton and wood. The engineered polymer makes it soluble in water by increasing the degree of substitution. The polymer is of high molecular weight with large pores and hence does not support the bioaccumulation of substances. The use of CMCs in clinical trials for breast implants has been investigated for the past two decades. The radio-translucency of the CMC gel is higher than the silicone gel (45).

1.7.   3D models in drug discovery

Accessing the possible effects of a new compound, there is the need to conduct cell-based assays. The costs incurred during these processes is quite high and is estimated at 1.3$ billion. The number of drugs that pass the clinical trials is about 21%. Comparing the cost of the tests and the production of a marketable drugs, it is evident that the process is quite expensive (46). The use of 3D models is necessary because it reduces the costs incurred during trials in the clinical phase because it closely mimics the response of the body cells to the drugs and hence the failures in the clinical phase of drug testing are reduced (47). According to research studies, stronger drug resistance is caused by signals from the surrounding cells and the ECM impact on their decision-making process (48). The limited access to the cells in the core of the spheroids make it easy to develop drug resistance in the 3D models. The variety of 3D models has attracted massive attention in drug screening assays. a number of 3D models are inaccessible because of their high cost, time consumption and their lack of reproducibility (49). The 3D cell cultures have great potential in the future of drug discovery (50) (Table 1.2).

Strengths	Weaknesses
• ECM components increase cell-cell interaction • Cell morphology and function largely mimic what seen in vivo • Matrix could contain growth factor and protein in tumor condition. • Heterogeneous cell population are like tumour cells • Gene and protein expression levels like *in vivo* levels. • Models using different cell types to build multicellular systems. • Decreasing the use of animal models	• Variability in biologically obtained matrices may lead to development of non-producible results. • Cost more than 2D monolayer culture systems. • Some models produce spheroids of varying sizes which cause high variability in a well. • 3D models lack the vasculature which is significant for tumour growth rate and drug delivery.

Figure 1.3: Advantages and disadvantages of 3D culture models for drug discovery applications (8).

1.8.   Growth of tumors

Tumours are a mass of cancer cells that grow under abnormal conditions enabling them to multiply bypassing apoptosis. The surrounding tissues are usually deprived of their nutrients by this mass of cells in its bid to survive. At the same time, the large amount of waste products overwhelms the surrounding healthy cells (51). The cancerous cells proliferate at a very high rate leading to the formation of the tumour which comprises of millions of cells. After a proportion of normal cells are deprived and die and hence fail to perform the normal cellular functions of the specific organ. The tumour cells continue occupying space and squeeze the normal ones to a diffusion-limited maximal size (52). The reason as to why tumour cells do not undergo apoptosis because of the low nutrient settings, but for their survival, they require less amounts of nutrients, oxygen and growth hormones than normal healthy cells. The tumour cells, furthermore, produce angiogenic factors that stimulate the growth of new blood vessels in a process referred to as angiogenesis (53).

The process of angiogenesis is important in the expansion of a solid tumour and hence, this process is targeted by researchers to shed some light on the anti-cancer drugs resistance abilities of the tumour. It is one of the research areas that has sparked a lot of interest in cancer researchers because of its ability to generate a complex interaction of molecular processes (54). These molecules impact on the endothelial cells, how they multiply and how they invade the lining of the blood cells. One of the most important stimulatory molecules is the vascular endothelial growth factor (VEGF), and another one is basic fibroblast growth factor (BFGF) (55).

The condition where oxygen requirements within a tissue drop to 5% of the normal physiological level called hypoxia often neighbouring areas of necrosis. Hypoxia outstrips the capability of the local vasculature to supply oxygen (53). In cancer tumours, hypoxia is related to poor projection of the diagnosis, resistance to treatment and increased probability of metastasis. The tumours are easily monitored using imaging techniques, for example, by positron emission tomography (56). To better understand hypoxia, 3D cell culture

models can help by mimicking the tissue hypoxia in vivo; image formation tumours can also be helpful. The high demand of oxygen in tissue and low vascular oxygen supply leads to hypoxia.

Although many studies have been carried out in tumour vascular networks, tumour oxygen consumption is mainly ignored (25). The hypoxic tissues are more radio resistant than well-oxygenated tissues, and this has a significant effect on treatment as the cells in these hypoxic tissues do not respond well to either radio and chemotherapy (57). Hypoxia as well as necrotic conditions give the researchers the ability to develop therapy that is selective to only the tumour cells without having to invade the normal cells. This is done by targeting genes that are responsible for hypoxia such as those that express hypoxia-inducible factor 1 transcription. Hence these approaches could use this impediment and turn that into a benefit for cancer therapy (58).
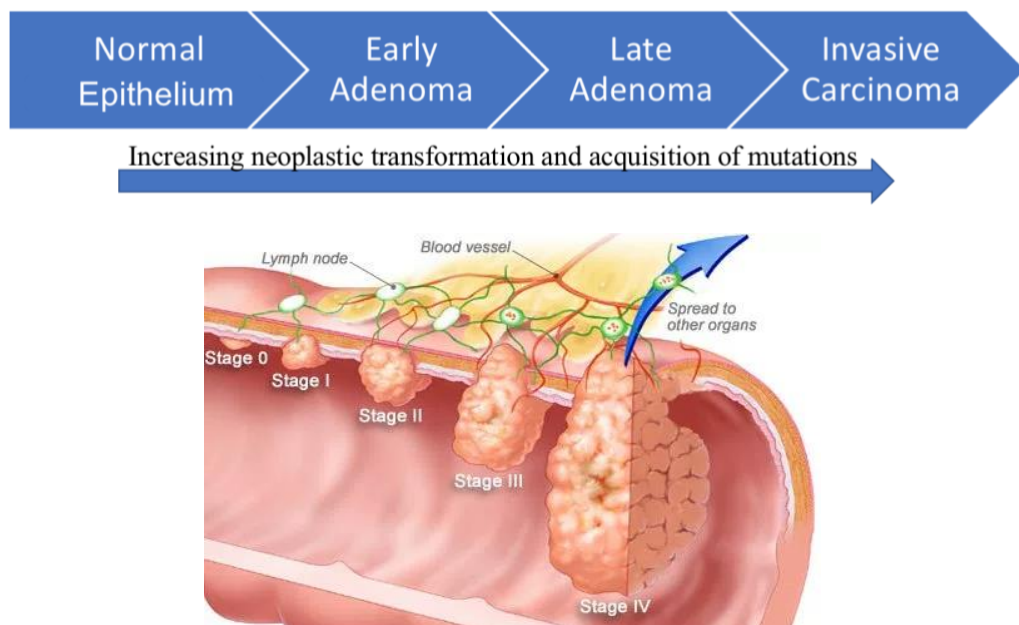
Figure 1.4: This shows tumour development from Stage 0 until stage IV and the process of determining how far a tumour has spread beyond its original location . (The cancer therapy option depend upon the stage of a tumour) (http://www.onlinecancerguide.com/colon-cancer/4-stages-of-colorectal-cancer/)

1.9. Targeting studies

Most of current cancer diagnostics and therapy usually include invasive procedures such as initial chemotherapy to reduce the tumours, and then surgical removal of the tumours if possible, and then more chemotherapy and radiation. The goal of the radiation and chemotherapy is to destroy the cancer cells as they are more likely to be harmed by the effects of the therapy due to their faster growth rate than normal healthy cells. For the past 20 years, the number of studies conducted to improve chemotherapy which has led to the development of the survival of patients has been on the rise. However, there is still a need for improvement.

Recent research areas include carriers' improvement to allow complementary dosing methods, new therapeutic targets such as blood vessels fuelling tumour growth and specific targeted therapeutics (59). Research studies have shown patients are willing to embrace new treatment methods of cancer diagnosis and treatment.

These new methods are aiming at ensuring that the patient leads a quality life and at the same time increasing survival rate (60). The level of effectiveness of these treatment methods, are determined by the ability of the drugs to target specific cancer cells and not the healthy cells. (61). The ability of the drug to specifically target the cancer cells would leave the rest of the cells intact and hence improve the patient's quality of life and life expectancy (62). The fact that can be used for more targeted treatment is that cancer cells tend to overexpress some their antigens on the cell surface (63). This makes it easy for the anti-cancer drugs to target the specific tumour cell without causing harm to the normal cells.

1.10. Targeting tumours using nanoparticles

The use of nanoparticles to target cancer cells is an interesting prospect in the diagnosis and treatment of cancer. However, the dosage delivered to the site

is too low and hence may take long to diffuse the tumour. This is the main reason why transferring nanotechnology to human use has been a slow journey (64). The possibility of engineering nanoparticles that selectively detect and destroy cancer cells in the body remains an exciting concept which has led scientists to plan a myriad of different nanoparticle designs demonstrating unique physicochemical properties (size, shape and surface chemistry) and programmed with a multitude of biological and medical functions (65).

When designing the ideal nanoparticles, their ability to deliver is of utmost importance. This is because the destruction of the tumour cannot happen if enough dosage of the drugs is not delivered to the site (66). The low delivery ability of the nanoparticles is the resistance it faces when travelling through the body including the shear, friction, protein adsorption and immune attacks (67). Nanoparticles that escape biological barriers could interact with the tumour tissue. The number of nanoparticles that can achieve this is stated as the nanoparticle delivery efficiency (68).

Gold nanoparticles (AuNPs) are important components for biomedical purposes. AuNPs have been broadly used for diagnostics and have seen increasing use in the area of therapeutics. AuNPs have useful features such as size and shape related optoelectronic properties, large surface to volume ratio, excellent biocompatibility, and low toxicity. These properties make AuNPs an essential tool in bio-nanotechnology. Important physical properties of AuNPs include surface plasmon resonance (SPR) and the ability to quench fluorescence (219).

Over the last two decades, fluorescent gold nanoclusters have been on the priority list of most researchers because of their outstanding photo stability characteristics (215, 69). Protein conjugated fluorescent gold nanoclusters (NCs) become more popular in the field of medical and nanotechnology because of their outstanding photo-stability characteristics such as unique advantages which include high sensitivity, cost effectiveness and diverse detection capabilities (70). Despite their great and promising future as innovative labelling agents, advance improvement of fluorescent gold

nanoclusters faces different challenges (71). Fluorescent gold nanoclusters (AuNCs) have a relatively low quantum yield (QY) compare to semiconductor QDs and natural dyes. Fluorescent gold nanoclusters produce unique multi-functional nano probes for fluorescence imaging and detection (72).

The interactions between proteins and fluorescent AuNCs have the significant impact on the biological behaviour of both proteins and fluorescent AuNCs (73). overall AuNCs as a biocompatible marker have amazing features for biological detection with good water-solubility, low toxicity, and high emission rates. The table below (1.3) is a summary of the recent advances in various biological applications of AuNCs in detection (74). They are still at an early stage, and further studies are required. Further development in design and synthesis of high-quality AuNCs lead to extensive applications in ultrasensitive molecular diagnostics and intercellular drug delivery in future.

AuNCs in biodetection		
	Detection of metal ions	11-MUA-capped AuNCs used for sensing Hg^{2+} based on Hg^{2+} induced aggreation of AuNCs.
	Detection of proteins	Glutathione-stabilized AuNCs are capable of GST-tagged proteins detection from cell lysates
	Detection of small biomolecules	11-MUA-AuNCs based on luminosence for quatntitaive determination of H_2O_2
	Detection of nucleic acids	Flourencence AuNCs use in nucleic acids delivery

Figure 1.5: Biomedical applications of AuNCs (74).

1.11. Tumor-specific targeting

Current studies have shown that tumour specific targeting is a vital system in cancer therapeutics and diagnostics. When a drug is still attached to a tumour specific carrier, then it remains inactive until it reaches its destination (75). This is made possible because of the markers on the cancerous cells that are not present in the healthy cells. Since 1975, studies have first shown antibodies'

ability to bind to specific tumour antigens. However, it took about 20 years to develop the antibodies into compounds that can fight cancer (76). In all cancer cells, targeted antigens should be expressed but not on host cells. The FDA has approved many of targeted cancer therapies using antibodies for various cancer types, such as anti-epidermal growth factor receptor antibodies (anti-EGFR cetuximab) and anti-HER2 antibody (Herceptin) (77).

Studies have shown that these therapeutic methods using antibodies directed to cancer targets will lead the market. For more efficient and less invasive cancer treatments, these antibodies will be used heavily as therapeutic agents or even carriers for drug transport processes (78). It is important to generate targeted treatment methods that alter the target in a way that inhibits its ability to promote the survival of cancer cells. The targeted therapy could prevent the targets from attachment to a receptor that they routinely activate, among other potential tools or reduce the target activity (79).

As it has been mentioned earlier, most of the targeted cancer therapies use antibodies. Antibodies are large, and they, therefore, cannot enter the cells. Hence, they are used only to target the surface of the cell (80). Typically, the antibodies are created by injecting the antigen to be targeted into a rat. The rat's immune system in the quest to fight the antigen develops antibodies against it. The antibodies are then tested for their selectivity in combating the antigens (81).

The next stage for the tested antibodies is to be used in humans a process referred to as "humanising." Humanising is essential for blocking the human immunity from demolishing the antibody and recognising it as "foreign" before it has a chance to bind to the target. In the Humanization procedure, a reasonable number of human antibodies are replaced with a consistent portion of mouse antibodies. Finally, small-molecule compounds are not usually recognised as foreign by the host. Hence, humanization is not an issue for that (82). Many appropriate cancer targeted therapies can be used such as signal transduction inhibitors, hormone therapies, gene expression, modulators,

apoptosis inducers, angiogenesis inhibitors, immunotherapies, and toxin delivery molecules (83). (Table 1.4)

Cancer targeted therapies	Explanation
Signal transduction inhibitors	when the cell has received a signal, the signal is transferred to the cell through a series of biochemical reactions that eventually provide the relevant responses.
Hormone therapies	The body interferes with the hormones action and stops from providing the hormones.
Gene expression	Proteins perform a role in regulating gene expression, by changing proteins function.
Apoptosis inducers	The apoptosis is a controlled cell death process caused by cancer cells.
Angiogenesis inhibitors	By stop the angiogenesis to tumours inhibits new blood vessels growth interfere with vascular endothelial growth factor (VEGF) action.
Immunotherapies	The recognition of specific antibodies on the cancer cells surface, to destroy cancer cells by trigger the immune system.
Toxin delivery molecules	The antibodies that deliver toxic molecules may cause the cancer cells die.

Figure 1.6: Different cancer targeted therapies (83).

There are other cancer therapies such as cancer vaccines, and gene therapy that interfere with the growth of specific cancer cells and antibodies as targeted therapies to specific cancer cell markers as shown in table 1.5 (84).

Antigen types	Antigen examples	Tumor types
Glycoproteins	EpCAM	Breast & Colon
Glycoproteins	CEA	Breast & Colon
Glycoproteins	gpA33	Colon
Glycoproteins	Mucins	Breast & Colon
Glycoproteins	TAG-72	Breast & Colon
Carbohydrates	Lewis-Y^2	Breast & Colon
Growth factor	EGFR	Breast & Colon
Growth factor	HER2	Breast & Colon
Growth factor	ErbB3	Breast & Colon
Growth factor	c-MET	Breast
Growth factor	IGF1R	Breast
Growth factor	EphA3	Colon
Growth factor	TRAIL-R1, TRAIL-R2	Colon
Stromal & extracellular matrix antigen	FAP	Breast & Colon
Stromal & extracellular matrix antigen	Tenascin	Breast

Figure 1.7: Currently available targeted cancer treatments using antibodies (85).

1.12.   Calreticulin (CRT)

The endoplasmic reticulum (ER) is a network of membrane-enclosed tubules and sacs that extends from the nuclear membrane throughout the cytoplasm. The whole endoplasmic reticulum is surrounded by a continuous membrane and is the largest organelle of most eukaryotic cells. Calreticulin (CRT) is a compound that is predominantly situated in the ER (86). CRT is also found in the nucleus, which means that it aids in the process of transcription regulation. Structural predictions show that the protein consists the N, P, and C-domain (87). CRT has got two main functions inside the ER; regulation and moving calcium ions. CRT can, therefore, act a target for the regulation of gene expression (88). The correlation between expression level of CRT and tumorigenesis has been widely studied in cancer research (89). The level of expression of CRT leads to different clinical outcomes. By increasing the levels of CRT, cancer development process would be damaged. When CRT is expressed in high levels, it can help develop a treatment for cancer (90). The interaction with integrins is a mediation tool that can be used for this process (91).

1.13.   Imaging of spheroids

The 3D spheroids have a high potential for use in cancer therapeutics in the future because they mimic the behaviour of tumour in vivo better than that seen in 2D culture systems (92). The imaging and analysis process of the 3D spheroids experience some challenges as documented in the table 1.6 below.

3D spheroids limitations in imaging and analyzing
Find the spheroid and focusing on that in every well so it can be imaged in a single field-of-view.
To confirm dye penetration and prevent disturbing the spheroid location the most effective compound and staining treatment required.
To get the representative images throughout the 3D matrices, background signal from above and below the imaging level or decreasing out-of-focus.

To analyze the images to produce meaningful result.

Figure 1.8: limitations in imaging of 3D spheroids (92).

There are some different biological records from spheroid assays that have been explained. High-contrast imaging techniques have been proven as promising methods for characterizing the effects of chemical compounds on spheroids. Recently, spheroid formation in low-attachment plates has become popular as the technique is suitable for high-content imaging (49). Imaging has advantages over other analytic procedures, such as plate reader-based fluorescence or luminescence, where no spheroids interference is required, and multiple biological records are possible, as indicated below (93).

The viability dyes, apoptosis dyes, DNA-binding dyes and fluorescence markers can be all used in fluorescence imaging. For example, cancer cells can be transfected with fluorescent proteins at the early stage before spheroid formation to allow detection of changes in spheroid size or intensity by fluorescence (92). This technique can be prolonged to more complex multicellular models that express fluorescent marker groups. Transmitted light (TL) imaging can be used to determine the spheroid size and, same density level (92). Normally, the large magnification index makes it easy to view a single cell and hence the collection of information of the spheroid is easy. Low-magnification is only used when the whole spheroid needs to be observed (94).

The confocal imaging system is another imaging technique. There are three tactics to be used for confocal imaging technique to achieve out-of-focus plane removal (95). 1) by using a blocked pin-hole gap in a conjugate focal plane to the specimen so that light transmitted away from the point in the sample being illuminated is physically blocked from reaching the detector 2) by illuminating a single point of the specimen at any one time with a focused beam. And 3) By using software deconvolution to use mathematical calculation to estimate the effects of out of focus plane for any plane and hence removing these distortions. In most biomedical applications, gold particles used for fluorescence imaging, however, can be used in immuno-gold labelling (96). Although in this reported growth, morphology hypoxia and targeting of the 3D spheroids were checked

at different time points for any changes in the area, volume and form were carried out with a new imaging technique using confocal microscopy.

1.14.   AIMS

The aim of this thesis was to develop a 3D culture matrix, which allows for the growth and subsequent harvesting of cancer cell spheroids for nanocluster investigations.

The specific objectives are:

1. Combining low temperature melting agar with collagen or egg white (albumin) to generate biomimetic 3D matrices for cultivating cancer cell spheroids was carried out.

2. Novel natural macromolecule based carboxymethyl cellulose (CMC) in combination with gelatine as 3D matrices was also developed for spheroid formation.

3. Formed spheroids were harvested from all matrices and used for targeting with fluorescent gold (AuNCs) for microscopy detection of a novel cancer marker.

4. Harvested spheroids were also used for co-cultivation with endothelial cells in extravasation studies.

5. Mature spheroids were examined for the detection of hypoxia within the spheroids

6. Water soluble fluorescent gold nanoclusters AuNCs were synthesized suitable for bio-conjugation for targeting purposes.

CHAPTER 2

Methods & Materials

2. Methods and Materials:

2.1.   Routine cell culture

The colorectal cancer cell line (HT29) a breast cancer cell line (MCF7) and the human umbilical vein endothelial cell line HUVECs have been used in this body of work (all purchased from the European Collection of Cell Cultures, ECACC, Salisbury, UK and Sigma-Aldritch, Dorset, UK). The cancer cell lines were grown in Dulbecco's Modified Eagle Medium (DMEM) with high glucose/L, GlutaMAX™-I, without phenol red, without HEPES and pyridoxine HCl (Sigma-Aldrich, D6046) supplemented with 10% Foetal Calf Serum (FCS, 5129, First Link UK Ltd, Birmingham, UK) and 1% Penicillin/Streptomycin with 10,000 units' penicillin and 10 mg streptomycin per mL in 0.9% NaCl, sterile-filtered, (P/S, GIBCO, Invitrogen, Paisley, UK). HUVECs were grown in Endothelial Growth Medium (PromoCell Heidelberg, Germany) with 1% Pen strep. All the cells were handled aseptically and cultured routinely as 2D monolayers in a humidified atmosphere with 5% CO_2/air at 37°C in a Forma Scientific CO_2 Incubator. Passaging for propagation and viable freezing (liquid Nitrogen stocks) was carried out enzymatically (1mg/ml Trypsin in EDTA/PBS, GIBCO) at between 75-90% confluence. Cells were purchased in passage 5. Cells were used within 30 passages, at which time more cells were taken out of stock. Regularly, cells were feed every three days. Routine plasticware was purchased from VWR (Leicestershire, UK) and Greiner Bio One (Stonehouse, UK)

2.2.   Optimum density on 2D

For 2D studies, cells (HT29, MCF7) were seeded in 96 well plates in the order of $10x10^3$ cells/ml up to $2x10^5$ cells/ml and after 24 h incubation at 37° C the metabolic activity was checked using alamarBlue. The alamarBlue assay is designed to measure quantitatively the proliferation of both cell lines (HT29, MCF7). The alamarBlue Assay incorporates a fluorometric/colorimetric growth indicator based on detection of metabolic activity. Specifically, the system incorporates an oxidation-reduction (REDOX) indicator that both fluoresces and

changes colour in response to chemical reduction of growth medium resulting from cell growth. The standard curve results show the optimum cell density to be used in 2D (concentrations were chosen from the linear part of the curve).

2.3.   3D in vitro model with two types of matrices (Agar & Collagen) (Agar & Egg white)

The following matrix components were used: Low melting agar (Sigma, UK), collagen type I with 2.05 % protein concentration (First Link, UK); eggs (MS Free range), which were surface sterilized by wiping with 70% ethanol under sterile conditions. The egg white was separated from the egg yolk by puncturing the shell at one end and transferring into sterilized universal containers (Greiner Bio One) and subsequently frozen down (-20°C) until needed.

To create the 3D, model the following steps were taken. The low melting agar, type I collagen and egg white were all maintained in a water bath at 40°C. For the experiments, 3 ml of type I collagen or 3 ml of egg white and 3 ml of low melting agar (1:1) were mixed; and equal volumes of fully supplemented DMEM added.

The final solution was dispersed into wells of ultra-low binding plates 12-well, or 24-well depending on experimental protocols (purchased from Sciencell, Carlsbad, USA). At the same time, sterilized individual Glass beads (5mm diameter, Sigma) were placed in the middle of the 3D mixture, just before starting to cool to form a gel while in the sterile tissue culture cabinet. After 10 min of gel formation the glass beads were removed to create a well within the 3D construct, which was then filled with 0.1 ml of cancer cell suspension containing optimum number of cells (HT29, MCF7) and let it to settle in the tissue culture cabinet for 20 min and topped up with fully supplemented medium and placed in the incubator.

2.4. Optimum density in 3D A/E and A/C

For 3D studies, cells (HT29, MCF7) were seeded in prepared A/E and A/C 3D matrices in order from $25x10^3$, $50x10^3$, $75x10^3$, $100x10^3$ cells/ml and incubated at 37° C. Afterwards the cell metabolic activity was measured on specific time points (Day 1,4,7 and 10) (Over 3 independent experiments). At each time point cell medium was removed and 300 µl of 10% alamarBlue reagent was added to each well, and the plate was incubated at 37°C for approximately 5 h (Incubation time varied between 4 h up to 8 h) to allow cells to convert resazurin to resorufin and produce their characteristic colour. After the incubation time the resultant absorbance signal was measured (Excitation 530, Emission 620). Metabolic activity results showed $75x10^3$ cells/ml is the optimum density to use in 3D A/E and A/C models.

2.5. Preparation of novel CMC matrix for 3D model

Sodium Carboxymethylcellulose and Bovine Gelatine comprised the new matrix (CMC mixture). 4g of CMC were dissolved by adding gradually to a stirring container in 100 ml of water and the mixture was boiled. After cooling and standing in the fridge overnight to complete dissolution, 1g of gelatine was weighed and added to the CMC solution and mixed thoroughly. To sterilize, the mixture autoclaved at 121° C for 25 min and allowed to cool. The mixture was now considered (x2), so to use it was diluted 1:2 with growth medium and mixed gently.

2.6. 3D CMC water swelling capability

The 24-well Ultra Low Binding plate was weighted before and after transferring 1 ml of the CMC mixture into the well. By using freeze-drying which is a dehydration process, CMC mixture froze and then reducing the surrounding pressure to allow the frozen water in the CMC mixture to sublimate directly from the solid phase to the gas phase. Eventually freeze-dried CMC mixture was weighted. This shows the weight of the plate contains 1 ml of CMC mixture before and after dehydration process.

2.7. Viscosity properties of Carboxymethycellulose and CMC+gelatine

Another physical property is viscosity of CMC; therefore, a viscometer was used to measure the viscosity of the fluid. 1 ml of CMC solution was added and the viscosity level of that compared with the viscosity of CMC+gelatine (CMC mixture). It is important when applying a sample that the correct amount is used. Over filling or under filling will result in errors in your data. The total test is carried out at room temperature. Many different measuring systems can be used on the rheometer.

To check the viscosity level of CMC mixture, the Cone/plate measuring system is recommended. The advantages of using this system are easy to clean, suitable sample position, small sample volume needed, shear rate constant across the sample, and finally high shear rates possible with small angle Cone. Cone/plate measuring system contains of a rotating upper Cone and a fixed lower plate with CMC mixture contained between them. Since the shear stress is constant (within 0.3%) with radial position for Cones with a small Cone angle, the viscosity of CMC mixture can be analysed directly from the experimental torque/speed relation. For Cone/plate measuring system, it is normally easier to slightly over fill and then trim off any excess sample after bringing the upper and lower measuring systems together. It is important to clean the rheometer after use. Samples left behind may damage the surfaces of the measuring systems.

2.8. Optimum cell density in 3D CMC+gelatine

To check the optimum density in 3D CMC+gelatine matrix, cancer cells (HT29, MCF7) were dispersed into prepared CMC+gelatine 3D matrices in 24-well ultra-low binding plate in order from 25×10^3, 50×10^3, 100×10^3, 150×10^3 cells/ml and incubated at 37° C. Afterwards cells metabolic activity was measured on specific time points (Day 1,4,7 and 10) (Over 3 independent experiments). At each time point cell medium was removed and 300 μl of 10% alamarBlue reagent was added to each well, and the plate was incubated at 37°C for approximately 5 h (Incubation time varied between 4 h up to 8 h) to allow cells

to convert resazurin to resorufin and produce the characteristic colour. After the incubation time the resultant absorbance signal was measured (Excitation 530, Emission 620). The final results showed 100×10^3 cells/ml is the optimum density to be used in CMC+gelatine 3D model.

2.9.   3D in vitro model with CMC+gelatine matrix

1 ml of the CMC mixture (CMC+gelatine) was transferred into each well of a 24-well ultra-low binding plate and the plate was placed into the fridge for 10 min to set the matrix. Same optimum density used in previous 3D model, hence 100×10^3 cells (HT29, MCF7) and HUVECs were dispersed into the matrix and after 10 min the cells settled within the matrix, the 3D CMC mixture was topped with DMEM.

2.10.   Live/Dead Assay - Propidium Iodide and FDA

Fluorescence-based live-dead assays can be used to evaluate the viability of mammalian cells. For this technique, the two chemical dyes used Fluorescein diacetate (Sigma-Aldrich Company. LLC, C-7521). FDA stock solution which was prepared by dissolving 5 mg of FDA in 1 ml acetone (stock solution kept at -20 °C). Propidium iodide (for example: Sigma-Aldrich Co. LLC, P4170). PI stock solution was prepared by dissolving 2 mg of PI in 1 ml PBS (stock solution kept at 4 °C). Simultaneous use of two fluorescent dyes allows a two-colour discrimination of the population of living cells from the dead-cell population. the current staining protocol used fluorescein diacetate (FDA) and propidium iodide (PI), which stain viable cells and dead cells, respectively.

The staining protocol is applicable to grown spheroids on CMC 3D matrix. Non-fluorescent FDA taken up by (HT29, MCF7) cancer spheroids and convert into the green fluorescent metabolite fluorescein. The measured signal acts as marker for viable cells, as the conversion is esterase dependent. In contrast, the nuclei staining dye PI cannot pass through a viable cell membrane. It reaches the nucleus of cancer cells by passing through disordered areas of dead cancer cell membranes and intercalates with the DNA double helix of the cancer cell. Hence, dead cells stain red. The staining solution mixture of

Fluorescein diacetate and Propidium iodide (PI) was freshly prepared to be used within 2 h. It was kept protected from light and placed it at 4°C when not needed. Spheroids were collected from their CMC 3D matrices using centrifugation with 800 rpm after 5 min. Afterwards the supernatant was removed, and 1 ml staining solution added to the spheroids, then the next step was the incubation of each sample at room temperature for 4 to 5 min in the dark. The staining solution was removed using same procedure centrifugation with 800 rpm after 5 min. The spheroids were washed by PBS and centrifuged with 800 rpm after 5 min. Eventually PBS or medium without FCS was added to sample, and the sample analysed by fluorescent microscopy (inverted fluorescent microscope with filter sets for Texas Red and FITC).

2.11. Hypoxia assay - to measure oxygen (O2) levels

Image-iT Hypoxia Reagent is a novel fluorogenic compound for measuring hypoxia in live cells. Therefore, hypoxia level of HT29 and MCF7 spheroids were checked through specific time points. It is non-fluorescent when live cells are in an environment with normal oxygen concentrations and becomes fluorescent when oxygen levels are decreased. Both cell lines were seeded into the CMC 3D matrices and hypoxia level were checked using Image-iT Hypoxia reagent. The reagent is fluorogenic when atmospheric oxygen levels are less than 5%. Image-iT Hypoxia Reagent is provided as a lyophilized powder. To make 1 mM stock solution, the lyophilized powder was dissolved in 1.40 mL of DMSO. The reagent was added to the cells at a final concentration of 5–10 µM and incubated for 15 to 30 min. cells were imaged under the fluorescence microscope with excitation/emission of 490/610 nm. Spheroids oxygen level with less than 5% indicate higher red fluorescence therefore, there are more hypoxic.

2.12. Harvesting spheroids from 3D matrices

Well-structure formed spheroids in A/E, A/C and CMC matrices are harvestable. At day 10 spheroids grown in all types of matrices. However, to use spheroids for further experiments the CMC matrix is less elaborate to use. Hence, grown spheroids collected from the 3D CMC matrix and transfer into

the universal using 5 min low speed, gentle centrifugation process 800 rpm, and when supernatant discarded, the spheroids are ready to be harvested again into the fresh CMC matrix.

2.13. Synthesis of AuNCs

Fluorescent AuNCs were made following a one pot synthesis method, by reducing gold salt with minimum amount of DMF in the presence of MSA: specifically, chemicals were introduced consecutively, beginning with MSA and then DMF in aqueous solution with strong mixing. The formation of a light brown colour is an indication of the production of ultra-small non-fluorescent NCs. The exposure of the prepared mixture to hydrothermal heating at 121° for a period of 25 min followed by a cooling phase resulted in the production of NIR-emitting NCs. Importantly, no fluorescence was detected prior to the heating process showing that exposure of the mixture to a high temperature as well as the gradual reduction by DMF contained in the AuNCs capped with MSA leads to luminescence of the nanoparticles.

The absorption and emission of MSA–AuNCs checked by spectroscopy. Therefore, toxicity and targeting fluorescent (800 nm) gold nanoclusters (AuNCs) were manufactured in house as above, TEM imaging of MSA–AuNCs also indicated an average core diameter of 2nm. These were further conjugated to antibodies against Calreticulin (CRT), a potential cancer biomarker or antibodies against epidermal growth factor (EGFR). The chemistry, manufacture and characterisation of the antibodies against CRT are not presented in detail in this report, as they had been previously raised for another study (kindly provided by Dr. B Ramesh, UCL Division of Surgery and Interventional Science). Antibodies against EGFR were purchased commercially (Abcam Company, UK).

2.14. AuNCs Conjugation to Anti-Calruticulin

Fluorescent AuNCs solution was diluted with equal volume of cold 100% ethanol and centrifuged at 4000 rpm for 30 min. The precipitated AuNCs were

vacuum dried to obtain as a powder. The precipitated dried NCs (approximately, 1 mg) were re-suspended in 1 mL phosphate buffer saline (PBS) and centrifuged at 4000 rpm for approximately 10 to 15 min. The obtained coated NCs (1 mL) solution was conjugated to anti-CRT using EDC as an acylating agent together with NHS. Briefly, 200 μL Au/MSA solution (1 mg/mL) was mixed with 200 μl EDC (1 mg/mL) and 200 μL NHS (1 mg/mL) in PBS for 30 min at room temperature. 100 μL of CRT solution (2 mg/mL) was added to the mixture and mixed for 2 h at room temperature. Double conjugation was carried out by repeating the above procedure but only with the synthetic CRT peptide to fully saturate the carboxylate functional sites. To separate the conjugation reagents, the mixture was diluted with ethanol (1:2 ratio) to precipitate the NCs-CRT and dried at room temperature. The purified NCs-(Anti-CRT) defined as Au/MSA conjugated to (Anti-CRT) was collected and stored at 4º C until further use. The sample was further characterized by NIR fluorescence and TEM microscopy.

2.15. Immuno-chemiluminescence detection for AuNCs-Anti-CRT

Dot blots were carried out for confirmation of conjugation of Anti-CRT antibodies and calreticulin synthetic peptide to gold nanoclusters. 5ul of 1:1000 dilution of anti-CRT antibodies conjugated to AuNCs (1mg/ml) in water was marked onto aqueous equilibrated PVDF membrane and allowed to dry at room temperature. On drying the membrane was washed gently in PBS with 0.05% Tween 20 (PBS/T; pH 7.4) and was incubated overnight at room temperature in 2% BSA with 0.005% sodium azide to block any remaining binding spots on the membrane. For the detection of the marked AuNCs-anti-CRT the membrane was washed for 5 min (3x) with PBS and then exposed to anti-rabbit conjugated to horse radish peroxidase (HRP). After 1 hour incubation rabbit AuNCs-anti-CRT bind together. The strip was washed in PBS for 5 min (5x) and used for chemiluminescence detection of the spots to check conjugation.

2.16. AUNCs conjugation to Anti-EGFR

The fluorescent AuNCs solution was diluted with 1 volume of cold 100% ethanol and centrifuged at 4000 rpm for about 10 min. Fluorescent AuNCs were conjugated to EGFR antibody from (Abcam Company, UK) using the N-(3-dimethylaminopropyl)-N-ethylcarbodiimide hydrochloride (EDC) coupling reaction. Based on the supplier's information of the EGFR antibody titer (1:2500), after conjugation, a titer of (1:2500) was found to be suitable to use throughout the experiments.

Briefly 100ul of Fluorescent AuNCs solution (about 200ug/ml, assessed by dry weight) was mixed with 100ul of Anti-Anti-EGFR. 200ug of EDC was then added to the mixture and mixed for 2 h. Due to the addition Anti-Anti-EGFR, Fluorescent AuNCs conjugates are larger than non-conjugated AuNCs and can be separated by centrifugal filter with a cut off 3 kD membrane.

2.17. Immuno-chemiluminescence detection for AuNCs-Anti-EGFR

Dot blots were carried out for confirmation of conjugation of Anti-EGFR antibodies by colleague in another report. 5ul of 1:1000 dilution of anti-EGFR antibodies conjugated to AuNCs (1mg/ml) in water was marked onto aqueous equilibrated PVDF membrane and allowed to dry at room temperature. On drying the membrane was washed gently in PBS with 0.05% Tween 20 (PBS/T; pH 7.4) and was incubated overnight at room temperature in 2% BSA with 0.005% sodium azide to block any remaining binding spots on the membrane. For the detection of the marked AuNCs-anti-EGFR the membrane was washed for 5 min (3x) with PBS and then exposed to anti-rabbit conjugated to horse radish peroxidase (HRP). After 1 hour incubation rabbit AuNCs-anti-EGFR bind together. The strip was washed in PBS for 5 min (5x) and used for chemiluminescence detection of the spots to check conjugation.

2.18.   Toxicity studies in 2D cultured cells

For toxicity studies, cancer cells (HT29, MCF7) and endothelial cells (HUVECs) were seeded into 24 well plates (40×10^3 per well) for 48 h, and then exposed to different concentrations of AuNCs or constituent compounds. After 24 h, metabolic activity (as a measure of proliferation) was measured, using the alamarBlue assay. Briefly, 300 alamarBlue the reagents were added to each well, the plates were incubated at 37°C approximately 4 h to allow cells to convert resazurin to resorufin, and the resultant absorbance signal was measured (Excitation 530, Emission 620). Results are presented by plotting the absorbance signal versus concentration of each test compound.

2.19.   Targeting studies in 2D fixed cancer cells

For primary targeting studies, 2D culture systems are optimal. The cancer cells (HT29, MCF7) and HUVECs were seeded in 24 wells plate (4×10^3 per well) incubated for 24 h and then fixed using Paraformaldehyde solution (4% in PBS). The fixed cells were rinsed in PBS and incubated with 100 µl of the 100 µl/ml conjugated AuNCs-Anti-CRT for 30 min at 37°C and washed with PBS to remove all excess off. To check the specificity of targeting the cancer cells and endothelial cells were seeded in 24 well plate (40×10^3 per well) incubated for 24 h and then fixed using Paraformaldehyde solution (4% in PBS). The fixed cells were washed in PBS and incubated with 100 µl of the 100 µl/ml non-conjugated AuNCs for 24 h at 37°C and washed with PBS to remove all non-specific bindings.

2.20.   Targeting studies in 2D live cultured cells

For primary targeting studies, 2D culture systems are optimal. The cancer cells (HT29, MCF7) and HUVECs were seeded in 24 wells plate (40×10^3 per well) incubated for 24 h. Cells were incubated with 100 µl of the 100 µl/ml conjugated AuNCs-Anti-CRT for 30 min at 37°C and then cells were washed with PBS to remove all non-specific bindings. For the control cancer cells and endothelial cells were seeded in 24 well plate (40×10^3 per well) incubated for 24 h and then

with 100 µl of the 100 µl/ml non-conjugated AuNCs for 24 h at 37°C and washed with PBS to remove excess off.

2.21. Targeting studies in 3D fixed spheroids

At day 10 when spheroids well-formed, spheroids were harvested using low speed, gentle centrifugation at 800 rpm for 5 min. Spheroids were fixed using Paraformaldehyde solution (4% in PBS). The fixed spheroids were rinsed in PBS and 100 µl of the 100 µl conjugated AuNCs-CRT applied. While for the controls, spheroids were fixed without applying any substance. After 1 hour both spheroids samples were washed using PBS and imaged by fluorescence microscopy.

2.22. Nucleic acid stain studies in 3D fixed spheroids

At day 10 when spheroids well-formed, spheroids were harvested using low speed, gentle centrifugation at 800 rpm for 5 min. Spheroids were fixed using Paraformaldehyde solution (4% in PBS). DAPI is a blue fluorescent nucleic acid stain that specially stains double-stranded DNA. It attaches to AT clusters in the DNA in fixed spheroids. DAPI binds to dsDNA and produce an approximate fluorescence enhancement. Fixed spheroids were imaged using florescence imaging. The fluorescence is directly proportional to the amount of DNA present, with emission maximum at 460nm. Although cations do considerably reduce its (blue) fluorescence, the fluorescence is unaffected over different pH range.

2.23. HUVECs grown on filter inserts

Crystal Violet assists in colorimetric measurement of cell viability. It has also been used for the staining of cells to study cell migration and invasion. Therefore, HUVECs were seeded on filter insert (0.45µm), after 48 h incubation, HUVECs were theoretically attached to the filter insert. However, to see the existence and attachment of HUVECs on membrane, HUVECs were stained using Crystal Violet staining solution. 100 ml of this staining solution

were applied onto the surface of filter insert and then briefly washed using PBS. Finally, the HUVECs imaged by fluorescence microscopy.

2.24. Specific targeting of grown 3D spheroids within the CMC+gelatine matrix

HUVECs were seeded on filter insert, after 48 h cells become confluent enough and cover the surface of filter inserts (0.45µm). At day 10 when spheroids were well-formed on CMC matrix, they were harvested using low speed, gentle centrifugation at 800 rpm for 5 min. Grown spheroids transferred into 6 well ultra-low binding plates within the new CMC 3D matrix. HUVECS seeded filter inserts placed on top of the 3D matrix, as a membrane and then 200 µl of 100 µl/ml conjugated AuNCs-Anti-CRT were applied to the membrane surface. For the control sample, empty filter inserts placed on top of the live spheroids and then 200 µl of 100 µl/ml conjugated AuNCs-Anti-CRT were applied onto the empty filter inserts.

This will lead to have better understanding of HUVECs behaviour that may affects targeting of grown spheroids. Afterwards spheroids were imaged in both conditions using fluorescence imaging microscopy and compared fluorescence intensity of them together, this will indicate any possible effects of HUVECs. To check the specificity of targeting in CMC 3D matrix, HUVECs were seeded on filter insert, after 48 h cells become confluent enough and cover the surface of filter inserts (0.45µm). The filter inserts placed on top of the 3D matrix without any spheroids, as a membrane and then 200 µl of 100 µl/ml conjugated AuNCs-Anti-CRT were applied onto empty 3D matrix. For the control 200 µl of the 100 µl/ml of conjugated AuNCs-Anti-CRT were applied onto the empty filter insert placed on top of the 3D matrix with no spheroids. Finally, both conditions were imaged using fluorescence imaging microscopy.

CHAPTER 3

Results

3. Results

The aim of this chapter is to investigate and characterize the growth of cancer cell lines in different 3D matrix conditions, natural and synthetic. Two cancer types took forward: 1) colorectal cancer and 2) breast cancer; endothelial cells were also used, as described below.

3.1. Basic growth characteristics of cell lines in 2D cell culture

3.1.1. Growth of colorectal cancer cells

The cancer cell line was used as an exemplar for colorectal cancer was HT29. In their routine media, their doubling time of cells is 3 to 4 days. HT29 are tumorigenic *in vivo* models, and they look different at high densities in 2D cell culture. However, the ATCC picture could be considered as the regular appearance, although, there is no "standard appearance." Their morphology under the current growth conditions appears "epithelial," and as they grow, they tend to arrange themselves in somewhat glandular structures (Figure 3.1).
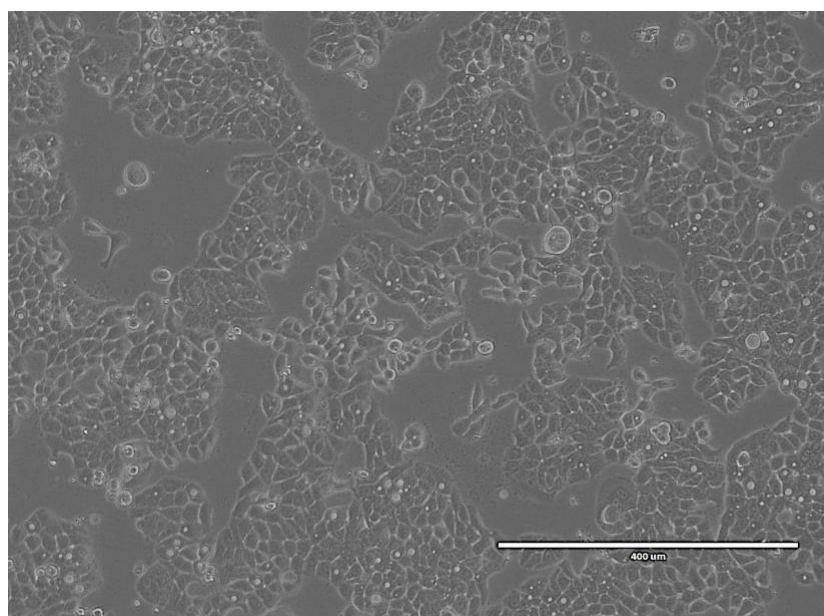
Figure 3.1. Human colon adenocarcinoma cell (line HT29) were seeded in T75 flask and at day 3 imaged using light microscopy in 10x magnification

3.1.2. Growth of breast cancer cells

The cancer cell line used as an example for breast cancer was MCF7. MCF7 is the acronym of Michigan Cancer Foundation-7, referring to the institute in Detroit where the cell line was established in 1973. MCF-7 cells are useful for *in vitro* breast cancer studies because the cell line has retained several ideal characteristics to the mammary epithelium. Their morphology in 2D cell culture appeared to retain epithelial characteristics and like HT29 they sometimes try to form glandular aggregates (3.2).
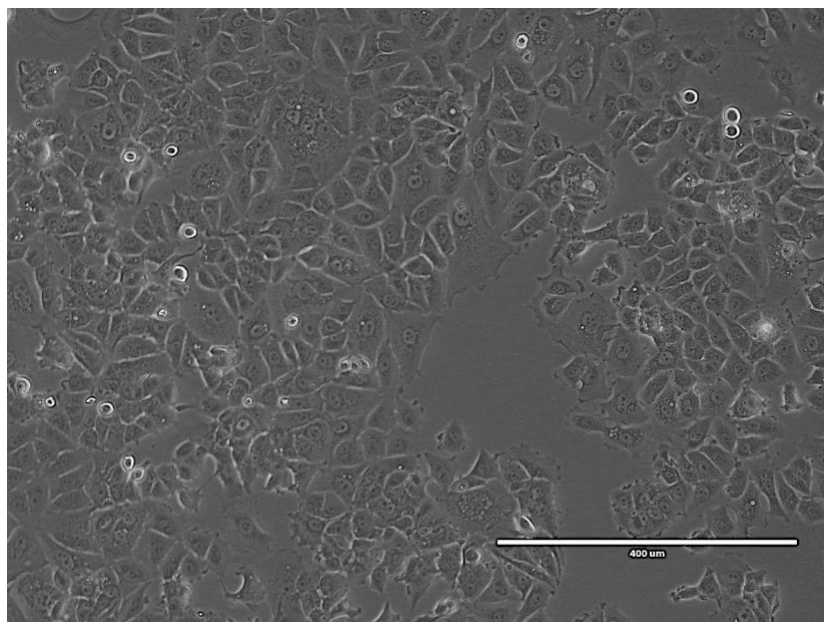
Figure 3.2. Michigan Cancer Foundation-7cell (line MCF7) were seeded in T75 flask and at day 3 imaged using light microscopy in 10x magnification.

3.1.3. Growth of endothelial cells (ECs)

A non-cancer, non-epithelial cell line was also used of endothelial cells to represent normal cells and to be able to incorporate later in complex 3D models as a cell type found in the tumour stroma. Human umbilical vein endothelial cells (HUVECs) are cells derived from the endothelium of veins from the umbilical cord and are commonly to be used for physiological and pharmacological investigations, such as macromolecule transport, blood coagulation, angiogenesis, and fibrinolysis. Human Umbilical Vein Endothelial Cells (HUVEC) single donor from Promo Cell Company was used. The cell

morphology in 2D cell culture was consistent with a typical cobblestone appearance, as expected (Figure 3.3).
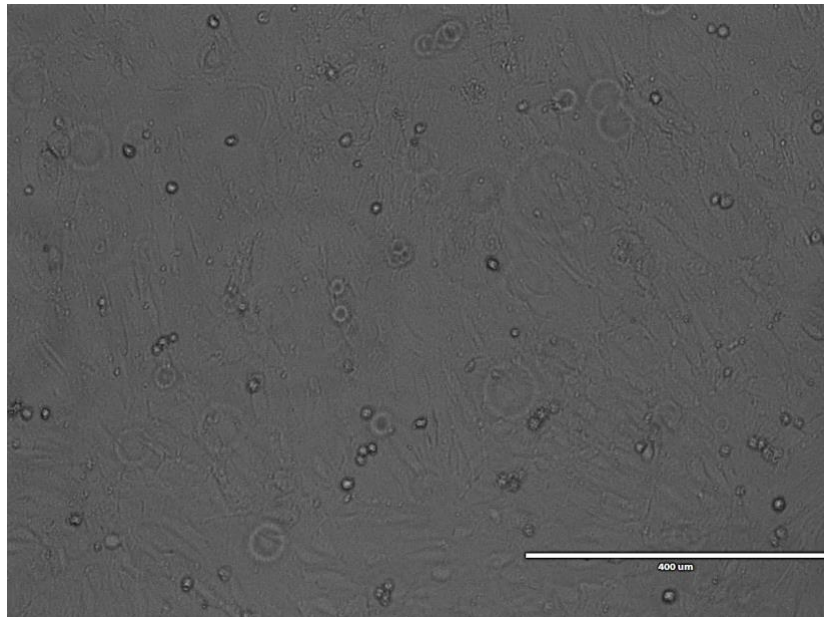
Figure 3.3. Human umbilical vein endothelial cells (line HUVECs) and at day 3 imaged using normal microscopy in 10x magnification

3.2. Metabolic activity of colorectal cancer cells and breast cancer cells in 2D and 3D cell culture (A/E & A/C)

3.2.1. Detection of cell growth of both cell lines using alamarBlue

The effectiveness of the alamarBlue assay for measuring cell proliferation, and cell growth was monitored (HT29, MCF7) for extended time periods. The figure below (3.4) was showed initial cell density for both cell lines in 2D after 5 h incubation with alamarBlue. The linear relationship demonstrated here gives confidence in the use of this assay, at the set parameters of dye concentration and time of exposure and was used for further experiments.
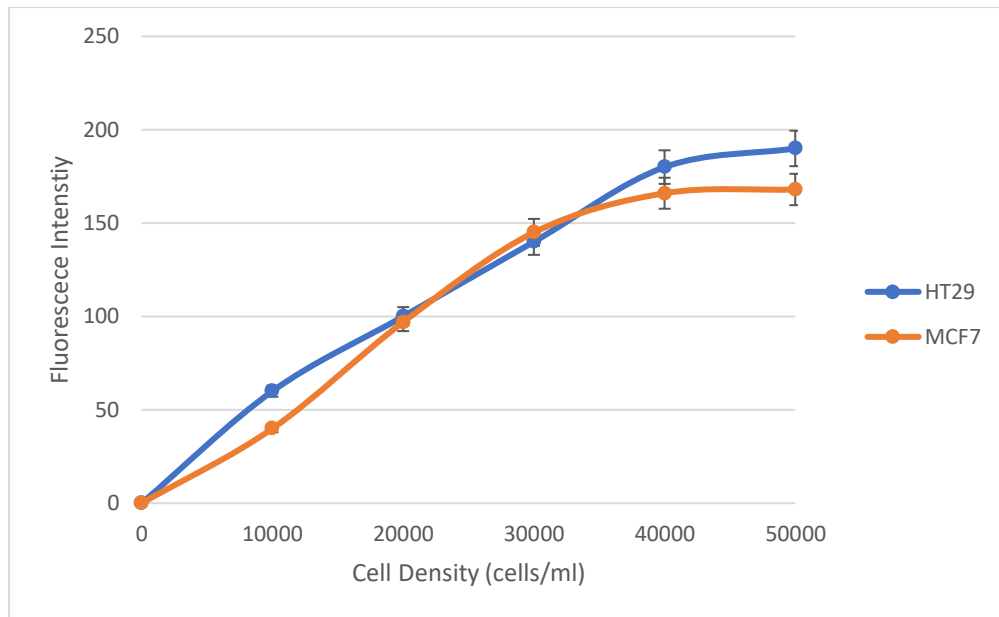
Figure 3.4: HT29 & MCF7 standard curve graph, shows initial cell density for both cell lines in 2D after 5 h incubation with alamarBlue. Absorbance intensity was measured as a measure of growth (Excitation 530, Emission 620). There was a statistically significant difference between groups as determined by one-way ANOVA ***P<0.05.

3.2.2. Optimum cell density for HT29 cancer cells in 3D cell culture using alamarBlue

To map the viability of HT29 cells, alamarBlue was used to quantify metabolic activity of HT29 cells in 3D. Cells seeded at different concentrations 25×10^3, 50×10^3, 75×10^3, 100×10^3 and metabolic activity was checked at each cell density. From day 1 up to day 10 cells gradually started to grow for all different concentrations. The lowest level 25×10^3 cells/ml, showed little metabolic activity up to day 7 followed by a small drop to 30% at day 10. For 50×10^3 cells/ml, cell viability slowly was increased from 10% to 50% at day10. For both 75×10^3 cells/ml and 100×10^3 cells/ml, cells demonstrated increased viability up to day 10.

The graph below (Figure 3.5) was showed results for HT29 cell line in 3D cell culture at different time points.
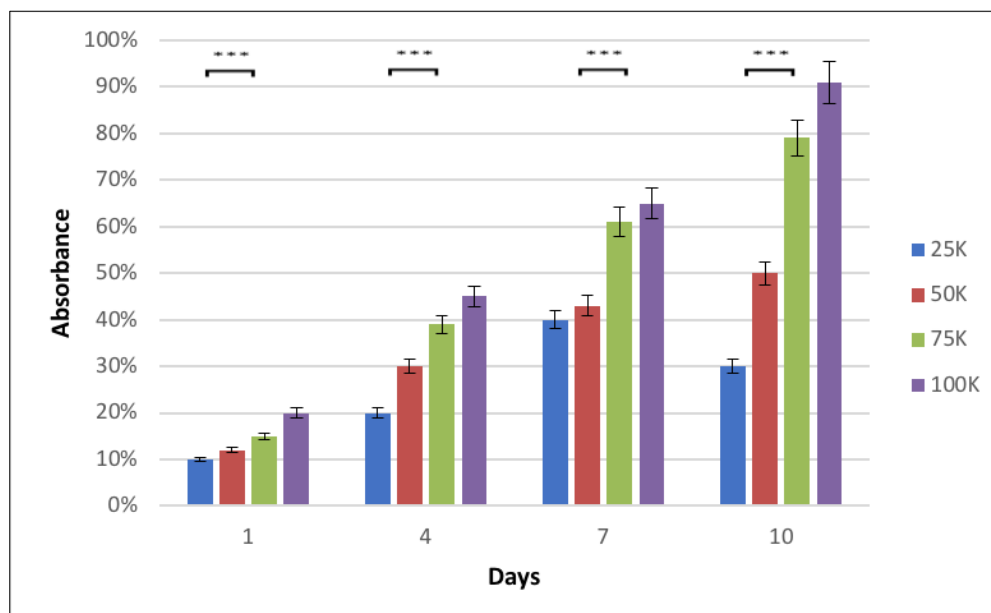
Figure 3.5: The metabolic activity of HT29 cells at 4 different time points, confirms $100x10^3$ is optimum cell density for 3D studies. Absorbance generated from the alamarBlue assay was used as a measure of growth. It increase significant over time compared to day1 for all time points (4,7,10). For each time point (mean ± SD obtained from triplicates) there is significant in growth with increasing seeding concentration from 25K. There was a statistically significant difference between groups as determined by one-way ANOVA ***P<0.05.

3.2.3. Optimum cell density for MCF7 cancer cells in 3D using alamarBlue

The metabolic activity of MCF7 cell in 3D was measured as follows: cells were seeded in different concentrations $25x10^3$, $50x10^3$, $75 x10^3$, $100x10^3$ and metabolic activity was checked using alamarBlue assay at each cell density. From day 1 up to day 10 cells gradually started to grow for all different concentrations. At $25x10^3$ cells/ml, cell viability increased only to 40% by day 10. At $50x10^3$ cells/ml, from day1 up to day10 viability rose from about 15% to approximately 50%. At $75x10^3$ cells/ml, from day1 viability was increased from 15% at day1 to almost 70% at the final day. And eventually, the highest concentration $100x10^3$ cells/ml was showed dramatic increases in viability from 15% to more 80% at day10.

Below graph (Figure 3.6) was showed results for MCF7 cell line in 3D at different time points.
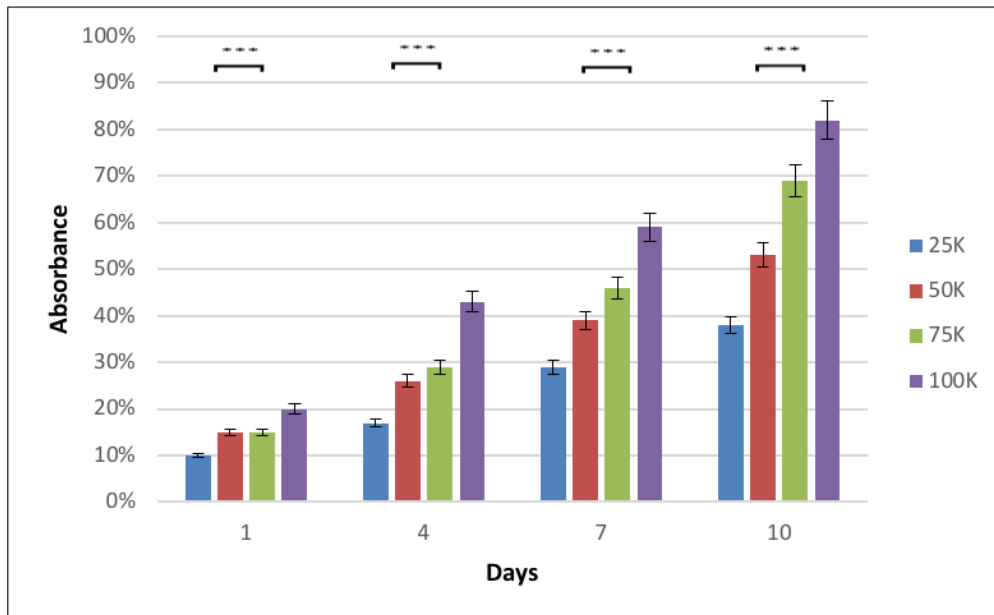
Figure 3.6: The metabolic activity of MCF7 cells at 4 different time points, confirms 100x103 is optimum cell density for 3D studies. Absorbance generated from the alamarBlue assay was used as a measure of growth. It increase significant over time compared to day1 for all time points (4,7,10). For each time point (mean ± SD obtained from triplicates) there is significant in growth with increasing seeding concentration from 25K. There was a statistically significant difference between groups as determined by one-way ANOVA ***P<0.05.

These results suggest that growth of both cell lines (HT29 and MCF7) are linear and demonstrable over the timeline of the experiments up to day 10, at seeding concentrations of 75x10^3 cells/ml and 100x10^3 cells/ml. 100x10^3 cells/ml was the level chosen for further experiments.

3.3. Growth of cancer cells in different 3D cell culture matrices (tumouroids)

3.3.1. Growth of colorectal cancer cells in the agar/collagen (A/C) matrix.

Colorectal cancer cells (HT29) were seeded at 100x10^3 cells/ml concentration in A/C matrices in 24 well plates, as described in the methodology chapter. Miniwells were created by the addition of glass beads in A/C, and this followed by filling in the wells formed by the beads with HT29 cells. The final construct termed a tumouroid. These were left to grow over time and observed at specific

time points. At day 1, HT29 cells appeared to reside within the wells formed by the glass beads, with no sign of cell clumping and attachment. At Day 4, cells started clumping together. At day 7 cells continued to clump or aggregate and hence began to grow into spheroids. Finally, at day 10, small numbers of spheroids were fully formed (Figure 3.7).
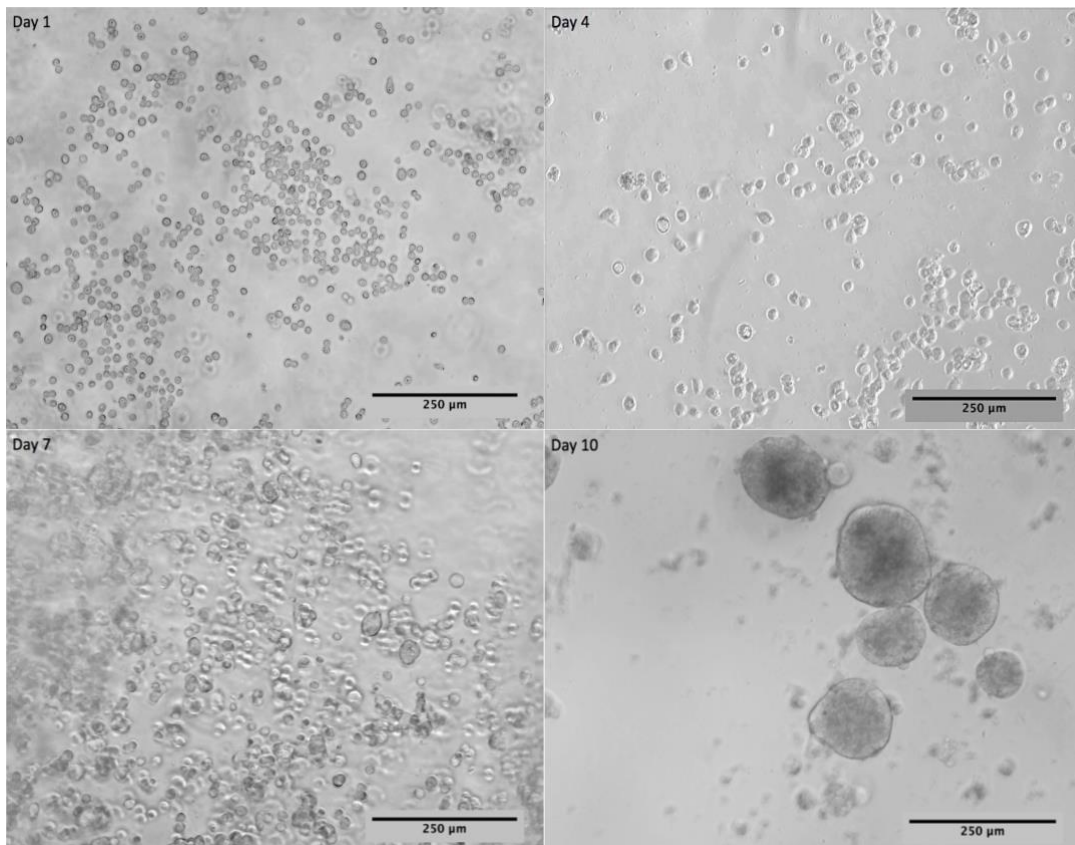
Figure 3.7: Cancer cells (HT29) growing in an agar/ collagen 3D matrix. Day1: Some cancer cells start clumping together, Day4: Some signs of small cell clumps, Day7: Clumps of cells slowly start to form spheroids. Day10: Small number of spheroids are completely formed. (Images taken using light microscopy in 20x magnification)

At day 10 spheroids were harvested for further experimentation. The figure below (3.8) shows the cancer spheroids growth rate in A/C from day 1 up to day 10. At day 1 and day 4 there was not much difference between spheroids sizes, with sizes less than 50 µm, however at day 7 spheroids roughly were about 50 µm and at day 10 they were about 80 µm in size.
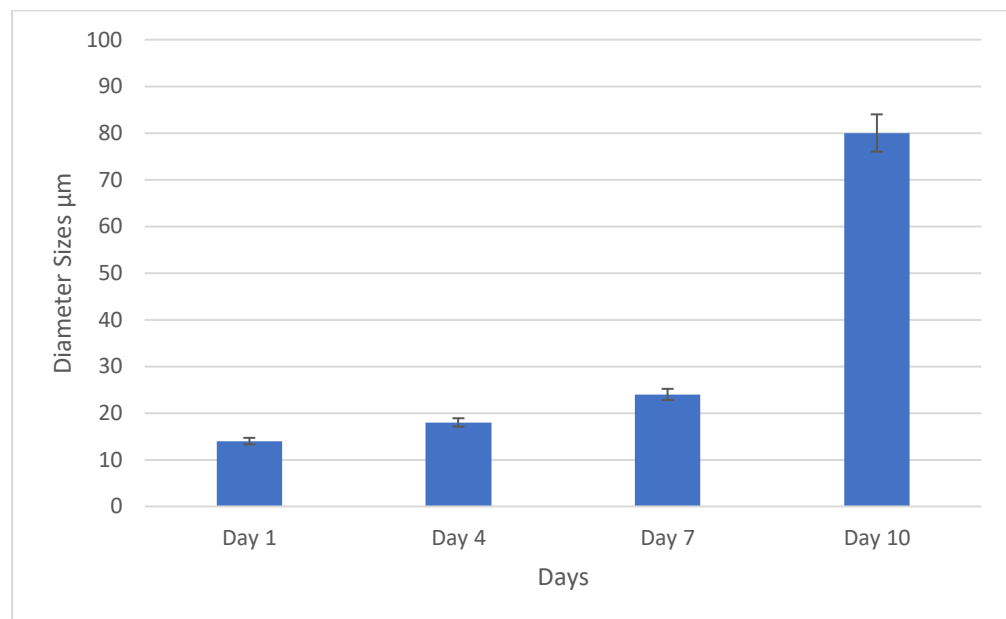
Figure 3.8: Cancer spheroids growth rate slightly increased from day 1 up to day 7. From day 7 diameter size dramatically increased. (numbers shown as averages of 100 spheroids over 3 independent experiments, measured by ImageJ). It increase significant over time compared to day1 for all time points (4,7,10) (mean ± SD obtained from triplicates). There was a statistically significant difference between groups as determined by one-way ANOVA ***P<0.05.

3.3.2. Growth of colorectal cancer cells in the A/E matrix.

Colorectal cancer HT29 cells also were seeded in the A/E matrix. Initial seeding concentrations and methods used were similar as those described above (1.3.1) and in methodology chapter. At day 1, HT29 cells were showed to reside within the wells formed by the glass beads. However, unlike in the A/C matrix, there were some signs of cell clumping and attachment. Also, there were some small spheroids already formed. At Day 4, more spheroids appeared in different sizes. At day 7 bigger spheroids formed and migrated outside the wells originally made by the addition of glass beads. 10 days after creating the 3D tumouroids, the large spheroids were evidently formed (Figure 3.9).

At day 10 only a few single cells appeared in A/E matrix compare to the A/C matrix. Therefore, the growth rate was better, and spheroids formed well; this was more accelerated growth compared to the growth in A/C matrix.
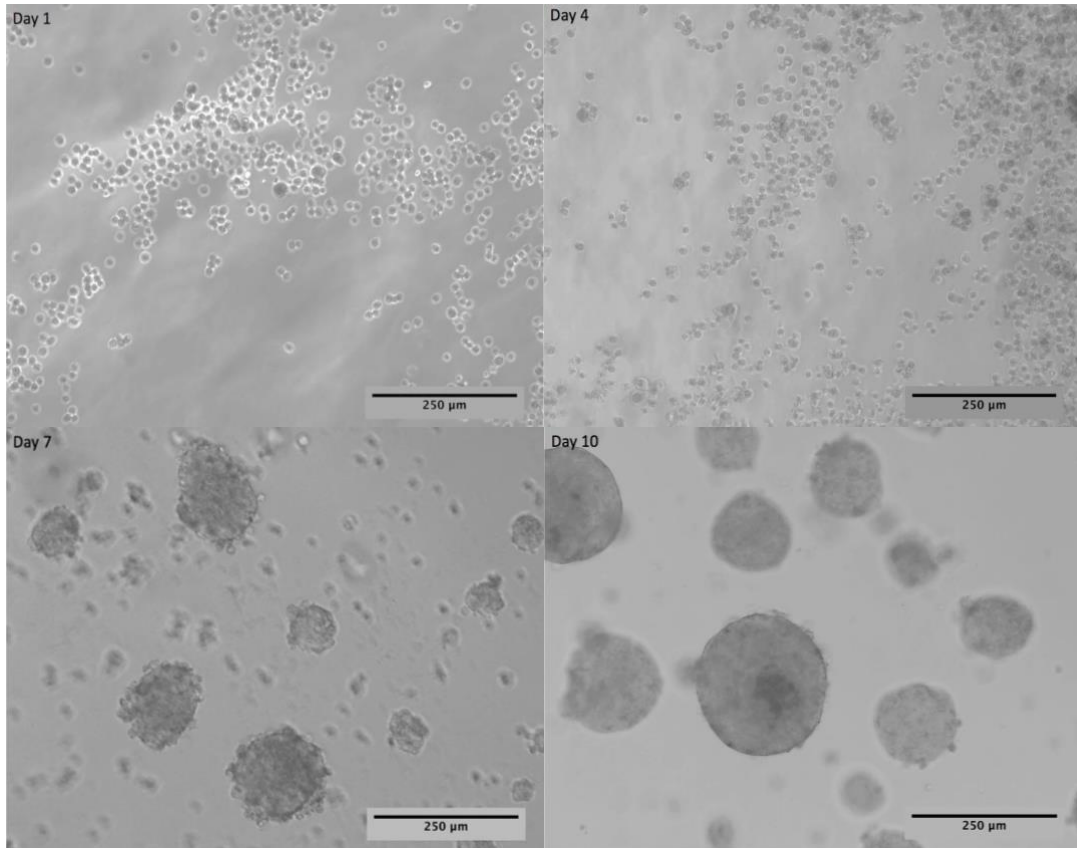
Figure 3.9: Cancer cells (HT29) growing in an agar/ egg white 3D matrix Day1: Some cancer cells start clumping together, Day4: Some sign of cell clumps, and spheroids formation. Day7: spheroid structure formed. Day10: Large structures of spheroids are completely formed. (Images taken using light microscopy in 20x magnification.)

The below (Figure 3.10) showed cancer spheroids growth rate in A/E from day 1 up to day 10, at which point spheroids were harvested. Hence, at day 1 spheroids sizes were about 20 µm (average of 100 spheroids), at day 4 there was some increase (50 µm), however at day 7 spheroids sizes were grown to about 80 µm and finally at day 10 there were highly dense of spheroids roughly about 140 µm.

Figure 3.10: Cancer spheroids growth rate slightly increased from day 1 up to day 7. From day 7 dramatically increased up to day 10. (numbers shown as averages of 100 spheroids over 3 independent experiments, measured by ImageJ). It increase significant over time compared to day1 for all time points (4,7,10) (mean ± SD obtained from triplicates). There was a statistically significant difference between groups as determined by one-way ANOVA ***P<0.05.

3.3.3. Growth of breast cancer cells in the A/C matrix

MCF7 breast cancer tumouroids were created in the A/C matrix, by the exact method described above. The creation of wells in the A/C matrix by the addition of glass beads and afterward filling in the wells created by the beads with MCF7 100×10^3 cells/ml. At day 1, MCF7 cells appeared to reside within the wells formed by the glass beads, with no sign of cell clumping and attachment. At Day 4, some cells started aggregating together. At day 7 all cells gradually began to clump and hence began to grow into spheroids. At day 10 there were some of the spheroids fully formed, and some cells appeared as single or in small spheroids, although some cells would just not aggregate together. (Figure 3.11)
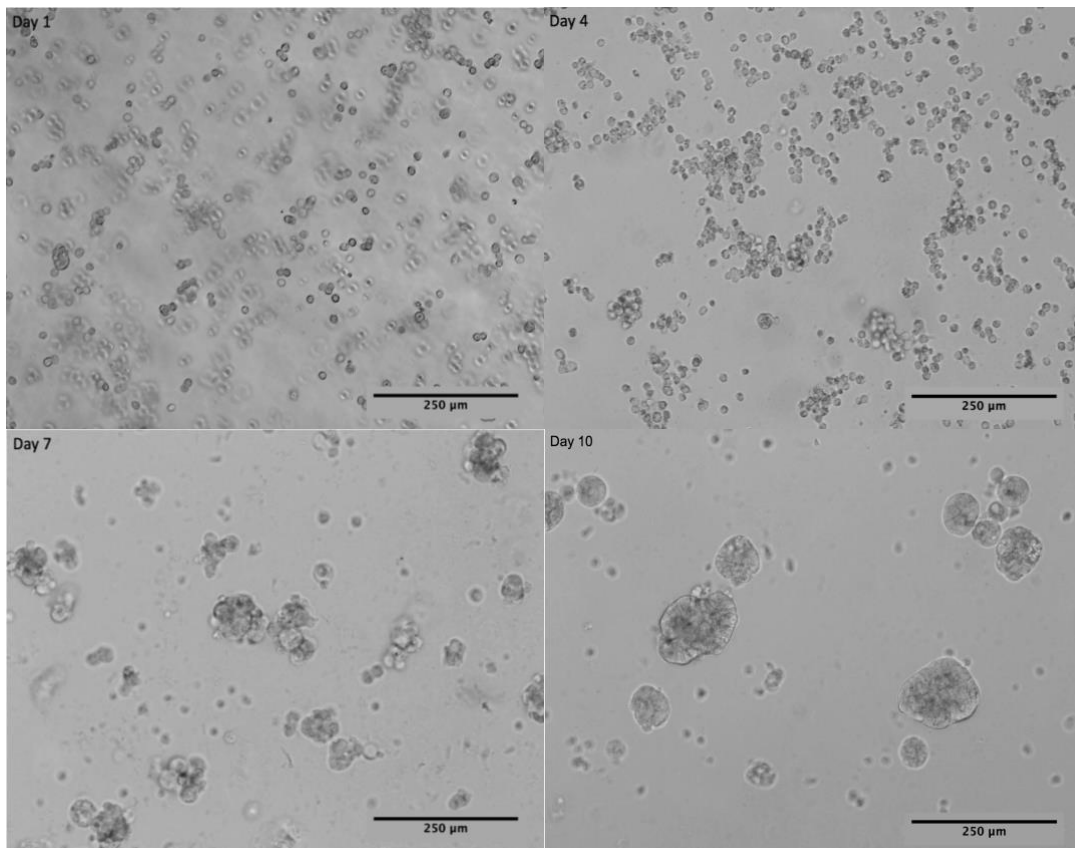
Figure 3.11: Cancer cells (MCF7) growing in an agar/ collagen 3D matrix Day1: Some cancer cells start clumping together, Day4: Some sign of cell clumps, Day7: Clumps of cells slowly start to form spheroids. Day10: Small number of spheroids is completely formed. (Images taken using light microscopy in 20x magnification.)

The below (Figure 3.12) shows cancer spheroids growth rate A/C from day 1 up to day 10, before harvesting spheroids. At day 1 the average sizes of clumping cells/spheroids were about 20 µm. At day 4 sizes slightly increased to about 30 µm, however at day 7 spheroids sizes sufficiently structured at about 50 µm, and finally, at day 10 spheroids sizes were roughly about 60 µm (average of 100 spheroids).
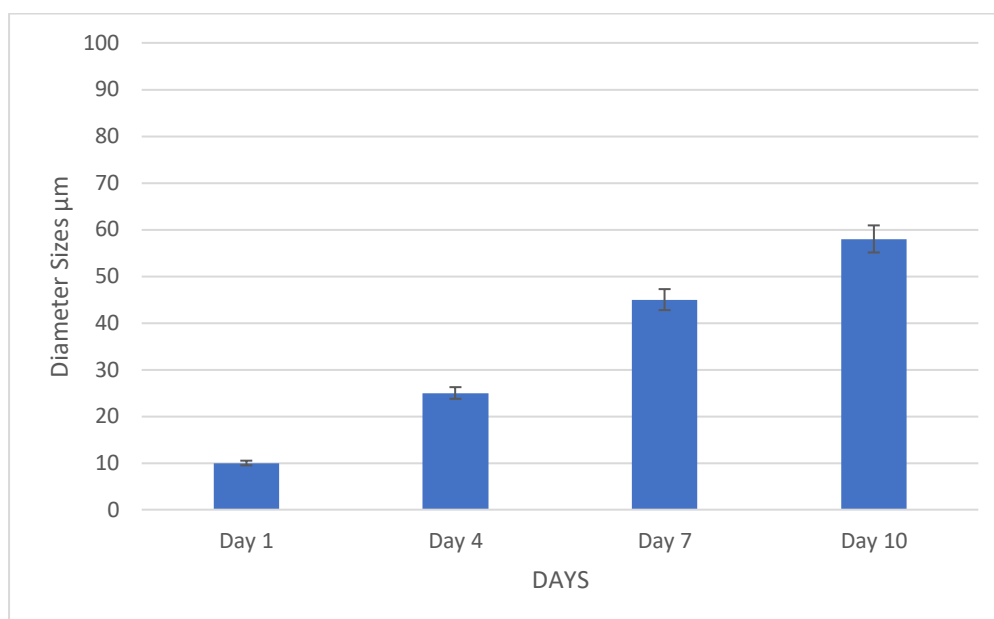
Figure 3.12: Cancer spheroids growth rate increased frequently from Day 1 up to Day 10. (numbers shown as averages of 100 spheroids over 3 independent experiments, measured by ImageJ). It increase significant over time compared to day1 for all time points (4,7,10) (mean ± SD obtained from triplicates). There was a statistically significant difference between groups as determined by one-way ANOVA ***P<0.05.

3.3.4 Growth of breast cancer cells in the A/E matrix

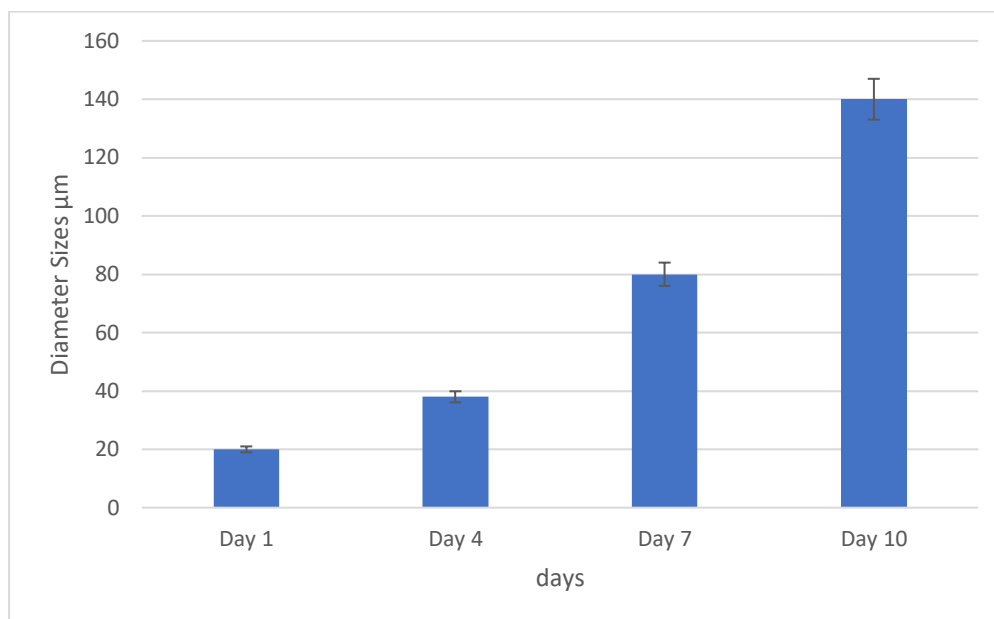MCF7 breast cancer tumouroids were created in the A/E matrix, by the exact method described above, the creation of wells in the A/E matrix by the addition of glass beads and filling in the wells created by the beads with 100×10^3 cells/ml MCF7 cells. At day 1, MCF7 cells appeared to reside within the wells formed by the glass beads, with some sign of cell clumping and attachment. At Day 4, there were some signs of clumping cells. At day 7 clumping cells started to grow into spheroids. 10 days after creating the 3D tumouroids, small numbers of structures of spheroids were fully formed (Figure 3.13). At day 10 a few single cells appeared in A/E matrix unlike in the A/C matrix; therefore, the growth rate

was better, and spheroids formed well and more efficiently that those in the A/C matrix.
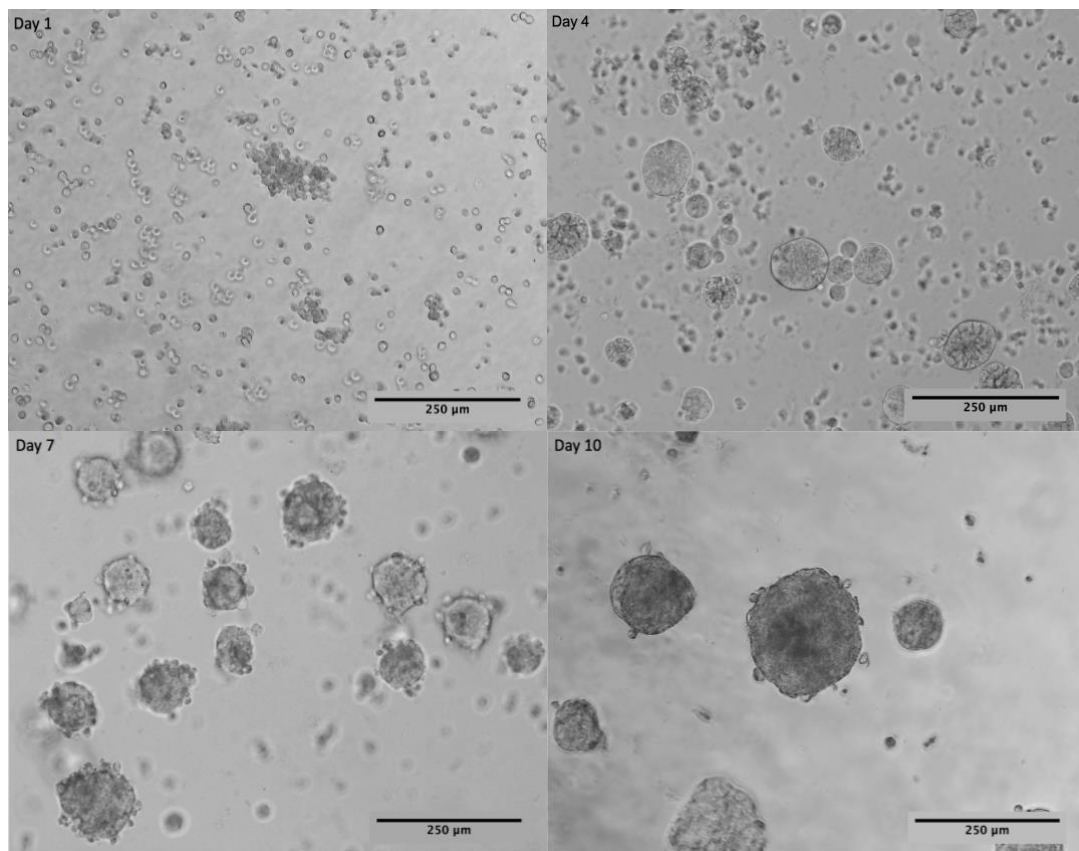
Figure 3.13: Cancer cells (MCF7) growing in an agar/ egg 3D matrix Day1: Some cancer cells start clumping together, Day4: Some sign of cell clumps, Day7: Clumps of cells slowly start to form spheroids. Day10: Small number of spheroids is completely formed. (Images taken using light microscopy in 20x magnification.)

The below (Figure 3.14) shows cancer spheroids growth rate in A/E from day 1 up to day 10, before harvesting spheroids. At day 1 the average sizes of clumping cells were about 20 µm, at day 4 small spheroids formed with an average size about 40 µm, however, at day 7 spheroids sizes increased to about 60 µm. Finally, at day 10 spheroids sizes dramatically increased to roughly about 120 µm (average of 100 spheroids).
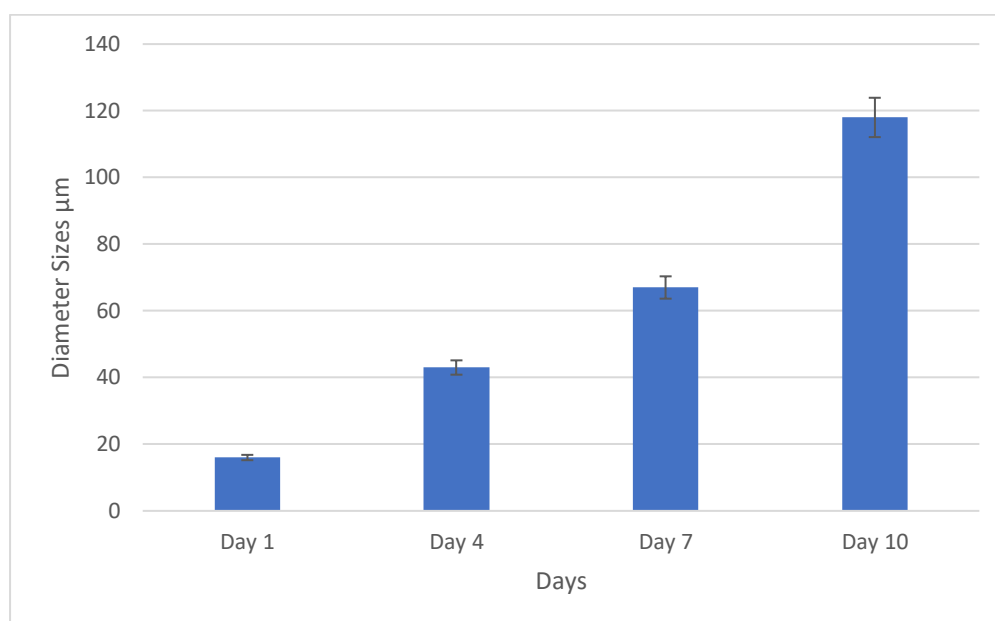
Figure 3.14: Cancer spheroids growth rate increases from Day 1 up to Day 7, and from Day 7 dramatically increases up to day 10. (numbers shown as averages of 100 spheroids over 3 independent experiments, measured by ImageJ). It increase significant over time compared to day1 for all time points (4,7,10) (mean ± SD obtained from triplicates). There was a statistically significant difference between groups as determined by one-way ANOVA ***P<0.05.

## 3.4. Propagation of cancer cells as spheroids, in 3D A/E matrix

Spheroids were harvested from the tumouroid constructs by centrifugation and reseeded into the 3D new matrix to demonstrate whether cells could passage in 3D or not. Harvesting was only attempted for the A/E model. At day 10 after manufacture of 3D tumouroids, when finally, HT29 & MCF7 spheroids were fully formed the whole soft tumouroid underwent 5 min gentle spinning using centrifuge at 80 g, and resultant spheroids were transferred back into the new A/E condition. The spheroids appeared to have kept their morphology, although their sizes may have diminished.

The below images (Figure 3.15) shows HT29 spheroids and (Figure 3.16) shows MCF7 spheroids just one hour after the transferring process into the fresh A/E matrix.
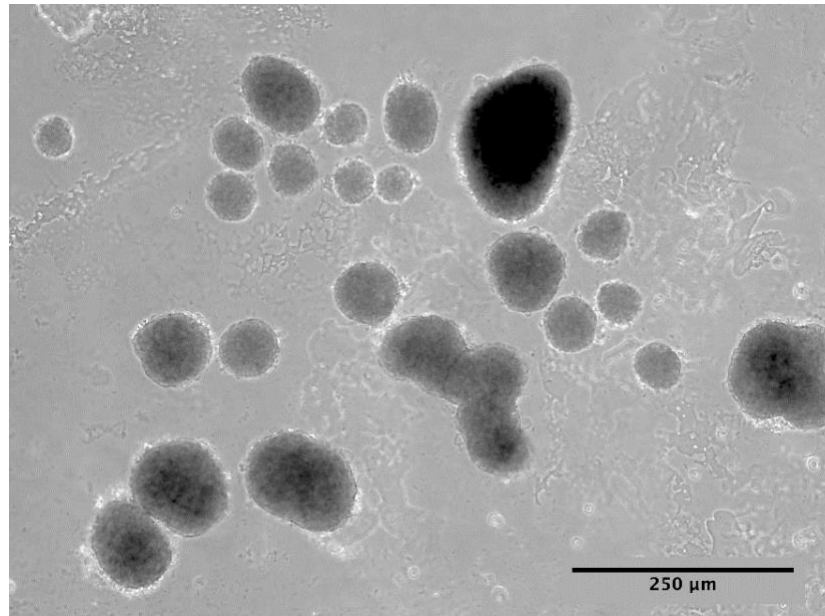
Figure 3.15: HT29 spheroids harvested and transferred back into fresh A/E matrix. (Images taken using light microscopy in 20x magnification.)
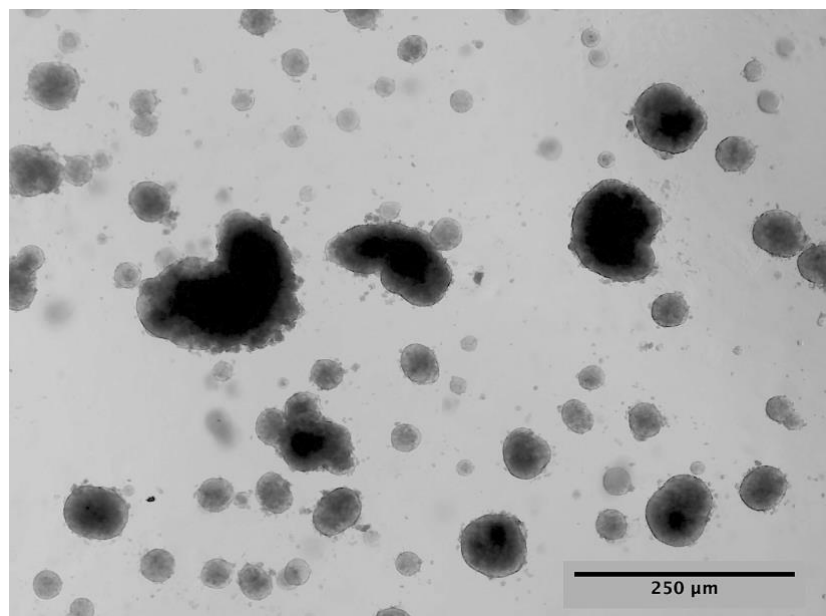
Figure 3.16: MCF7 spheroids harvested and transferred back into fresh A/E matrix. (Images taken using light microscopy in 20x magnification.)

3.5. The physical properties of the new 3D matrix

3.5.1. Sodium Carboxymethylcellulose + Bovine Gelatine

As described in the methodology chapter CMC was dissolved in water and brought to the boil. After cooling and standing in the fridge overnight to complete dissolution, gelatine was added to the CMC solution and mixed thoroughly. The compound was autoclaved at 121°C for 25 mins to be sterilized and cooled. The mixture was now x2 concentrated, so to use it was diluted 1:2 with growth medium and mixed gently, diluted further if too viscous.

As it has mentioned in the method section physical property is essential to record, therefore viscosity level and water swelling capability of the solution was analysed.

3.5.2. Viscosity properties of Carboxymethycellulose (CMC)+gelatine & Carboxymethycellulose (CMC)

A viscometer was used as an instrument to measure the viscosity of fluid. 1 ml of CMC+gelatine solution was added to rheometer (the lower measuring system), and viscosity level checked using viscometer and compared with the viscosity of CMC solution (No gelatine) at room temperature. The figure 3.17 below shows the rheometer (Cone/plate system).
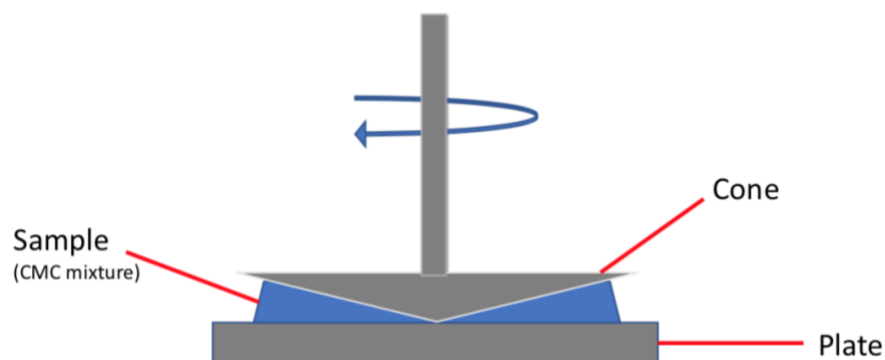
Figure 3.17: Rheometer (Cone/plate) measuring system contains of a rotating upper Cone and a fixed lower plate with CMC mixture contained between them. Since the shear stress is constant (within 0.3%) with radial position for Cones with a small Cone angle, the viscosity of CMC mixture can be analysed directly from the experimental torque/speed relation. For Cone/plate measuring system, it is normally easier to slightly over fill and then trim off any excess sample after bringing the upper and lower measuring systems together.

The below figures show the viscosity level of CMC+gelatine and CMC solution (No gelatine). Therefore, the results showed CMC+gelatine viscosity was slightly higher than CMC solution (No gelatine). Although the viscosity level is significant, it is important that it does not interfere with 3D harvesting.
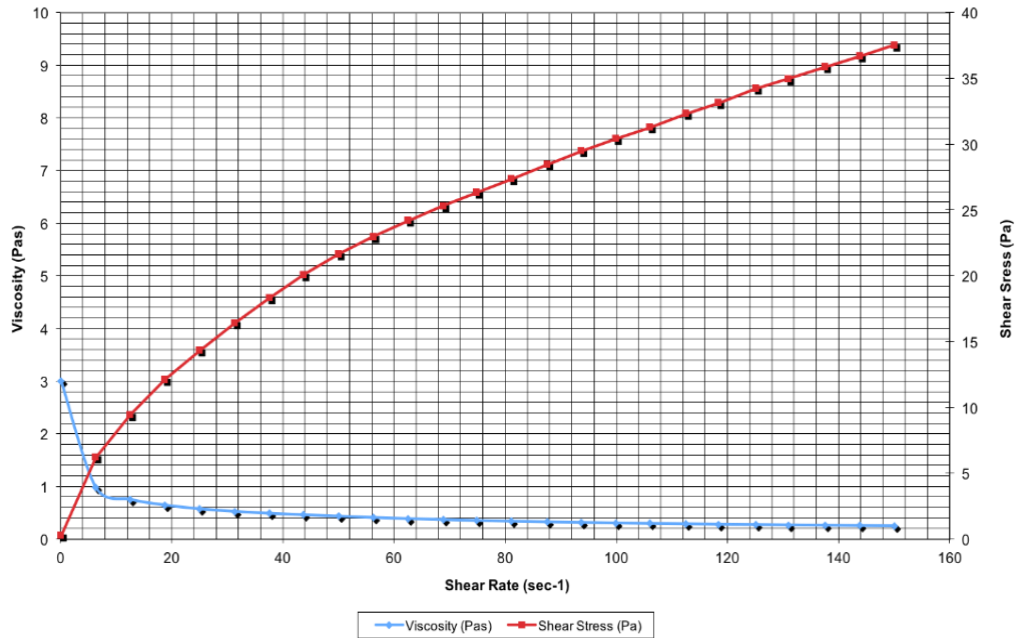
Figure 3.18: The (blue line) indicates viscosity level of CMC+gelatine and (Red Line) represent shear stress, measured by Cone/plate measuring system.
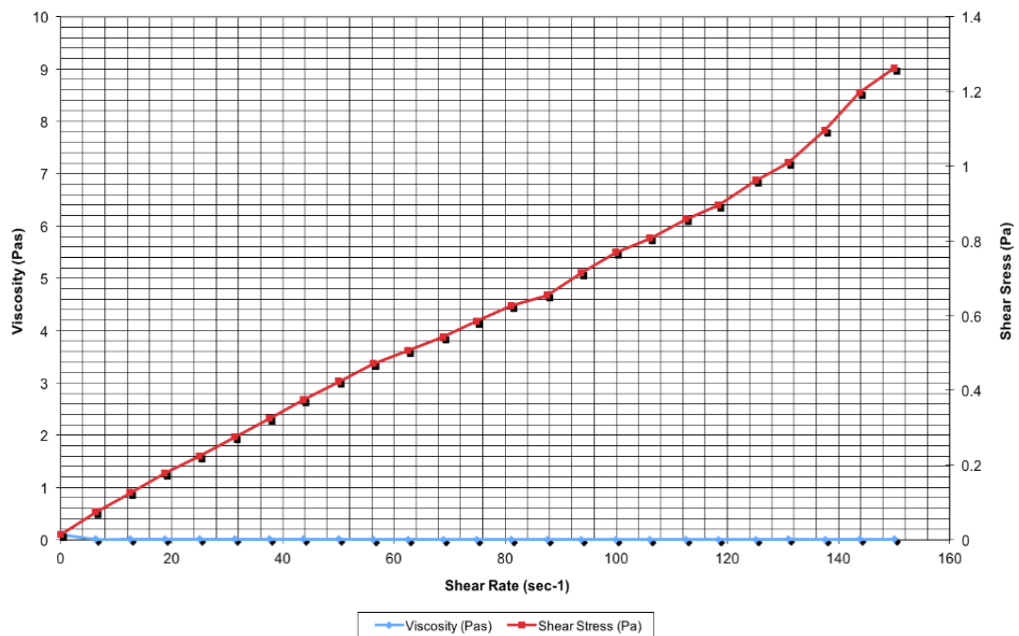
Figure 3.19: The (blue line) indicates viscosity level of CMC and (Red Line) is shear stress. measured by Cone/plate measuring system.

3.5.3. 3D CMC water swelling capability

Water swelling capability properties was checked using freeze-drying which is a dehydration process. The below (Figure 3.19) shows water swelling capability process, where freeze dried CMC mixtures was weighted, and compared with the actual weight of CMC mixture. The 24 ultra-low binding plate weighed 71.00 gr (+/-). Then the 24 ultra-low binding plate containing 1 ml of solution weighed 73.00 gr (+/-) and eventually after freeze-drying the 24 ultra-low binding plate containing dried CMC+gelatine solution weighed 69.00 gr (+/-).
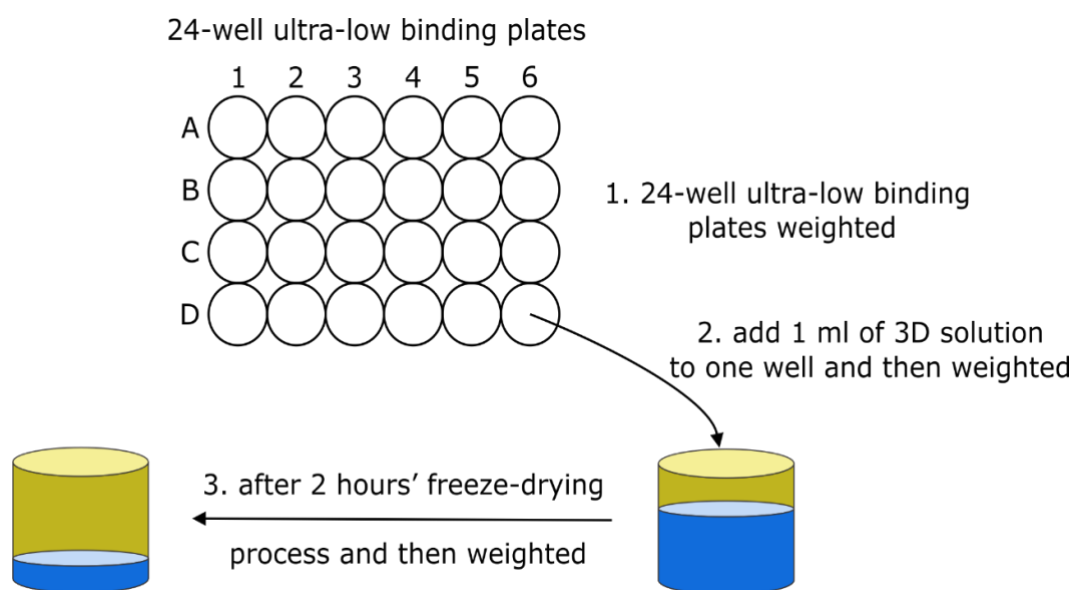
Figure 3.20: Three stages of water swelling capability process,1. The 24 Ultra Low Binding plate weighted. 2. The 24 Ultra Low Binding plate weighted after adding of 1 ml solution. 3. The 24 Ultra Low Binding plate contains 1 ml solution weighted after freeze-drying process.

3.6. Metabolic activity of cancer cells in the novel 3D matrix

As it has mentioned in the methodology section, different cell densities were seeded into CMC mixture (in 24 ultra-low binding plates) for both HT29 and MCF7 cancer cells. The below (Figures 3.20, 3.21) show results of growth, measured as metabolic activity (alamarBlue) over 3 independent experiments.

3.6.1. Optimum cell density of colorectal cancer cells in CMC+gelatine

The lowest seeding concentration of HT29 $25x10^3$ cells/ml showed an increase in metabolic activity/growth from day 1 up to day 7 however, at day10, this dropped to less than 60%. $50x10^3$ cells/ml cell density showed a smooth increase from day 1 up to day 10. $100x10^3$ cells/ml showed the highest continuous increase from day 1 up to day 10. And eventually the highest concentration $150x10^3$ cells/ml showed a dramatic increase from day 1 up to day 7, and a dramatic drop for day 10 from over 90% to less than 70%.
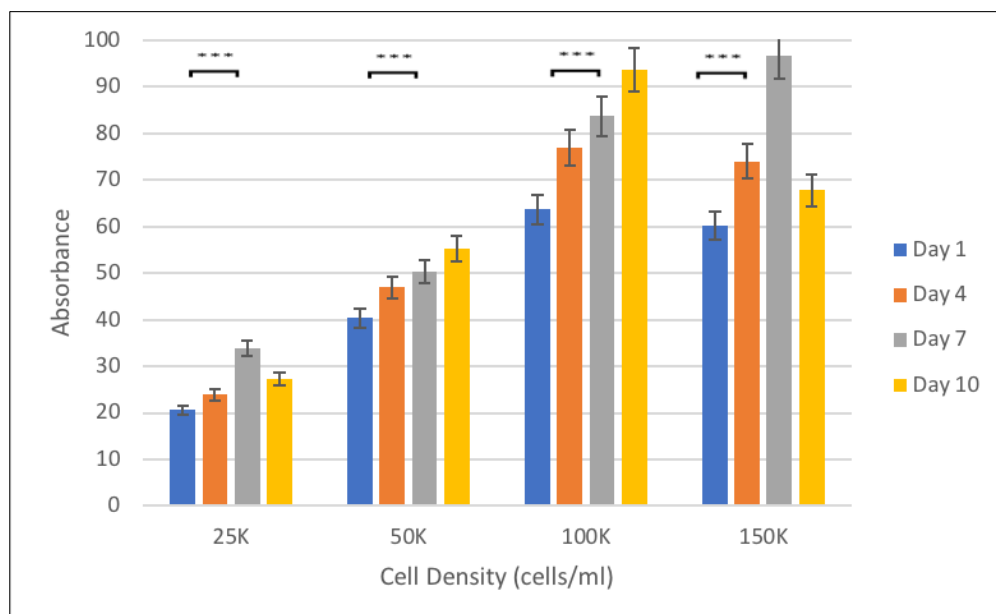
Figure 3.21: The metabolic activity of different HT29 seeding concentrations compared at four different time points. Metabolic activity was measured by alamarBlue and taken as an indication of growth. The results show 100K is the optimum cell density. It increase significant over time compared to day1 for all time points (4,7,10). For each time point (mean ± SD obtained from triplicates) there is significant in growth with increasing seeding concentration from 25K. There was a statistically significant difference between groups as determined by one-way ANOVA ***P<0.05.

3.6.2. Optimum cell density of breast cancer cells in CMC+gelatine

The below (Figure 3.21) shows MCF7 growth slightly increased from day 1 up to day 7, however, there was a plateau between day 7 and day 10 at the lowest concentration 25×10^3 cells/ml. The 50×10^3 cells/ml cell density of MCF7 showed the continuous increase from day 1 up to day 10. By increasing cell density of MCF7 to 100×10^3 cells/ml the measurements showed a constant increase from day 1 up to day 10 which was larger than that observed for 50×10^3 cells/ml. Finally, MCF7 showed a dramatic increase from day 1 up to day 7, and dramatic drop at day 10 for the highest seeding concentration of 150×10^3 cells/ml.
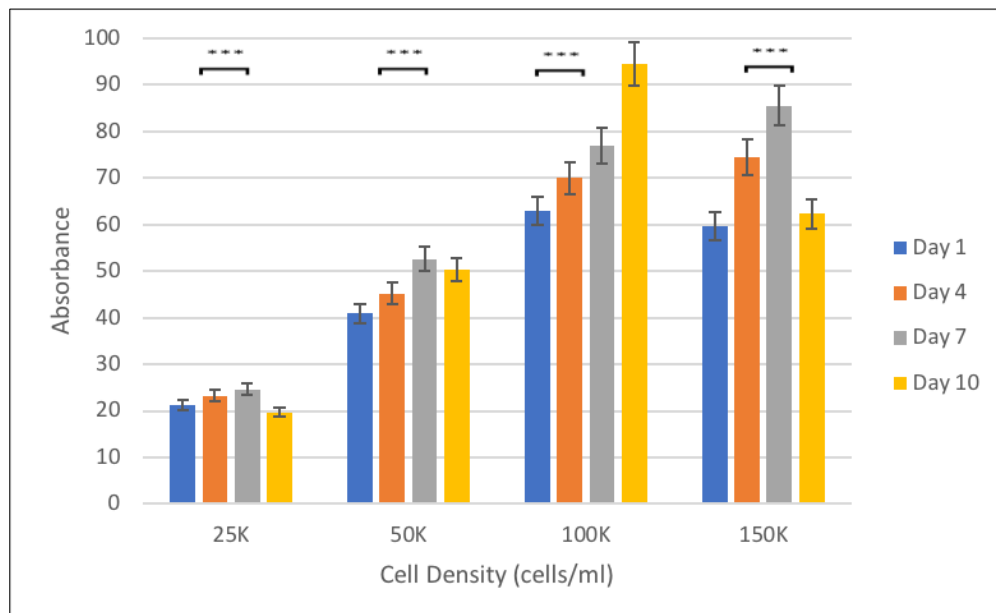
Figure 3.22: The metabolic activity of different MCF7 seeding concentrations compared at four different time points. Metabolic activity was measured by alamarBlue and taken as an indication of growth. The results show 100K is the optimum cell density. It increase significant over time compared to day1 for all time points (4,7,10). For each time point (mean ± SD obtained from triplicates) there is significant in growth with increasing seeding concentration from 25K. There was a statistically significant difference between groups as determined by one-way ANOVA ***P<0.05.

3.7. Growth of cancer cells in the novel 3D matrix (CMC+gelatine matrix)

100×10^3 cells/ml were seeded into the 3D CMC+gelatine matrix and growth rate of spheroids tracked and compared over different time points. The below figures show results from 3 independent experiments.

3.7.1 Growth of colorectal cancer cells in CMC+gelatine matrix.

At day 1 HT29 small spheroids were already formed with sizes of about 80 μm in average. At day 4 spheroid size considerably increased to about 175 μm in average, at day7 spheroid size increased to more than 200 μm and finally at day10 growth (as measured by diameter) started slowing down, with highly dense spheroids of about 220 μm in average (Figures 3.22, 3.23).
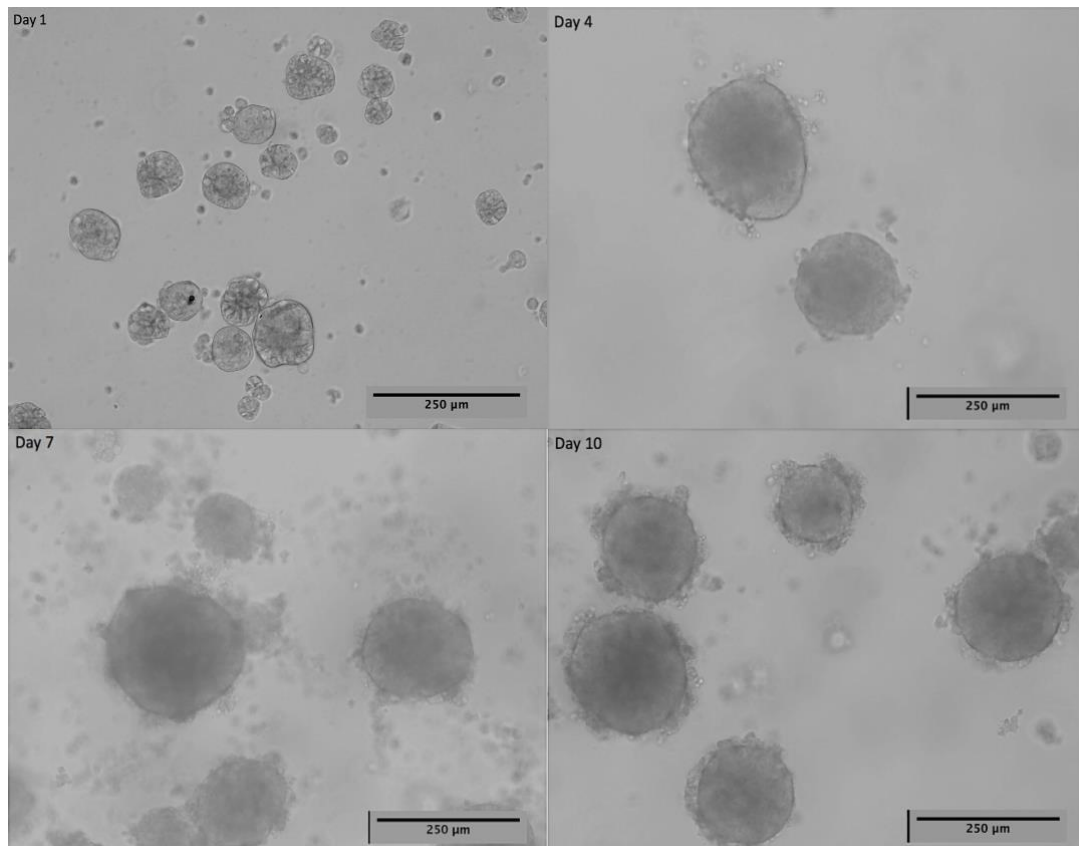
Figure 3.24: colorectal cancer cells growth in 3D CMC+gelatine. Day1: small spheroids formed. Day4: spheroids fully structured. Day:7 spheroid size increased. Day10: highly dense spheroids ready for harvesting.
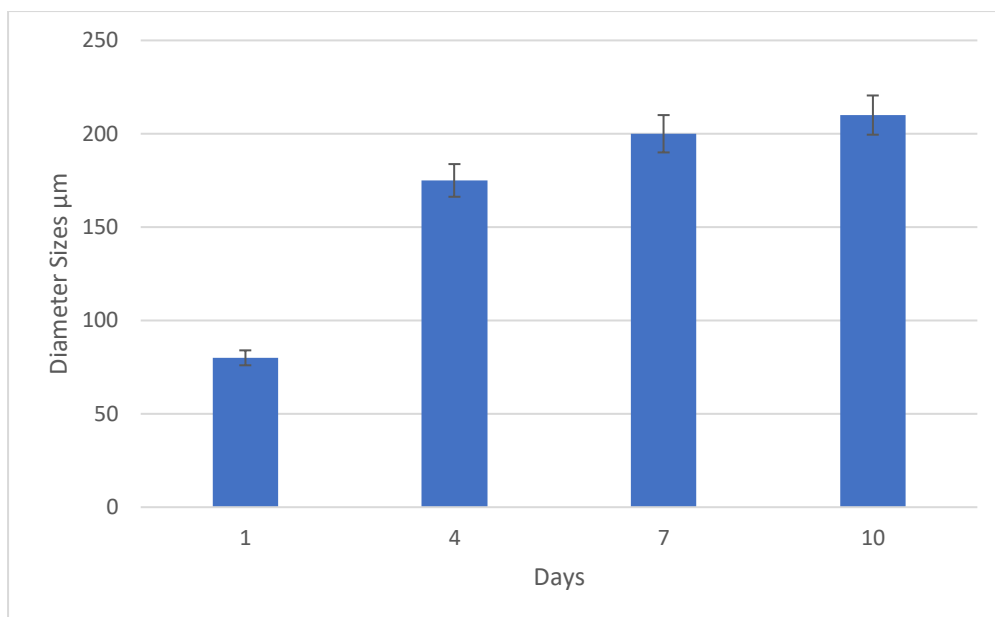
Figure 3.25: Growth rate of HT29 cancer cells in 3D CMC+gelatine matrix, Spheroid size increases between 1- 7 days' post seeding, with sizes starting to reach a plateau by day 10. Day1: spheroid size about 75 mm. Day 4: spheroids size about 170 mm. Day7: spheroids size increased to 200 mm. Day10: spheroids size about 210 mm. (numbers shown as averages of 100 spheroids over 3 independent experiments, measured by ImageJ). It increase significant over time compared to day1 for all time points (4,7,10) (mean ± SD obtained from triplicates). There was a statistically significant difference between groups as determined by one-way ANOVA ***P<0.05.

3.7.2 Growth of breast cancer cells in CMC+gelatine matrix.

At day1 post seeding, MCF7 cells appeared to start forming into small spheroids, which were about 75 μm in average. At day 4 spheroid size dramatically increased to about 85 μm. At day 7 spheroids size was increased to more than 135 μm. And finally, at day 10 growth, as measured by diameter, started slowing: there were highly dense spheroids within the matrix with sizes which slightly increased to about 180 μm (Figures 3.24, 3.25). Overall, the growth rate of breast cancer spheroids was a little less than colorectal cancer spheroids.
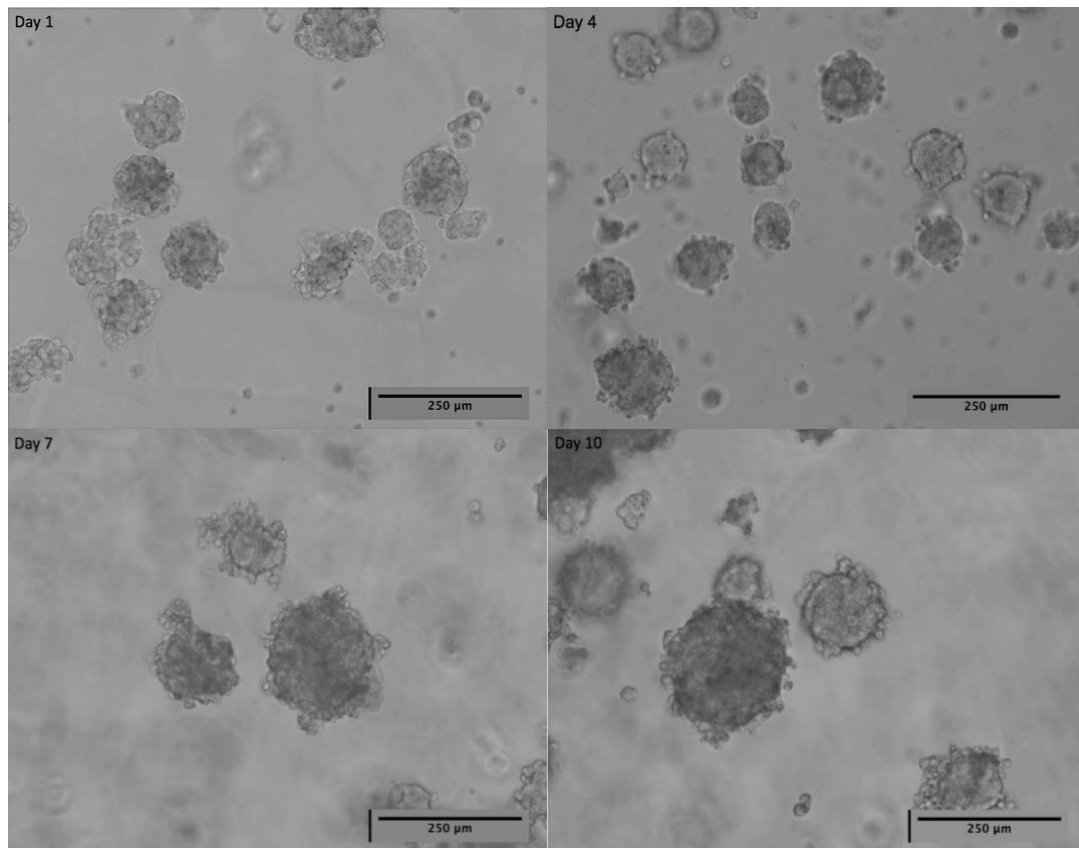
Figure 3.26: breast cancer cells growth in 3D CMC+gelatine. Day1: small spheroids formed. Day4: spheroids fully structured. Day:7 spheroid size increased. Day10: highly dense spheroids ready for harvesting.
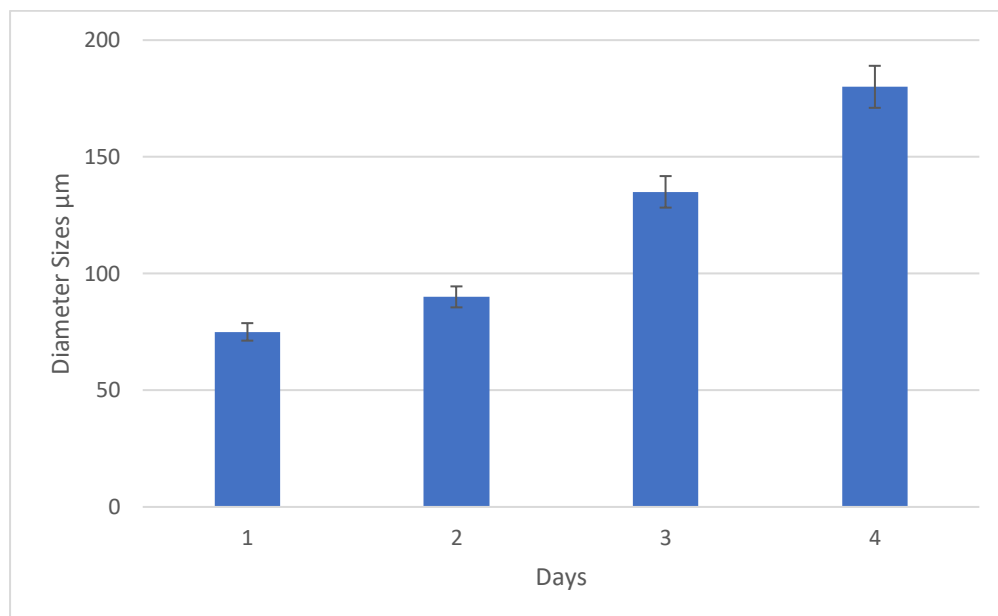
Figure 3.27: Growth rate of MCF7 cancer cells in 3D CMC+gelatine matrix, Spheroid size increases between 1- 7 days' post seeding, with sizes starting to reach a plateau by day 10. Day1: spheroid size about 55 mm. Day 4: spheroids size about 85 mm. Day7: spheroids size increased to 135 mm. Day10: spheroids size about 180 mm. (numbers shown as averages of 100 spheroids over 3 independent experiments, measured by ImageJ). It increase significant over time compared to day1 for all time points (4,7,10) (mean ± SD obtained from triplicates). There was a statistically significant for each time points difference between groups as determined by one-way ANOVA ***P<0.05.

3.8. Growth of human umbilical vein endothelial cells in CMC+gelatine matrix.

100×10^3 cells/ml HUVECs seeded into the 3D matrix and growth rate tracked and compared over different time points, Days 1, Day 5 and Day 10. The (Figure 3.26) below shows representative results, of HUVECs morphology in 3D; this was changed compared to 2D (Figure 3.3), with cells in 3D appearing rounded. The number of HUVECs seemed to have slightly increased from day 1 up to day 10. Finally, at day10 HUVECs were transferred back into the 2D condition to check whether they are live or dead. Crucially, HUVECs did not grow as spheroids or aggregates, which was the behaviour observed with cancer cell lines.
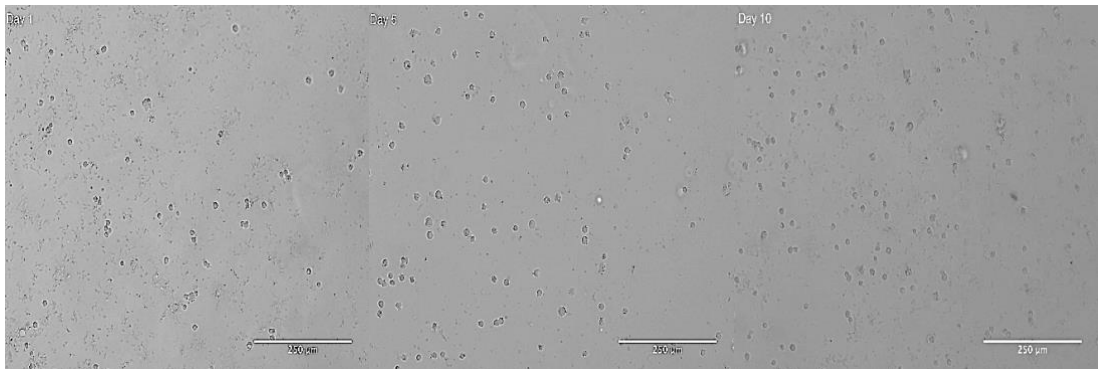
Figure 3.28: HUVECs compared over 3 different time points from day1 up to day10. (Images taken using light microscopy.)
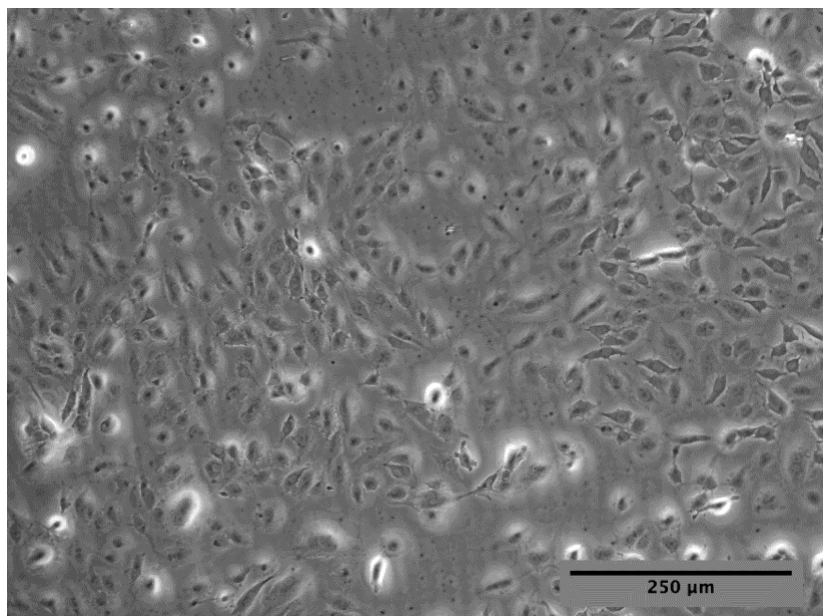
Figure 3.29: At day10 HUVECs were transferred back into the 2D condition to check whether they alive or not. Image taken using fluorescence microscopy.

3.9. Live/Dead Evaluation (Propidium Iodide and FDA)

It is crucial to determine and confirm the viability of spheroids either while growing within the 3D matrices or harvested after centrifugation of the 3D tumouroids, which was determined by the live/dead assay, using Propidium Iodide and FDA, which are detectable by fluorescent microscopy. Results for both colorectal cancer cells and breast cancer cells are shown below, at different time points after tumouroid manufacture, days 1, 5 and 10.

3.9.1 Viability of colorectal cancer cells in CMC and gelatine matrix (Live/Dead Assay)

At day1 staining of HT29 spheroids showed a weak signal of composite of FDA and PI signal due to small spheroids (Figure 3.26). At day 5 HT29 spheroids showed better signal and high cell viability. Eventually at day10 spheroids showed slightly weaker signal, mostly the internal structure of the spheroids surrounded by a layer of viable cells.
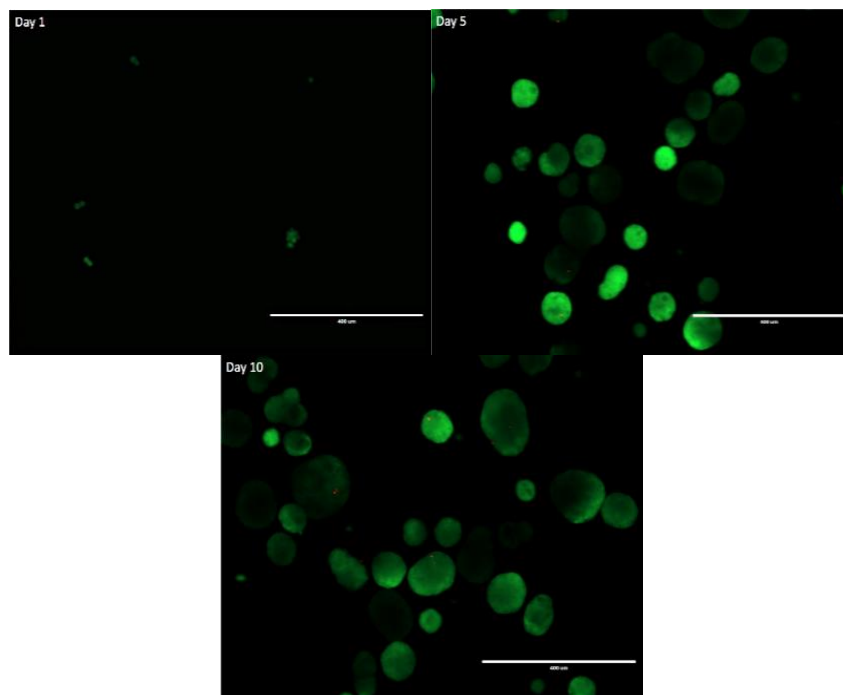
Figure 3.30: Live/Dead Assay in HT29 3D spheroids CMC+gelatine, Day1 clumping cells and small spheroids show weak signal. Fluorescein diacetate (FDA) and propidium iodide (PI), which stain viable cells (Green) and dead cells (Red), respectively.

3.9.2 Viability of breast cancer cells in CMC and gelatine matrix (Live/Dead Assay)

At day1 staining of MCF7 small spheroids showed a weak signal of composite of FDA and PI signal (Figure 3.27). At day 5 MCF7 spheroids showed the stronger signal of composite of FDA and PI. At day10 most MCF7 spheroids revealed high cell viability, mostly the internal structure of the spheroids surrounded by a layer of viable cells.
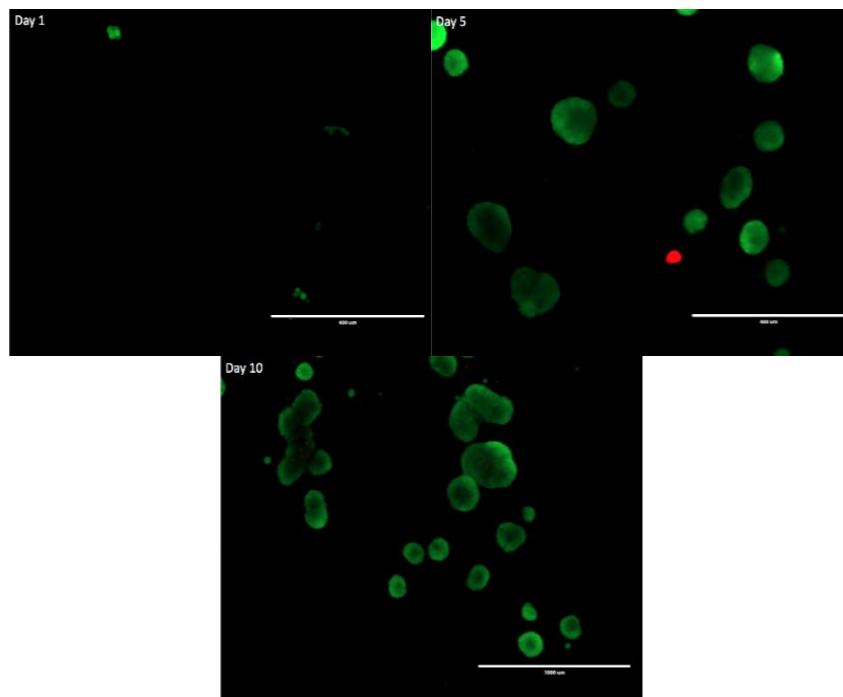
Figure 3.31: Live/Dead Assay in MCF7 3D spheroids CMC+gelatine, Day1 clumping cells and small spheroids show weak signal. Fluorescein diacetate (FDA) and propidium iodide (PI), which stain viable cells (Green) and dead cells (Red), respectively.

3.10. Levels of oxygen/ Hypoxia of 3D cultured cancer cells.

Hypoxia levels of HT29 and MCF7 spheroids were checked through specific time points. Both cell lines were seeded into the CMC+gelatine 3D matrices and hypoxia level was checked using Image-iT Hypoxia reagent. It is non-fluorescent when live cells are in the 3D model with normal oxygen concentrations and becomes fluorescent when oxygen levels decrease. Spheroids oxygen level with less than 5% indicates higher red fluorescence, therefore, there were more hypoxic than live cells in 3D model with no fluorescent.

Image-iT Hypoxia reagent was added to HT29 spheroids within CMC+gelatine 3D matrix. HT29 spheroids (Figure 3.28) tracked and imaged using confocal imaging microscopy over different time points, at day1 there is no sign of any fluorescence when live cells were within CMC 3D matrix. At day 4 while spheroids were well-formed, oxygen level started to drop to less than 5%. At day 7 larger size of spheroids were formed with higher fluorescence intensity according to the fluorescence scale bar. Eventually at day 10 whole 3D matrix and large spheroids showed the highest level of intensity, before the harvesting step. For the control group, HT29 spheroids within CMC+gelatine 3D model was tracked and imaged over different time points, using confocal imaging microscopy without any reagent added to the matrix.

Image-iT Hypoxia reagent was added to MCF7 spheroids within CMC+gelatine 3D model. MCF7 spheroids (Figure 3.28) were tracked and imaged using new instructed confocal imaging microscopy over the particular time frame, at day 1 there is no sign of any fluorescence when live cells were within CMC 3D matrix. At day 4 while spheroids were well-formed, oxygen level started to drop to less than 5%. At day 7 larger size of spheroids was formed shown stronger fluorescence intensity. At final time point, whole 3D matrix and large spheroids were showed the highest level of intensity, before the harvesting step. To check the effects of reagent MCF7 spheroids within CMC+gelatine 3D model was tracked and imaged over different time points, using new instructed confocal imaging microscopy without any reagent added to the matrix.
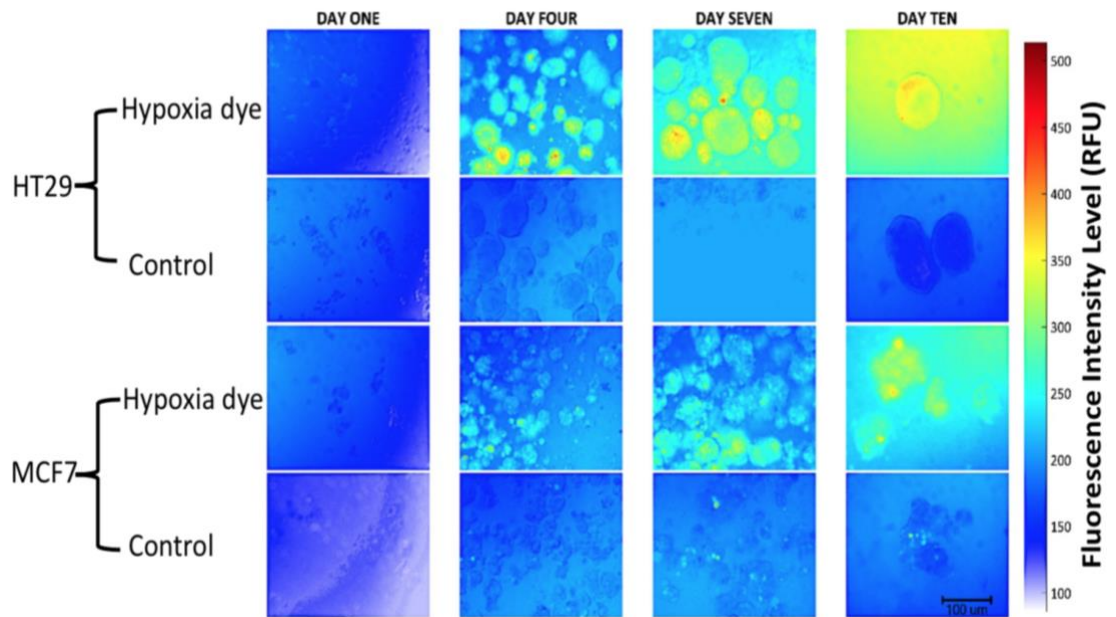
Figure 3.32: shows oxygen gradient (fluorescence) of grown spheroids on both cell lines within 3D matrix at different time points based on fluorescence intensity.

3.11. Propagation of cancer cells as spheroids, in 3D CMC+gelatine matrix

Once live/dead assay and oxygen level of spheroids were checked, at day 10 when grown spheroids were ready to be harvested for further studies. Grown spheroids were transferred into the new 3D matrix, where spheroids could be stained for targeting studies or eventually, for live precise targeting studies.

The (Figure 3.29) below shows the harvested grown HT29 spheroids at day 10 after being transferred into the new CMC+gelatine matrix.
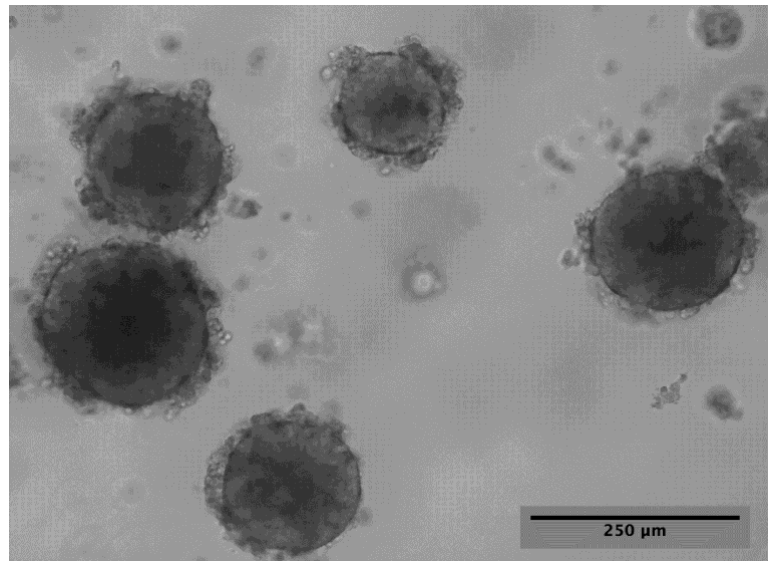
Figure 3.33: shows harvested HT29 grown spheroids at day 10 (20x).

The (Figure 3.29) below shows the harvested grown MCF7 spheroids at day 10 after being transferred into the fresh new CMC+gelatine matrix.
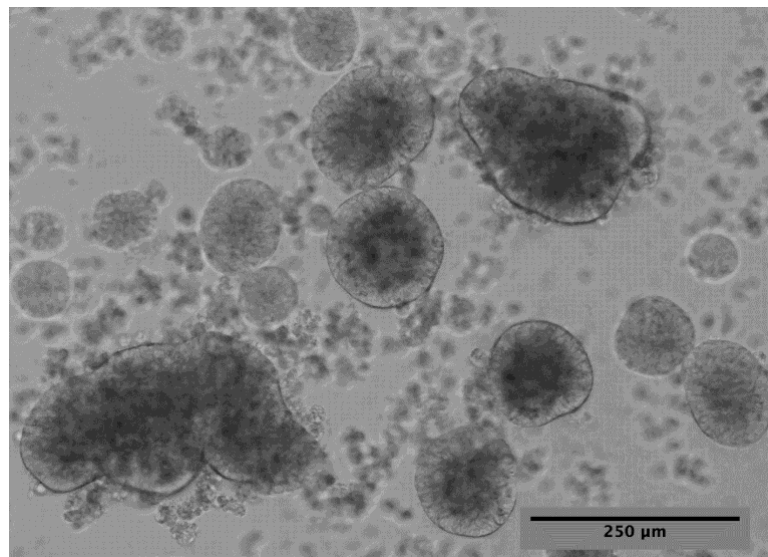
Figure 3.34: shows harvested MCF7 grown spheroids at day 10 (20x).

3.12. AuNCs

3.12.1. Synthesis of AuNCs

AuNCs manufacture is not presented in detail in this report, as their synthesis was part of another study (kindly provided by Dr. B Ramesh, UCL Division of Surgery and Interventional Science). The figure below shows the AuNCs final chemical structure (Figure 3.31).
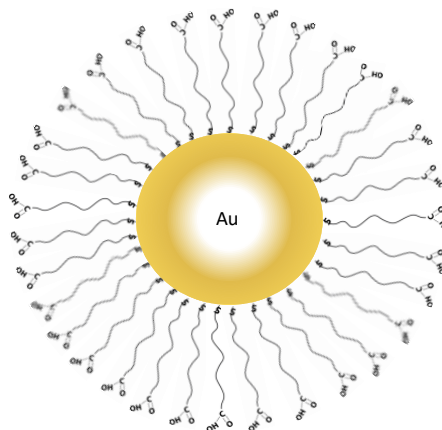
Figure 3.35: Schematic diagram of AuNC surrounded by the structures of COOH: carboxyl

3.12.2. Measuring AuNCs size

The AuNCs sizes were measured using TEM imaging, (Figure 3.32) which indicated an average core diameter size of AuNCs 2 nm (standard division 0.67 +/-). According to dynamic light scattering analysing, the hydrodynamic diameter size was 3.5 nm. The AuNCs are considered as appropriate fluorescence probes for bio-conjugating and high-resolution detection.
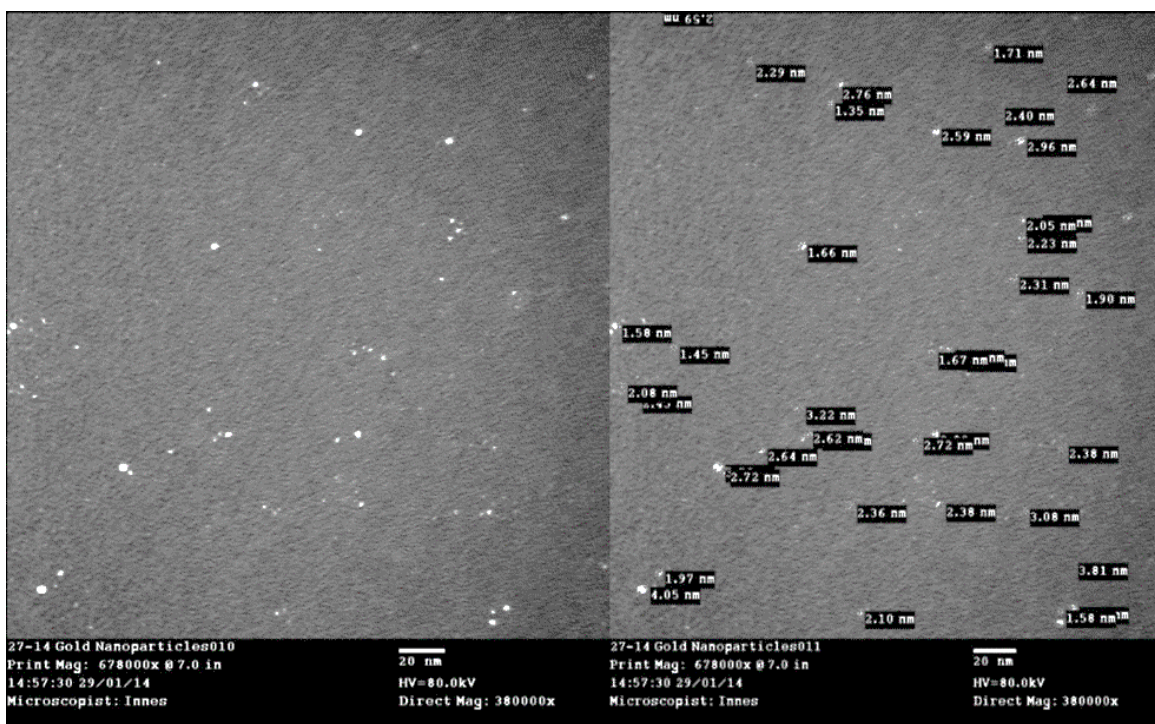
Figure 3.36: TEM image of dispersed AuNCs show the average diameter of (2nm) (standard division 0.67 +/-).

3.13. Toxicity of AuNCs in 2D cultures of all cell lines.

The (Figure 3.36) below shows cells exposed to equivalent concentrations of AuNCs and the primary chemical salts used for AuNCs manufacture $HAuCL_4$ (Mercaptosuccinic acid, Gold (III) chloride trihydrate, and Dimethylformamide). The results for HT29 colorectal cancer cells indicated that gold salts ($HAuCL_4$) conferred a higher level of toxicity compared to AuNCs, over all concentrations. From the lowest concentration 50 µg/ml to the largest concentration of $HAuCL_4$ the number of viable cells dramatically dropped to less the 50%. The AuNCs conferred less toxicity than $HAuCL_4$ compared to each salt concentration. However, exposure to AuNCs resulted in a drop-in viability to approximately 70%.

The results for MCF7 breast cancer cells indicated a decreased viability with exposure to increasing ($HAuCL_4$) gold salt concentrations ranging from relatively small decreases to 75% for 50, 100 and 150 µg/ml to a dramatic drop to less than 50% for 200 µg/ml. Contrary to this exposure to AUNCs resulted in significantly smaller reductions in viability, with a maximum of 20% drop (80%

73

viability) or the highest concentrations of the AUNCs. The decrease in viability caused by the gold salts was significant compared to control untreated cells, while the reduction in viability caused by AuNCs was only significant versus control for the high concentration of 200 µg/ml.

Finally, the results for HUVECs indicated that gold salts (HAuCL$_4$) decreased viability (increased toxicity) with exposure to increasing (HAuCL$_4$) gold salt concentrations. The results show a dramatic drop to less than 20% for all 50, 100, 150 and 200 µg/ml. The AuNCs conferred less toxicity than HAuCL$_4$ compared to each salt concentration. However, exposure to AuNCs resulted in a dramatic drop in viability at higher concentrations to approximately 60% (Figure 3.37).
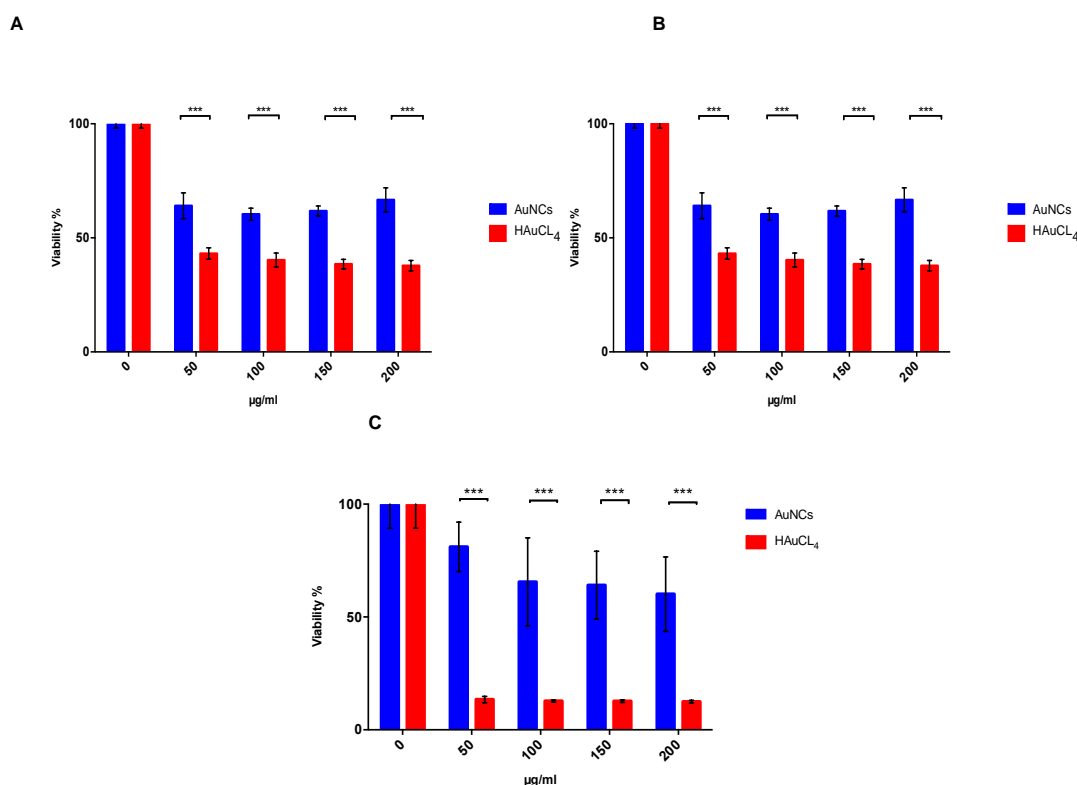
Figure 3.37: (A) alamarBlue assay measurements showing HT29 colorectal cancer cell viability. AuNCs confer a level of toxicity, which remains constant at different concentrations. With HAuCL$_4$ cell viability dramatically dropped to less than 50% over all concentrations, P < 0.0001. Results are shown as % of untreated controls. (B) alamarBlue assay measurements showing MCF7 cell viability. AuNCs confer a level of toxicity, which remains constant at different concentrations. With HAuCL$_4$ cell viability resulted in small decreases to 75% lower concentrations to a dramatic drop to less than 50% for 200 µg/ml, P < 0.0001. Results are shown as % of untreated controls. (C) alamarBlue assay shows HUVECs cell viability. AuNCs frequent toxicity level at different concentrations. HAuCL4 cell viability dramatically dropping to very least amount at different concentrations, ***P<0.05. for each condition (mean ± SD obtained from triplicates). Significantly different compared the AuNCs to HAuCL$_4$ in the same condition.

3.14. Targeting cells in 2D (fixed), using AuNCs-Anti-EGFR

Fluorescent AuNCs were conjugated to commercial EGFR antibody. HT29 and MCF7 cancer cells (2D) were fixed and then targeted using AuNCs-Anti-CRT and AuNCs.

3.14.1. Binding of AuNCs to fixed HT29 cells in 2D.

Both AuNCs-Anti-EGFR and AuNCs were applied to fixed HT29 colorectal cancer cells, which had been grown in 2D culture. Incubation lasted for one hour, cells were then washed and imaged using confocal imaging microscopy. Binding on HT29 cells was demonstrated only for targeted AuNCs-Anti-EGFR, but not for non-targeted AuNCs. A degree of binding, as shown by the NIR fluorescent (Pseudo colour) apparent mostly on the cell surface, was evident in most HT29 cells. The results (Figure 3.38) are shown as light transmission, fluorescence and merged images (respectively, A, B, C).
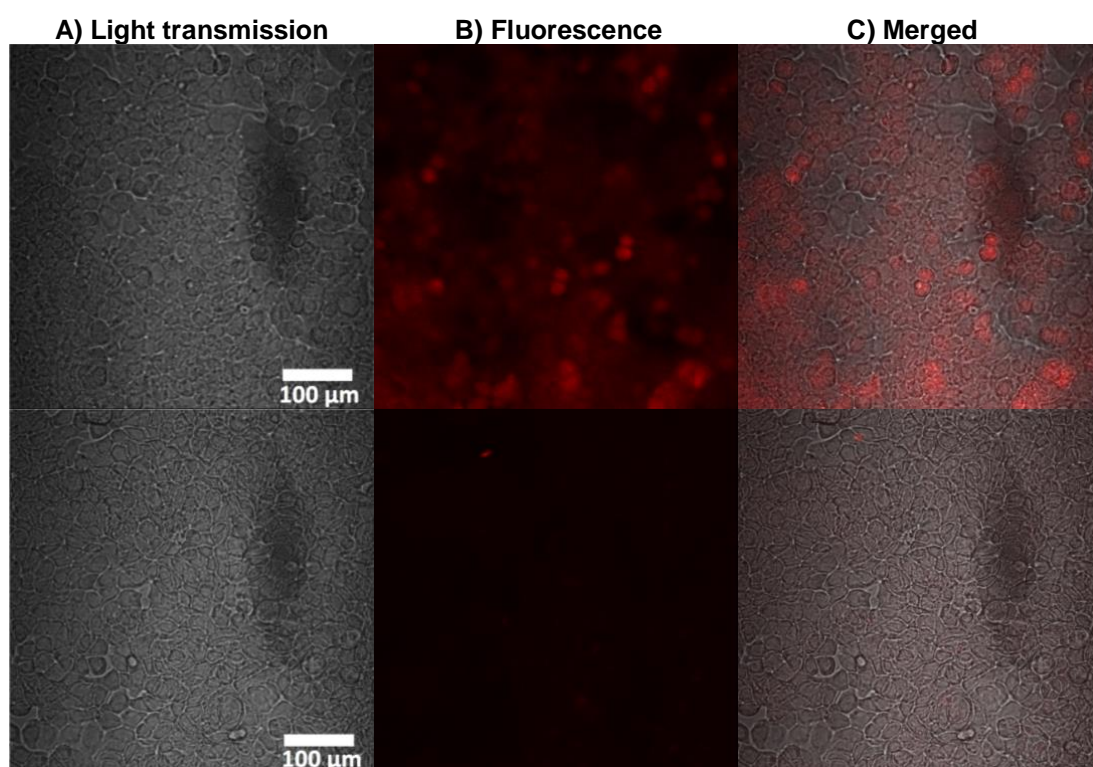
Figure 3.38: The top panel shows light transmission, fluorescence and merged images of fixed EGFR-expressing HT29 colorectal cancer cells grown in 2D, after incubation with targeted AuNCs-Anti-EGFR. For the control the bottom panel shows light transmission, fluorescence and merged of fixed EGFR expressing HT29 cells grown in 2D, after exposure to untargeted AuNCs. Both AuNCs molecules emit in the near infrared (700 nm) and therefore can be imaged at red colour by confocal microscopy.

3.14.2. Binding of AuNCs to fixed MCF7 cells in 2D.

Both AuNCs-Anti-EGFR and AuNCs were applied to fixed MCF7 breast cancer cells, which had been grown in 2D culture. Incubation lasted for one hour, cells were then washed and imaged using confocal imaging microscopy. Binding on MCF7 cells was demonstrated only for targeted AuNCs-Anti-EGFR, not for non-targeted AuNCs. A degree of binding, as shown by the NIR fluorescent (Pseudo colour) apparent mostly on the cell surface, was evident in most MCF7 cells. The results (Figure 3.39) are shown as light transmission, fluorescence and merged (respectively, A, B, C).
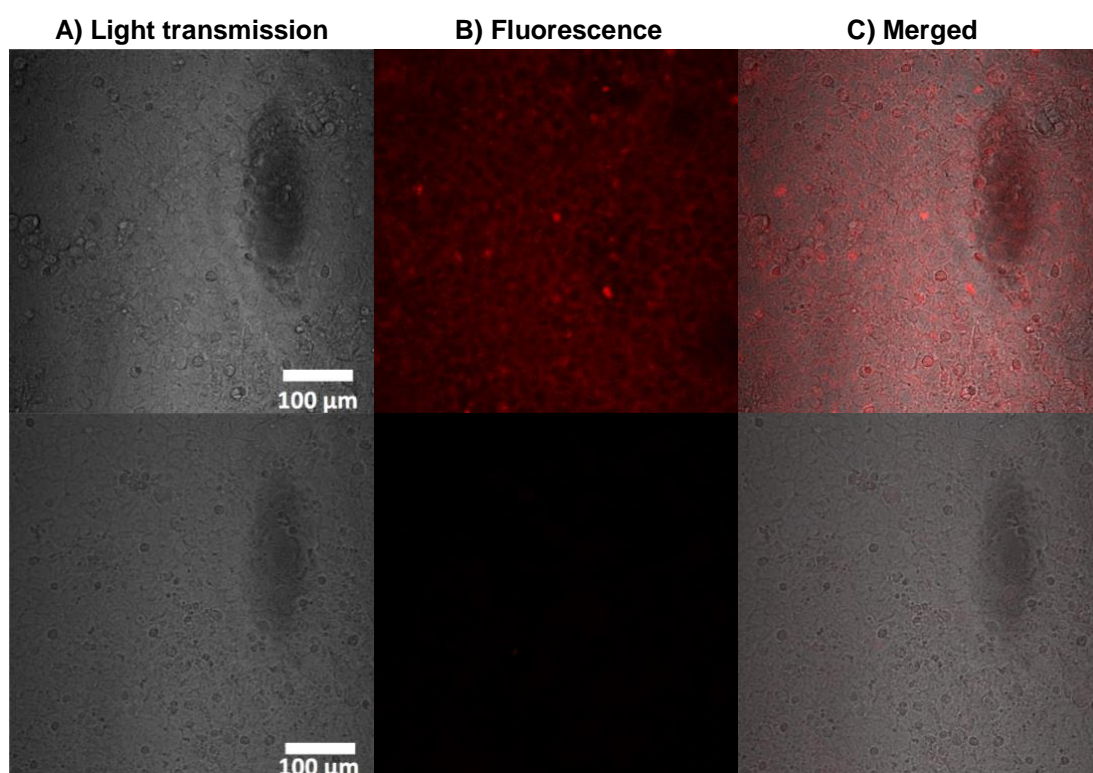
Figure 3.39: The top panel shows light transmission, fluorescence and merged images of fixed EGFR-expressing MCF7 breast cancer cells grown in 2D, after incubation with targeted AuNCs-Anti-EGFR. For the control the bottom panel shows light transmission, fluorescence and merged of fixed EGFR expressing MCF7 cells grown in 2D, after exposure to untargeted AuNCs. Both AuNCs molecules emit in the near infrared (700 nm) and therefore can be imaged at red colour by confocal microscopy.

3.15. Immuno-chemiluminescence detection of bio conjugated AuNCs

AuNCs were conjugated to Anti-Calreticulin and kindly provided by Dr. B Ramesh, UCL Division of Surgery and Interventional Science). Immuno-chemiluminescence detection was carried to further validate conjugation of the AuNCs-Anti-CRT via dot blot. There were no changes in fluorescence intensity or shift in spectra position despite modification. CRT peptides spotted onto PVDF membrane, were targeted using AuNCs-Anti-CRT. The following spots, A, B, C confirmed the conjugation of AuNCs-Anti-CRT via dot blot, although as different amounts of AuNCs-Anti-CRT were applied, hence, amounts of targeted CRT peptide changed. The (Figure 3.40) below showed decreasing amounts of targeted CRT peptide from A, B, C respectively. For the control, D showed glutathione peptide.
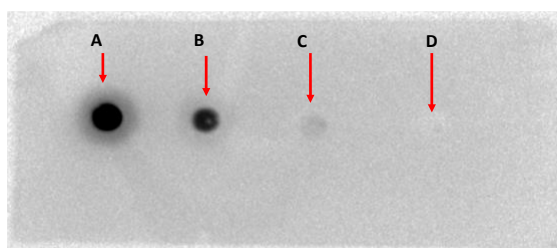
Figure 3.40: Dot blots of AuNCs-Anti-CRT (titre 1:1000) binding to CRT peptides spotted on PVDF membranes. Decreasing amounts of CRT (A-C) and control dot (D, glutathione peptide). (triplicate blots)

3.16. Targeting cells in 2D (fixed cells), using AuNCs-Anti-CRT

For primary targeting studies, 2D culture systems are optimal, as the flat morphology allows for clarity of imaging. The cancer cells HT29, MCF7 and endothelial cells HUVECs were fixed and then targeted using AuNCs-Anti-CRT and AuNCs as a negative control.

3.16.1. Colorectal cancer cells targeted using AuNCs-Anti-CRT (2D fixed cells)

The (Figure 3.37) below showed the application of AuNCs-Anti-CRT and AuNCs on fixed (2D) HT29 cancer cells. 100 µl of AuNCs-Anti-CRT and AuNCs applied to HT29 cells in 2D format. 1-hour after applying, HT29 cells were washed x3 with PBS and imaged using confocal imaging microscopy.

Both AuNCs-Anti-CRT and AuNCs were applied to fixed HT29 colorectal cancer cells, which had been grown in 2D culture. Incubation lasted for one hour, HT29 cells were then washed and imaged using confocal imaging microscopy. Binding on HT29 cells was demonstrated only for targeted AuNCs-Anti-CRT, not for non-targeted AuNCs. A degree of binding, as shown by the NIR fluorescent (Pseudo colour) apparent mostly on the cell surface, was evident in most HT29 cells. The results (Figure 3.41) are shown as light transmission, fluorescence and merged (respectively, A, B, C).
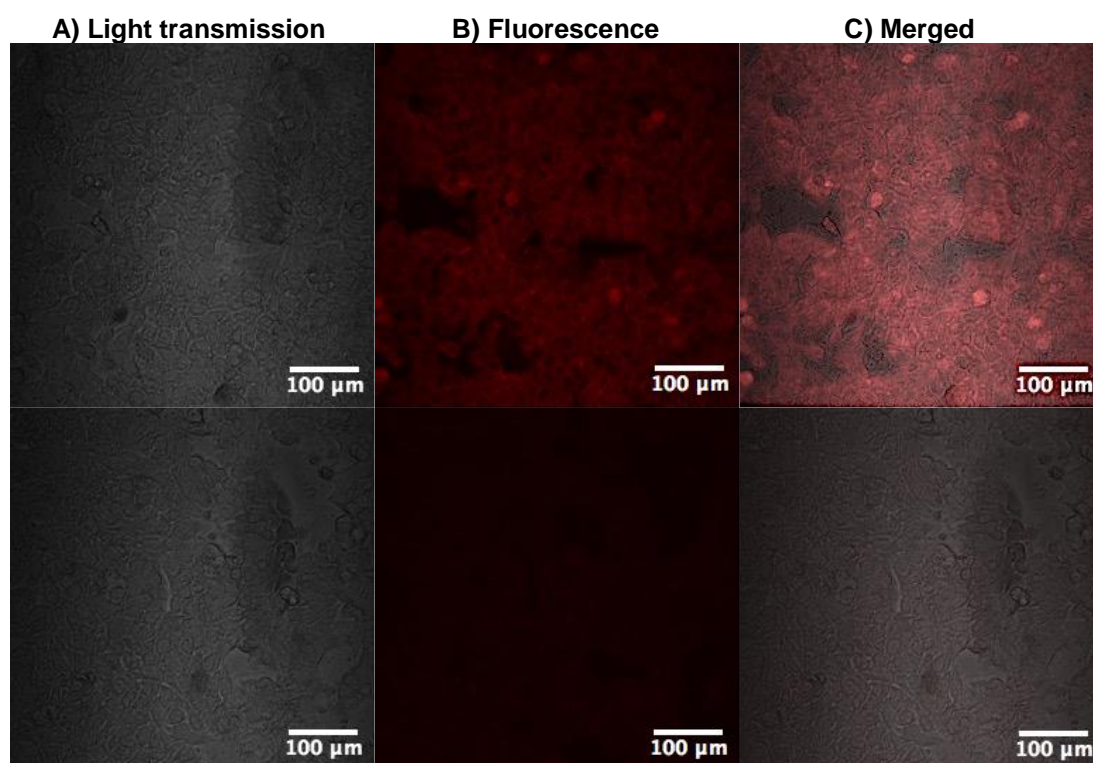
Figure 3.41: The top panel shows light transmission, fluorescence and merged images of fixed CRT-expressing HT29 colorectal cancer cells grown in 2D, after incubation with targeted AuNCs-Anti-CRT. For the control the bottom panel shows light transmission, fluorescence and merged of fixed CRT expressing HT29 cells grown in 2D, after exposure to untargeted AuNCs. Both AuNCs molecules emit in the near infrared (700 nm) and therefore can be imaged at red colour by confocal microscopy.

3.16.2. Breast cancer cells targeted using AuNCs-Anti-CRT (2D fixed cells)

Both AuNCs-Anti-CRT and AuNCs were applied to fixed MCF7 breast cancer cells, which had been grown in 2D culture. Incubation lasted for one hour, cells were then washed and imaged using confocal imaging microscopy. Binding on MCF7 cells was demonstrated only for targeted AuNCs-Anti-CRT, not for non-targeted AuNCs. A degree of binding, as shown by the NIR fluorescent (Pseudo colour) apparent mostly on the cell surface, was evident in most MCF7 cells. The results (Figure 3.42) are shown as light transmission, fluorescence and merged (respectively, A, B, C).
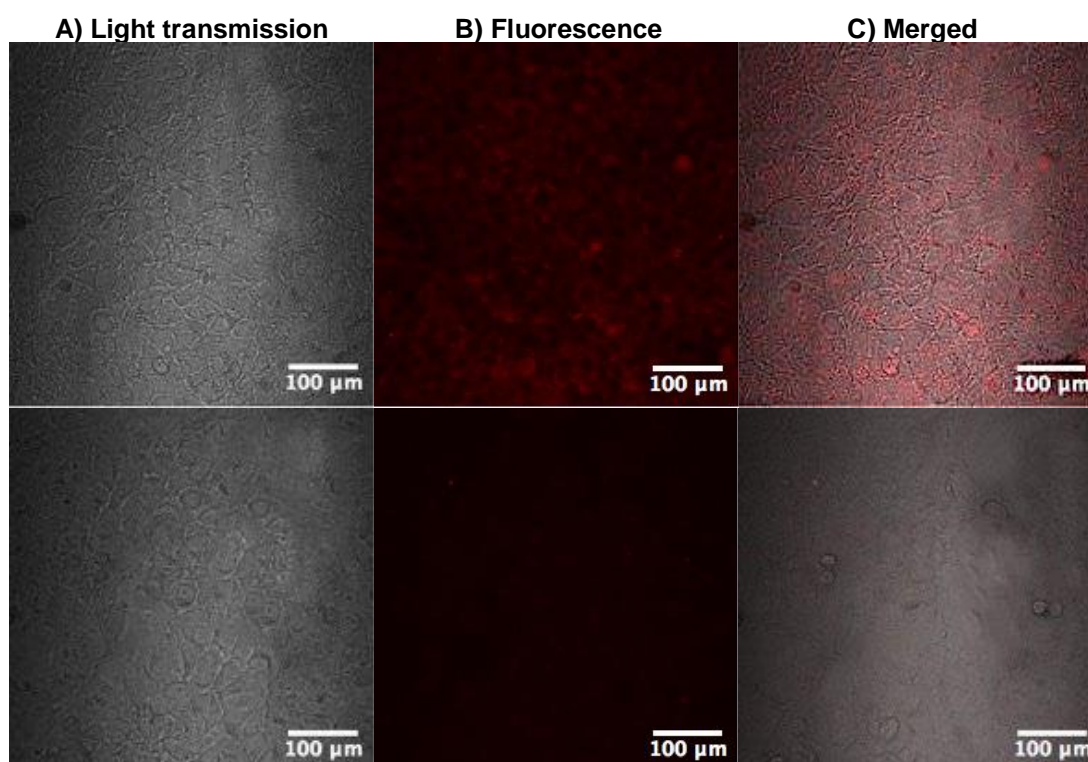
Figure 3.42: The top panel shows light transmission, fluorescence and merged images of fixed CRT-expressing MCF7 breast cancer cells grown in 2D, after incubation with targeted AuNCs-Anti-CRT. For the control the bottom panel shows light transmission, fluorescence and merged of fixed CRT expressing MCF7 cells grown in 2D, after exposure to untargeted AuNCs. Both AuNCs molecules emit in the near infrared (700 nm) and therefore can be imaged at red colour by confocal microscopy.

3.16.3 HUVECs targeted using AuNCs-Anti-CRT (2D fixed cells)

Both AuNCs-Anti-CRT and AuNCs were applied to fixed HUVECs endothelial cells, which had been grown in 2D culture. Incubation lasted for one hour; endothelial cells were then washed and imaged using confocal imaging microscopy. Binding on endothelial cells was not revealed for either of targeted AuNCs-Anti-CRT and non-targeted AuNCs. The results (Figure 3.43) are shown as light transmission, fluorescence and merged (respectively, A, B, C).

A) Light transmission   **B) Fluorescence**   **C) Merged**
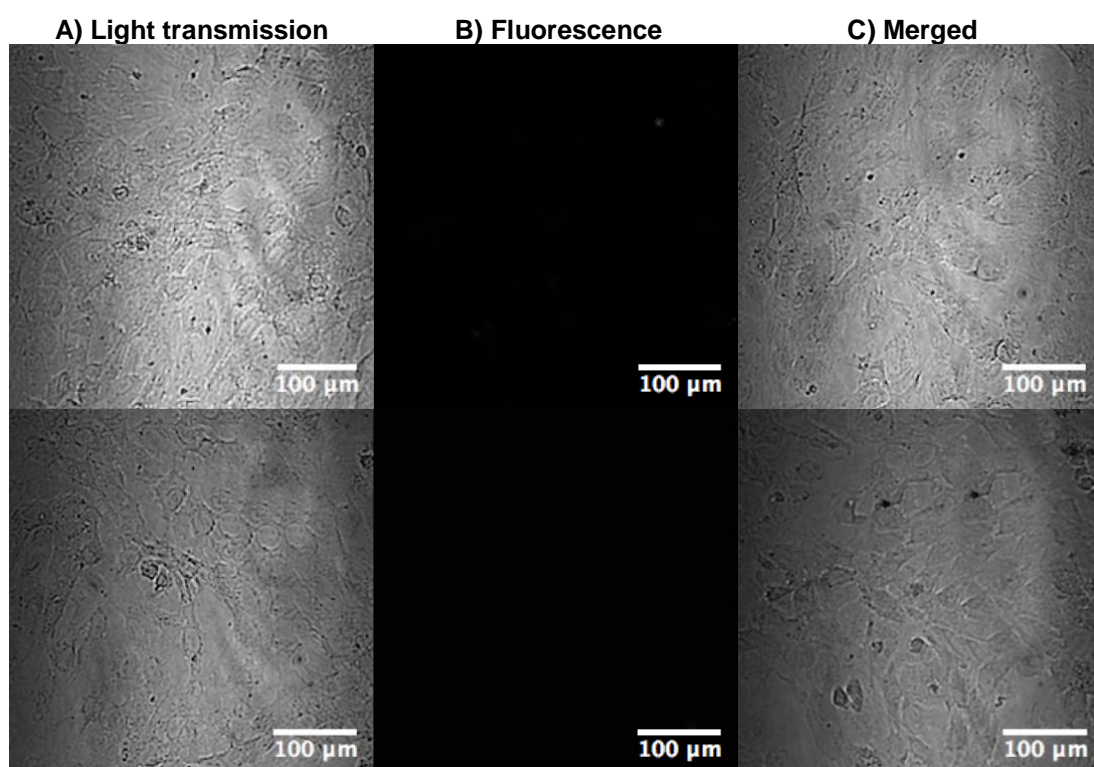
Figure 3.43: The top panel shows light transmission, fluorescence and merged images of fixed CRT-expressing HUVECs endothelial cells grown in 2D, after incubation with targeted AuNCs-Anti-CRT. For the control the bottom panel shows light transmission, fluorescence and merged of fixed CRT expressing HUVECs cells grown in 2D, after exposure to untargeted AuNCs. Both AuNCs molecules emit in the near infrared (700 nm) and therefore can be imaged at red colour by confocal microscopy.

3.17. Targeting cells in 2D (live), using AuNCs-Anti-CRT and AuNCs

### 3.17.1 Colorectal cancer cells targeted using AuNCs-Anti-CRT and AuNCs (2D live)

Both AuNCs-Anti-CRT and AuNCs were applied to live HT29 colorectal cancer cells, which had been grown in 2D culture. Incubation lasted for one hour; cells were then washed and imaged using fluorescence imaging microscopy. Binding on HT29 cells was determined only for targeted AuNCs-Anti-CRT, not for non-targeted AuNCs. A degree of binding, as shown by the NIR fluorescent (Pseudo colour) apparent mostly on the cell surface, was evident in most HT29 cells. The results (Figure 3.44) are shown as light transmission, fluorescence and merged (respectively, A, B, C).

A) Light transmission   **B) Fluorescence**   **C) Merged**
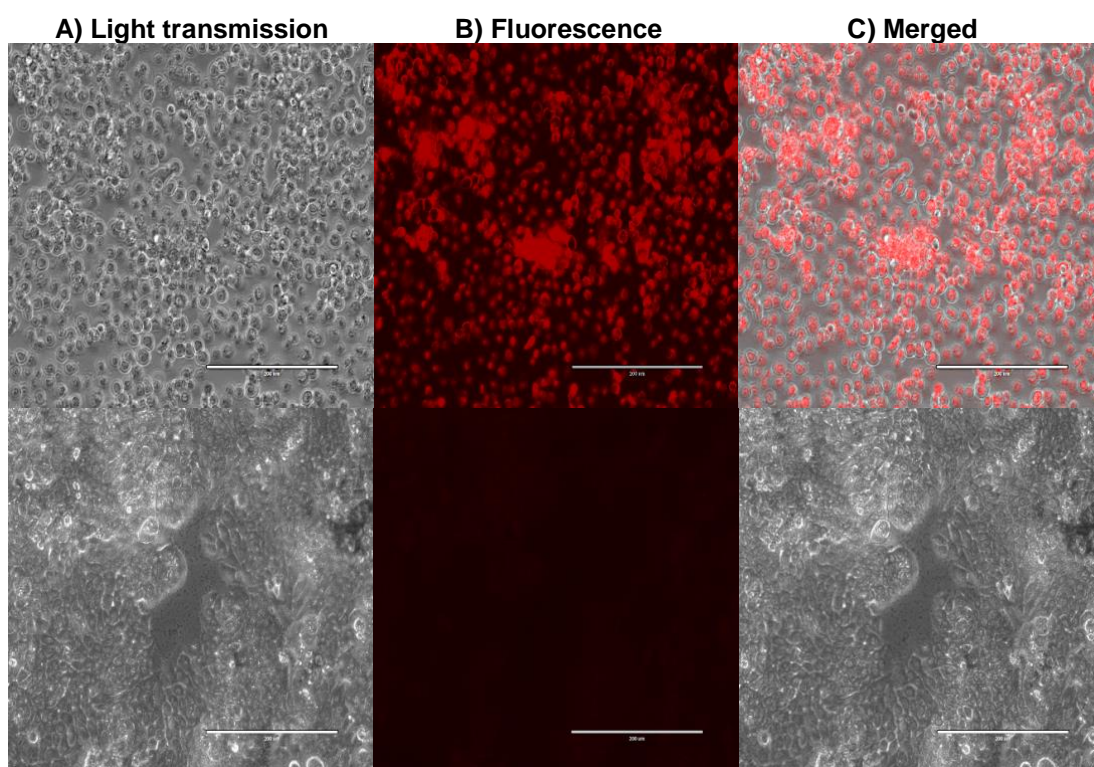
Figure 3.44: The top panel shows light transmission, fluorescence and merged images of live HT29 cells grown in 2D, after incubation with targeted AuNCs-Anti-CRT. For the control the bottom panel shows light transmission, fluorescence and merged of live HT29 cells grown in 2D, after exposure to untargeted AuNCs, (Images taken using fluorescence microscopy.)

## 3.17.2 Breast cancer cells targeted using AuNCs-Anti-CRT and AuNCs (2D live)

Both AuNCs-Anti-CRT and AuNCs were applied to live MCF7 breast cancer cells, which had been grown in 2D culture. Incubation lasted for one hour; cells were then washed and imaged using fluorescence imaging microscopy. Binding on MCF7 cells was demonstrated only for targeted AuNCs-Anti-CRT, not for non-targeted AuNCs. A degree of binding, as shown by the NIR fluorescent (Pseudo colour) apparent mostly on the cell surface, was evident in most MCF7 cells. The results (Figure 3.45) are shown as light transmission, fluorescence and merged (respectively, A, B, C).
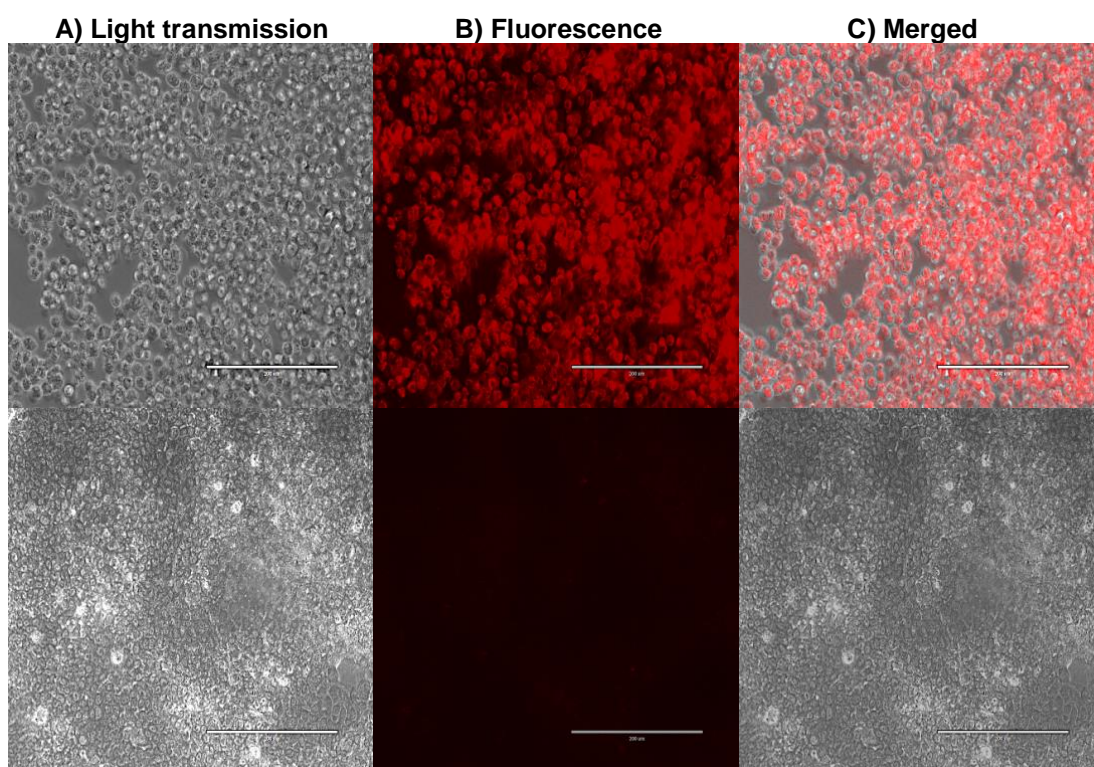
Figure 3.45: The top panel shows light transmission, fluorescence and merged images of live MCF7 cells grown in 2D, after incubation with targeted AuNCs-Anti-CRT. For the control the bottom panel shows light transmission, fluorescence and merged of live MCF7 cells grown in 2D, after exposure to untargeted AuNCs, (Images taken using fluorescence microscopy.)

3.18. Targeting 3D fixed spheroids using AuNCs-Anti-CRT and AuNCs

The spheroids harvested by centrifugation, after 10 days' growth in CMC+gelatine 3D matrix was fixed and incubated with AuNCs, either

conjugated AuNCs-Anti-CRT or untargeted AuNCs, for control studies. After incubation, spheroids were gently centrifuged rinsed to remove excess and imaged using fluorescence microscopy.

3.18.1. Colorectal cancer cells targeted using AuNCs-Anti-CRT (3D fixed)

Fixed HT29 spheroids which were incubated with AuNCs-Anti-CRT showed uptake of the targeted AuNCs-Anti-CRT, as demonstrated by the red fluorescent images (Figure 3.46). Uptake appears more intense on the periphery/outer boundary of the spheroids. Counterstaining using DAPI (which binds to the A-T rich regions in the DNA and emits blue fluorescence) enabled the identification of cell nuclei and showed that spheroids are well populated, with probably more cells towards the periphery of the spheroid, and fewer cells at the core of the spheroid. (Figure 3.46) demonstrates targeting, showed by red fluorescence.

A) DAPI Stain   **B) AuNCs-Anti-CRT**
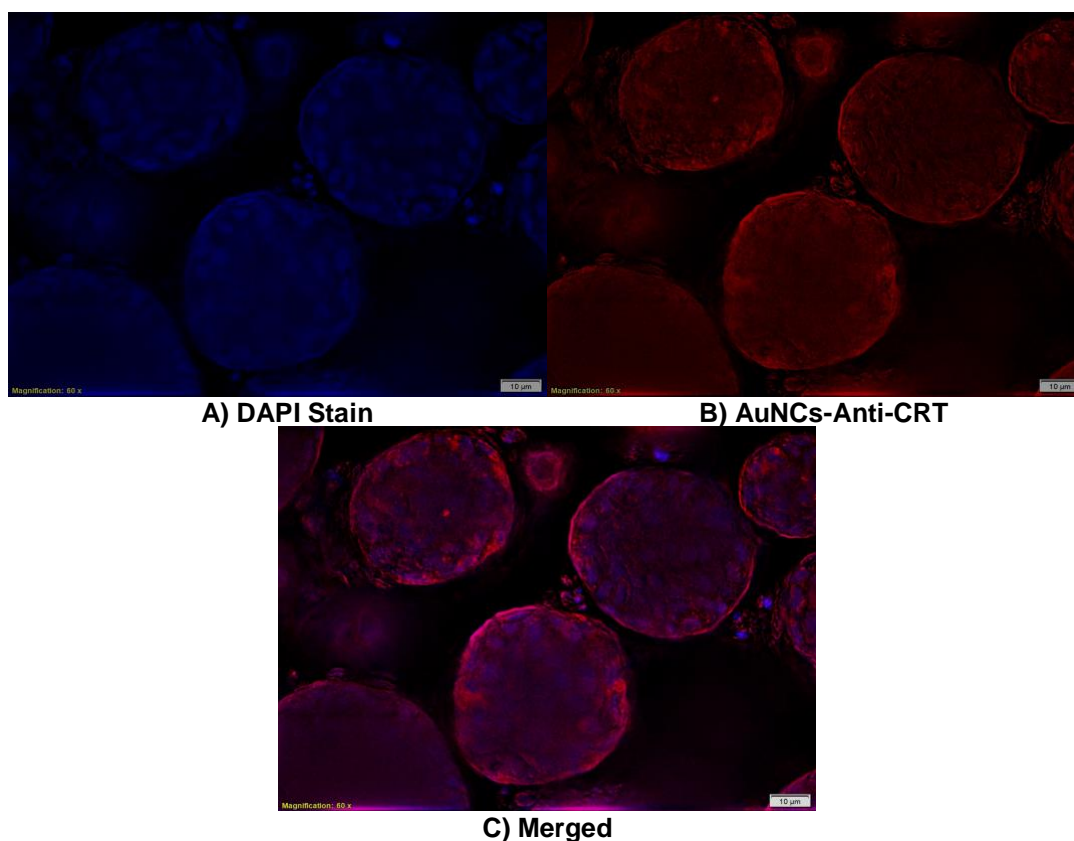
C) Merged

Figure 3.46 A) shows staining HT29 spheroids with DAPI that releases blue fluorescence by bind to the A-T rich regions in DNA. B) shows targeted HT29 spheroids using conjugated AuNCs-Anti-CRT. C) shows merged images of A and B.

3.18.2. Colorectal cancer cells targeted using AuNCs (3D fixed)

For the control, fixed HT29 spheroids which were incubated with AuNCs showed uptake of the targeted AuNCs, as demonstrated by the red fluorescent images (Figure 3.47). Uptake appears in lower levels of fluorescence compared to spheroids in section (1.14.1) on the periphery/outer boundary of the spheroids. Counterstaining using DAPI (which binds to the A-T rich regions in the DNA and emits blue fluorescence) enabled the identification of cell nuclei and showed that spheroids are well populated, with probably more cells towards the periphery of the spheroid, and less cells at the core of the spheroid. (Figure 3.47) demonstrates targeting, demonstrated by red fluorescence.

A) DAPI Stain

B) AuNCs-Anti-CRT
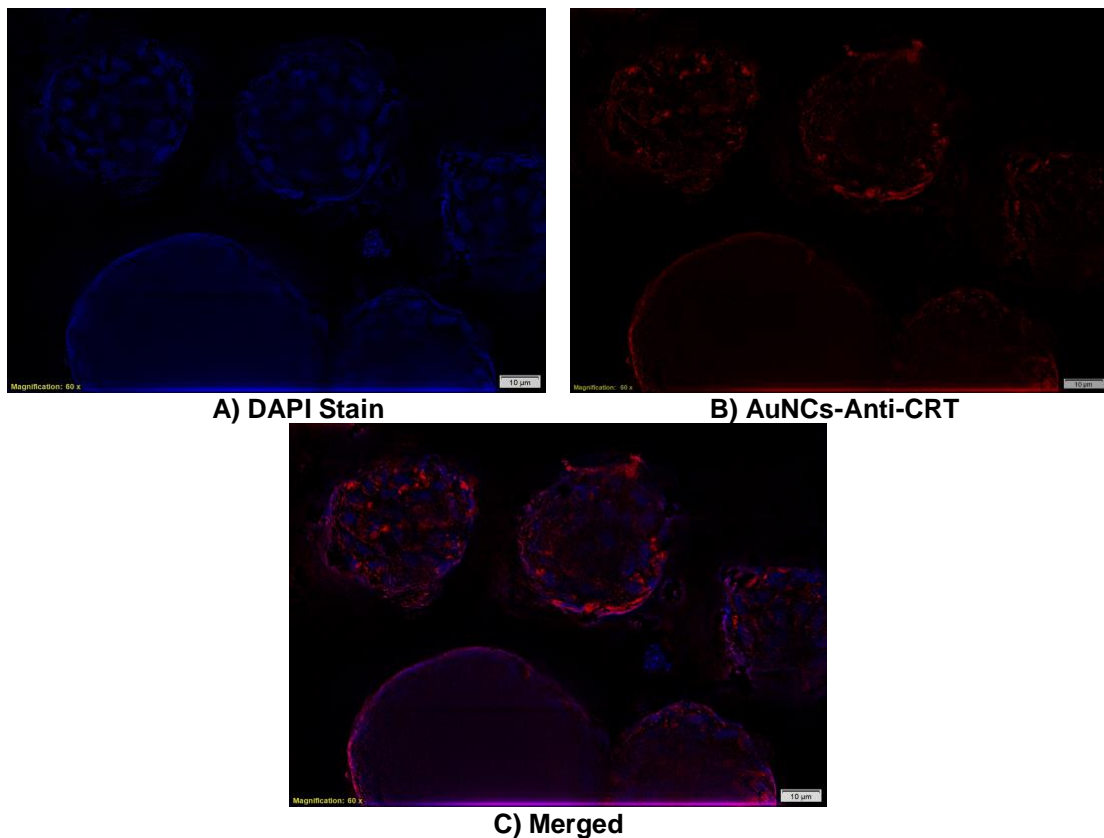
C) Merged

Figure 3.47: A) shows staining HT29 spheroids with DAPI that releases blue fluorescence by bind to the A-T rich regions in DNA. B) shows targeted HT29 spheroids using conjugated AuNCs. C) shows merged images of A and B.

3.18.3. Breast cancer cells targeted using AuNCs-Anti-CRT (3D fixed)

Fixed MCF7 spheroids which were incubated with AuNCs-Anti-CRT showed uptake of the targeted AuNCs-Anti-CRT, as demonstrated by the red fluorescent images (Figure 3.48). Uptake appears more intense on the periphery/outer boundary of the spheroids. Counterstaining using DAPI (which binds to the A-T rich regions in the DNA and emits blue fluorescence) enabled the identification of cell nuclei and showed that spheroids are well populated, with probably more cells towards the periphery of the spheroid, and fewer cells at the core of the spheroid. (Figure 3.48) demonstrates targeting, showed by red fluorescence.

A) DAPI Stain   **B) AuNCs-Anti-CRT**
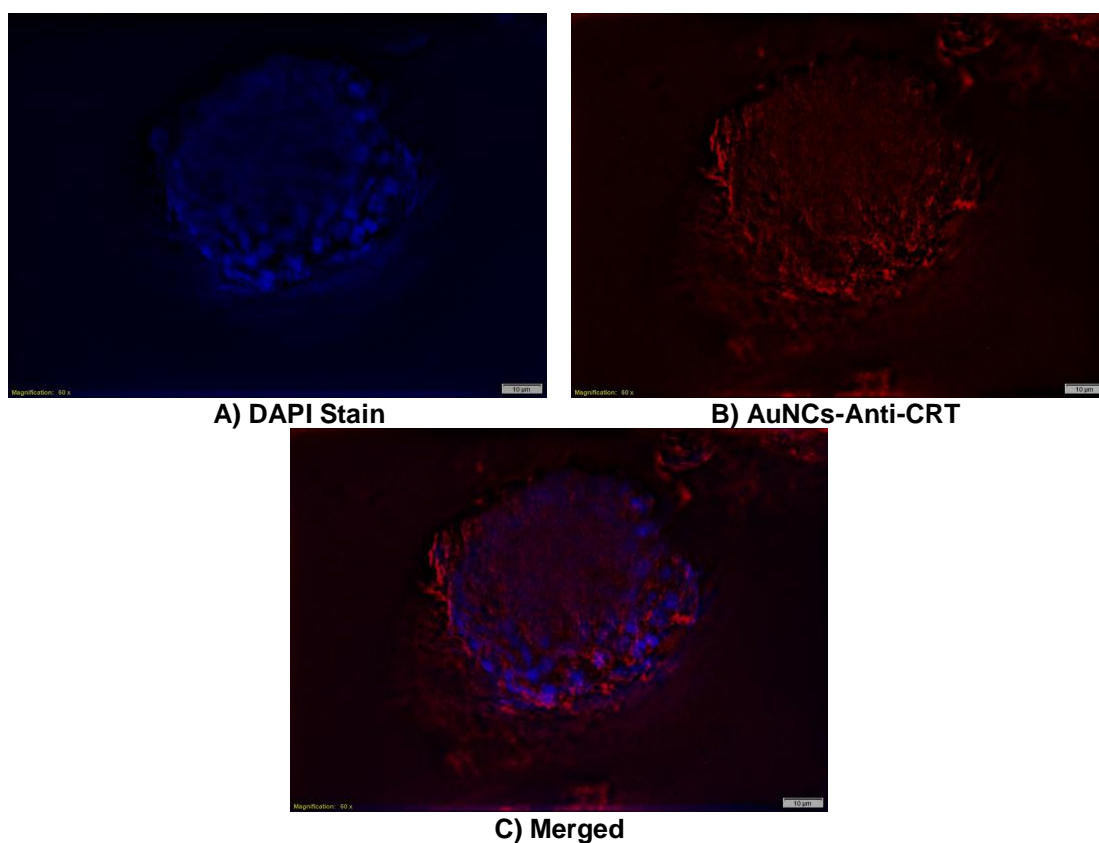
C) Merged

Figure 3.48: A) shows staining MCF7 spheroids with DAPI that releases blue fluorescence by bind to the A-T rich regions in DNA. B) shows targeted MCF7 spheroids using conjugated AuNCs-Anti-CRT. C) shows merged images of A and B.

3.18.4. Breast cancer cells targeted using AuNCs (3D fixed)

For the control, fixed MCF7 spheroids which were incubated with AuNCs showed uptake of the targeted AuNCs, as demonstrated by the red fluorescent images (Figure 3.49). Uptake appears in lower levels of fluorescence compared to spheroids in section (1.14.3) on the periphery/outer boundary of the spheroids. Counterstaining using DAPI (which binds to the A-T rich regions in the DNA and emits blue fluorescence) enabled the identification of cell nuclei and showed that spheroids are well populated, with probably more cells towards the periphery of the spheroid, and less cells at the core of the spheroid. (Figure 3.49) demonstrates targeting, demonstrated by red fluorescence.

A) DAPI Stain   **B) AuNCs-Anti-CRT**
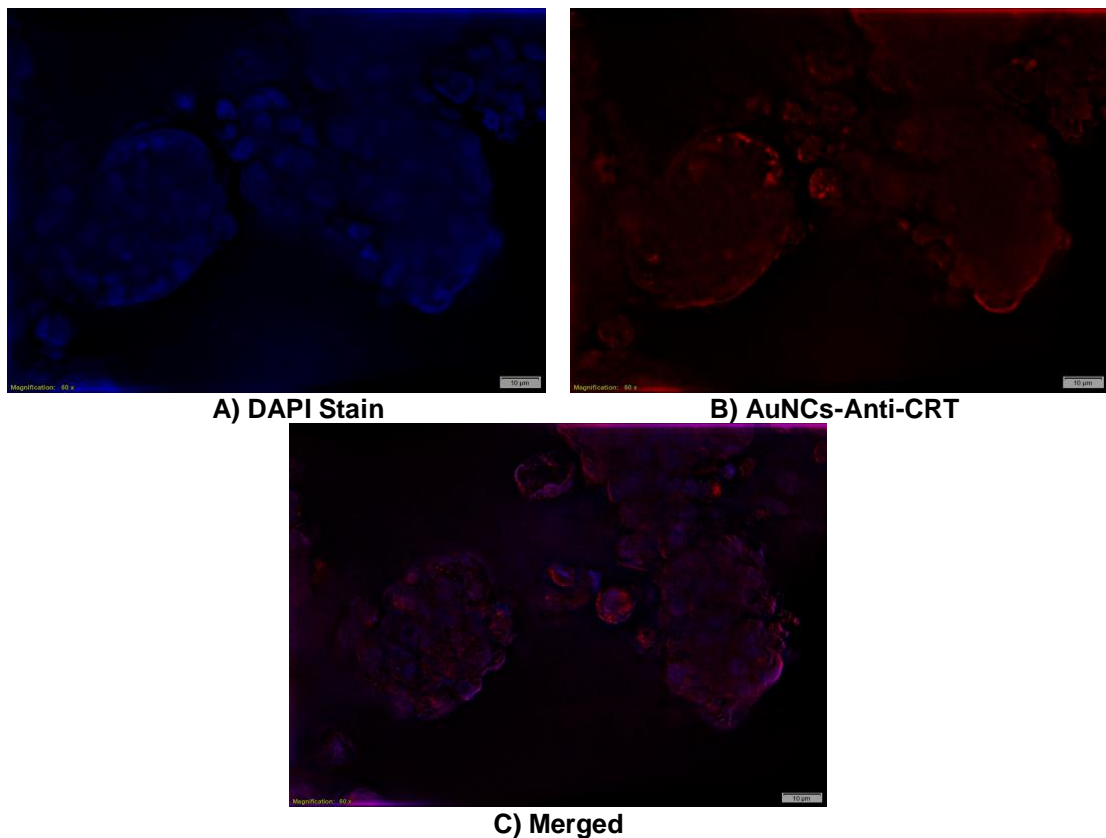
C) Merged

Figure 3.49: A) shows staining MCF7 spheroids with DAPI that releases blue fluorescence by bind to the A-T rich regions in DNA. B) shows targeted MCF7 spheroids using conjugated AuNCs. C) shows merged images of A and B using fluorescence microscopy.

3.19. Targeting live cancer spheroids through an endothelial cell barrier in a complex tumouroid construct, using AUNCs-anti-CRT

Having shown appropriate targeting capabilities of the AUNCs-Anti-CRT molecules, using variously fixed and live cell cultures, the purpose of this section was to investigate whether targeted AuNCs would differentiate their targets (CRT-expressing cancer cells) within a more complex 3D construct, which incorporates an endothelial barrier.

To achieve this, HUVECs were seeded on a filter insert for 48 h. Now spheroids grown for 10 days were harvested and transferred into new CMC+gelatine 3D matrix at 6 well ultra-low binding plates, and the HUVEC-populated filters were placed on top. Shortly after this, conjugated AuNCs-Anti-CRT were applied onto the HUVEC-populated membrane and investigations of the fate of AuNCs took place 2 h later, using confocal microscopy.

Control groups included constructs where "empty" (no HUVEC cells) filter inserts were placed on top of the 3D matrix containing grown spheroids. This helped to determine the barrier function of HUVECs. Further control groups consisted of constructs with HUVEC populated filters but no cancer spheroids in the CMC+gelatine 3D matrix. And a group where empty filter inserts were placed on top of CMC+gelatine 3D matrix with no spheroids. The procedure is schematically presented in (Figure 3.50).
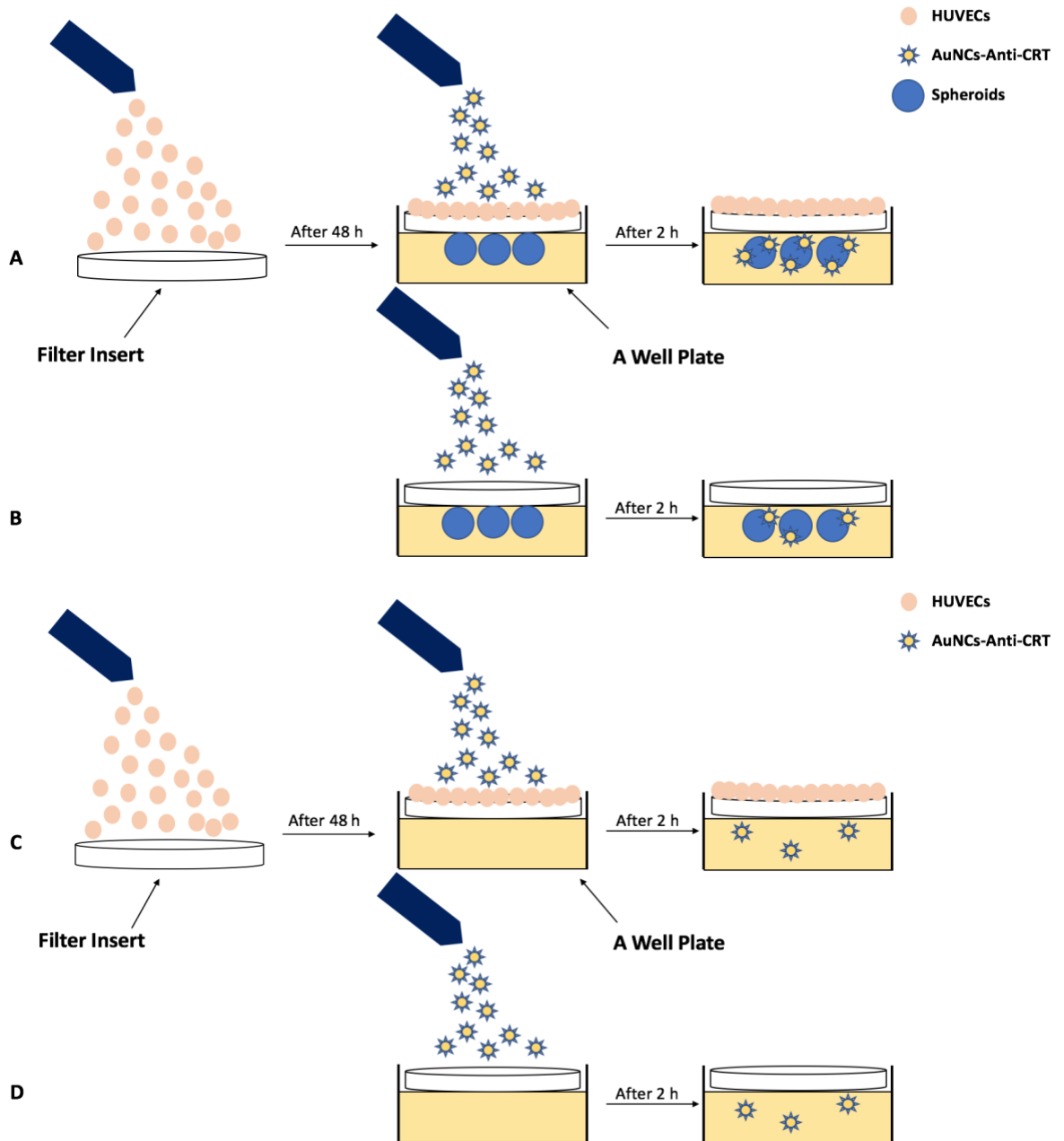
Figure 3.50: The process of manufacturing complex 3D constructs, which contain both cancer spheroids in CMC+gelatine matrix and an endothelial cells barrier. A) shows the HUVECs seeded on filter insert, after 48 h, the grown spheroids harvested and transferred into new CMC+gelatine 3D matrix and then conjugated AuNCs-Anti-CRT applied onto the HUVECs membrane. B) shows the empty filter insert placed on top of the grown spheroids harvested and then conjugated AuNCs-Anti-CRT applied. C) HUVECs were seeded on filter insert, after 48 the filter inserts placed on top of the 3D model and then AuNCs-Anti-CRT applies onto empty CMC+gelatine 3D matrix. D) shows the empty filter insert placed on top of the 3D model and then AuNCs-Anti-CRT applied onto empty CMC+gelatine 3D matrix.

3.19.1. HUVECs growth on filter insert

HUVECs were grown on filter inserts for 48 h to attempt to grow a layer of cells as confluent as possible. To demonstrate this, cells were stained with crystal violet and imaged by florescence microscopy. Figure 3.51 shows that cell nuclei took up crystal violet (green fluorescence).
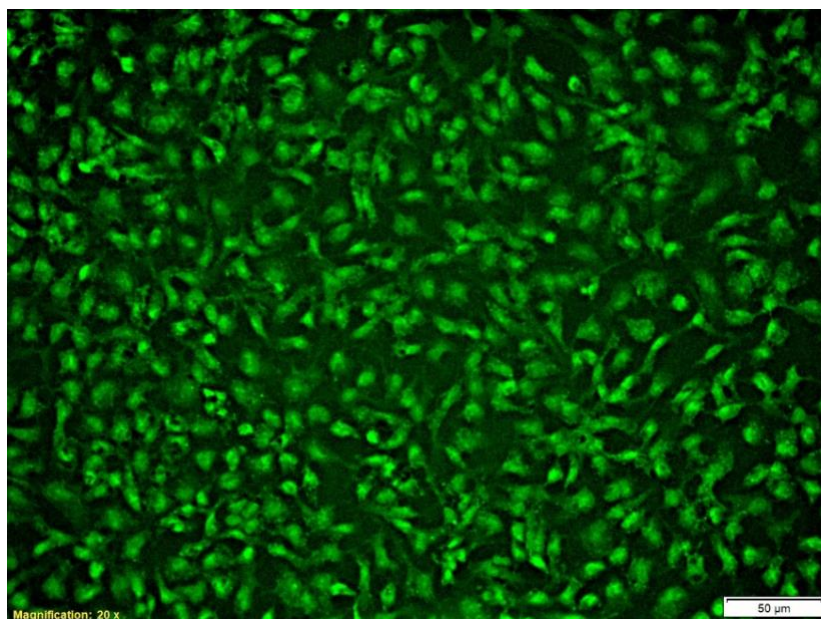
Figure 3.51: HUVECs were seeded on filter insert and 48 h later stained with crystal violet and imaged by fluorescence microscopy. The stain (green fluorescence) shows nuclear uptake.

3.19.2. HT29 grown spheroids targeted using AuNCs-Anti-CRT

The (Figure 3.52) below showed HT29 grown spheroids targeted using 100 µl of AuNCs-Anti-CRT by passing through HUVECs seeded on filter insert. The (Figure 3.52) also showed HT29 grown spheroids targeted using 100 µl of AuNCs-Anti-CRT by passing through empty filter insert. Both conditions were imaged using new imaging system 2 h after applying AuNCs-Anti-CRT and indicated HT29 grown spheroids targeted by passing through HUVECs seeded filter inserts, higher fluorescence intensity compared to the empty filter insert condition.

The (Figure 3.52) also showed specificity of targeting in grown spheroids by indicating low fluorescence intensity at these conditions. At this stage grown HT29 targeted spheroids harvested again for further studies.
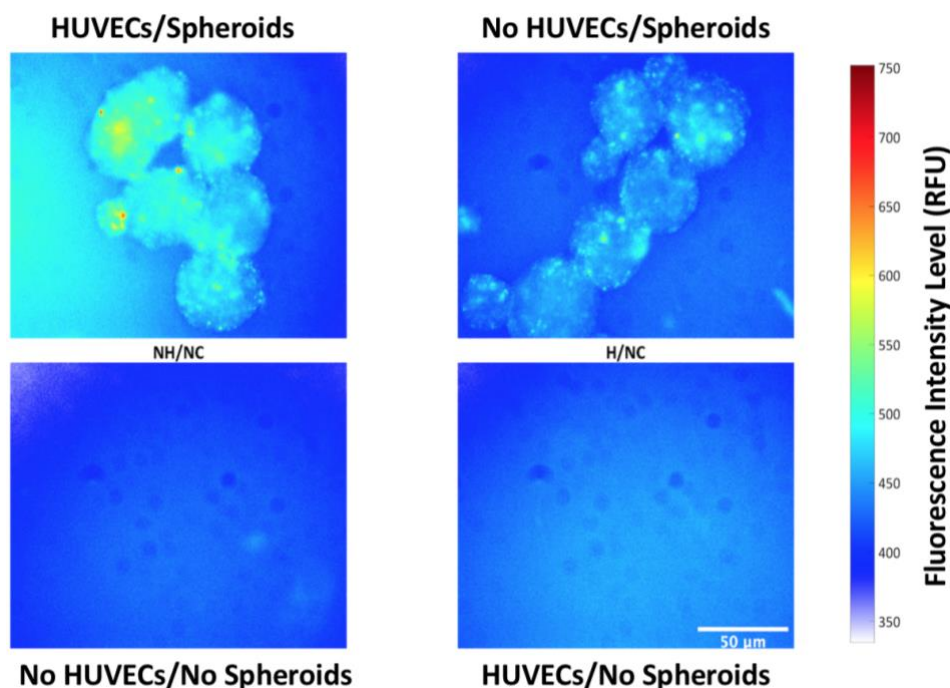
Figure 3.52: H/C shows HT29 grown spheroids targeted using AuNCs-Anti-CRT by passing through HUVECs seeded on filter insert. NH/C shows HT29 grown spheroids targeted using AuNCs-Anti-CRT by passing through empty filter insert. H/NC shows a condition when HUVECs seeded on filter insert and placed on top of the 3D model and then AuNCs-Anti-CRT applies onto empty CMC+gelatine 3D matrix. NH/NC shows the empty filter insert placed on top of the 3D model and then AuNCs-Anti-CRT applies onto empty CMC+gelatine 3D matrix. These images taken use new optimised confocal microscopy.

3.19.3. MCF7 grown spheroids targeted using AuNCs-Anti-CRT

The (Figure 3.53) below showed MCF7 grown spheroids targeted using 100 µl of AuNCs-Anti-CRT by passing through HUVECs seeded filter insert. The (Figure 3.53) showed MCF7 grown spheroids targeted using 100 µl of AuNCs-Anti-CRT by passing through empty filter insert. Both conditions imaged, 2 h after applying AuNCs-Anti-CRT using new imaging system and indicated MCF7 grown spheroids targeted by passing through HUVECs seeded filter insert higher fluorescence intensity compared to the empty filter insert condition.

The (Figure 3.53) showed specificity of targeting in grown spheroids by indicating low fluorescence intensity at these conditions. At this stage grown MCF7 targeted spheroids harvested again for further studies.
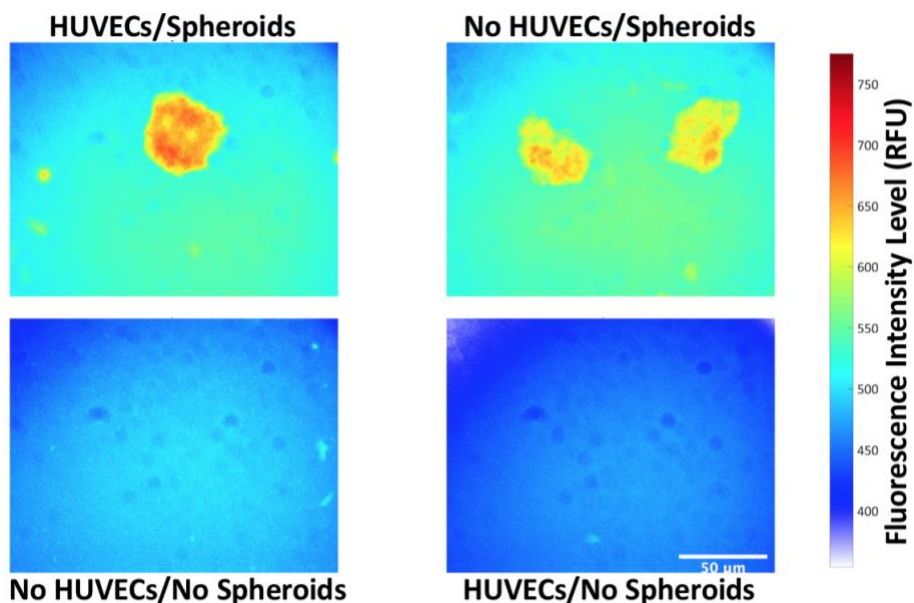
Figure 3.53: H/C shows MCF7 grown spheroids targeted using AuNCs-Anti-CRT by passing through HUVECs seeded on filter insert. NH/C shows MCF7 grown spheroids targeted using AuNCs-Anti-CRT by passing through empty filter insert. H/NC shows a condition when HUVECs seeded on filter insert and placed on top of the 3D model and then AuNCs-Anti-CRT applies onto empty CMC+gelatine 3D matrix. NH/NC shows the empty filter insert placed on top of the 3D model and then AuNCs-Anti-CRT applies onto empty CMC+gelatine 3D matrix. These images taken use new optimised confocal microscopy.

3.20. Monitoring and localizing of AuNCs-Anti-CRT within spheroids

Following the above experiments, HT29 and MCF7 grown spheroids were targeted using AuNCs-Anti-CR and then fixed to allow for further investigations of how the AuNCs-Anti-CRT interacted within the spheroids.

3.20.1. AuNCs-Anti-CRT within HT29 spheroids

The (Figure 3.54) below showed grown HT29 targeted spheroids after fixing process. AuNCs-Anti-CRT mostly is on edges, to the better understanding of this targeting (Figure 3.55) showed 3D view of this spheroid (from top to bottom). And (Figure 3.56) showed stacking view of this spheroid. AuNCs-Anti-CRT is mostly on edges and bottom of the spheroid.
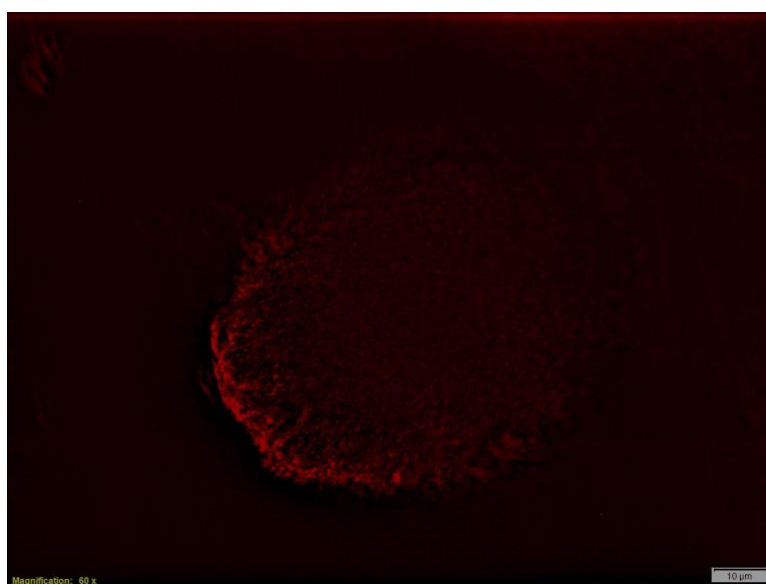
Figure 3.54: shows the single view of HT29 spheroid targeted using conjugated AuNCs. Uptake appears more intense on the periphery/outer boundary of the HT29 spheroid. Using fluorescence microscopy.
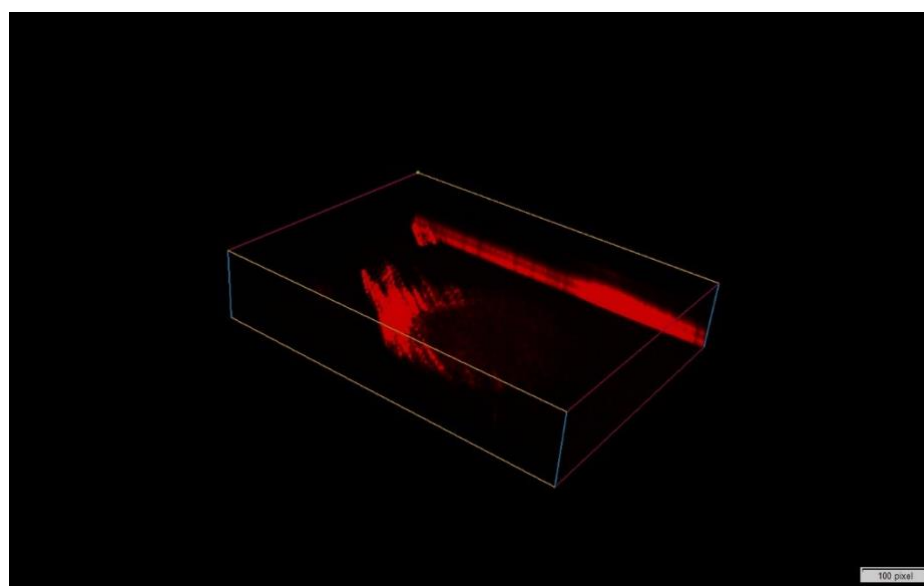
Figure 3.55: shows 3D view of the HT29 spheroid, targeted using conjugated AuNCs. Uptake appears more intense on the periphery/outer boundary and bottom layer of the HT29 spheroid. Using fluorescence microscopy.
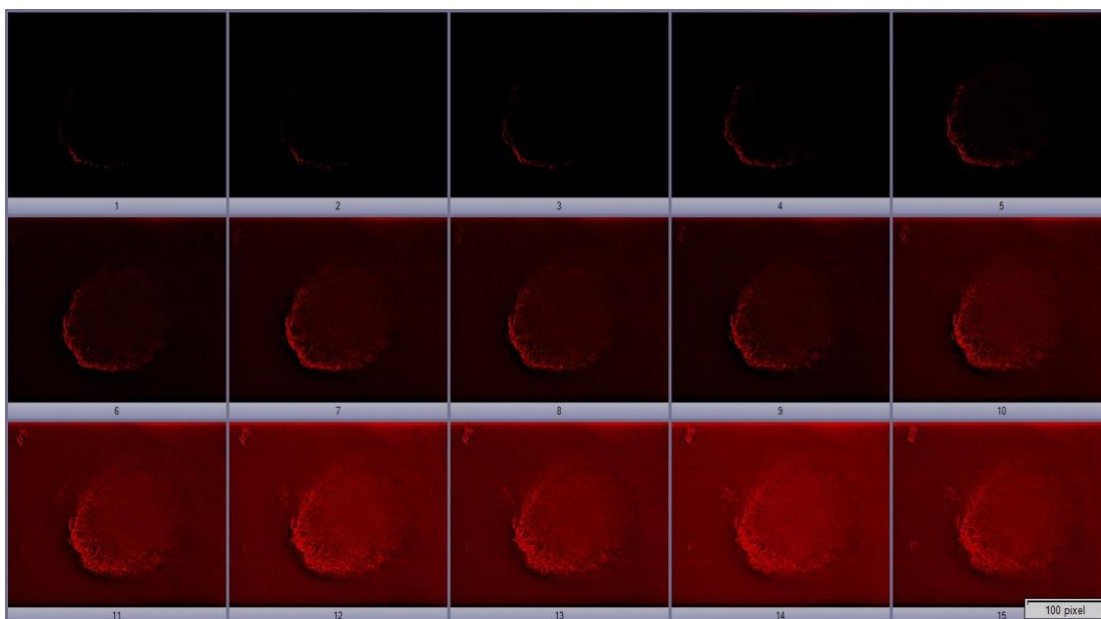
Figure 3.56: shows stacking view of the HT29 spheroid, targeted using conjugated AuNCs. it shows uptake appears more intense on the periphery/outer boundary and bottom layer of the HT29 spheroid. Higher level of fluorescence (from top to bottom). Using fluorescence microscopy.

3.20.2. AuNCs-Anti-CRT within MCF7 spheroids

The (Figure 3.57) below showed grown MCF7 targeted spheroids after fixing process. AuNCs-Anti-CRT was seen mostly around the periphery/edges, to the better understanding of this targeting (Figure 3.58) showed 3D view of this spheroid (from top to bottom). And (Figure 3.59) showed stacking view of this spheroid. AuNCs-Anti-CRT is mostly on edges and bottom of the spheroid.
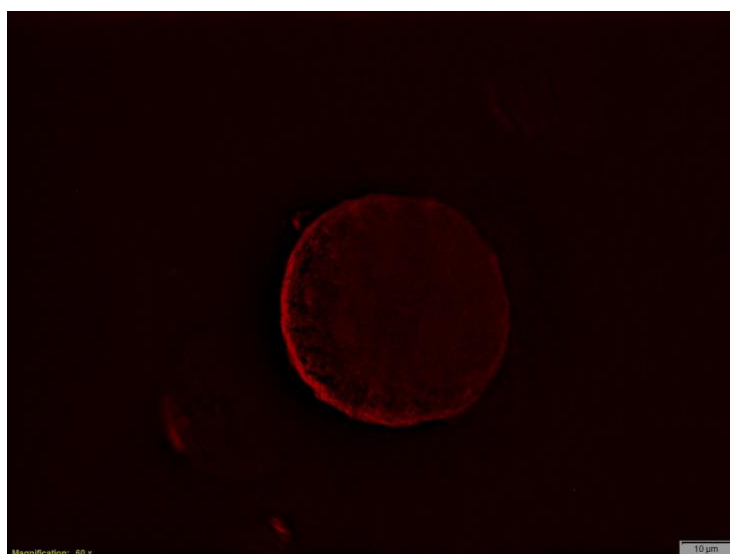
Figure 3.57: shows the single view of the MCF7 spheroid targeted using conjugated AuNCs. uptake appears more intense on the periphery/outer boundary of the HT29 spheroid. Using fluorescence microscopy.
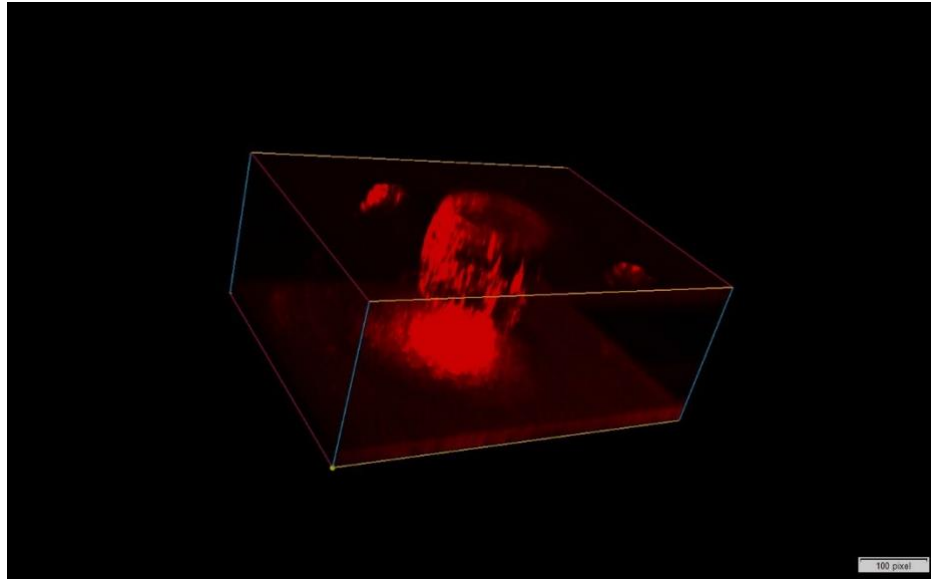
Figure 3.58: shows 3D view of the MCF7 spheroid, targeted using conjugated AuNCs. Uptake appears more intense on the periphery/outer boundary and bottom layer of the MCF7 spheroid. Using fluorescence microscopy.
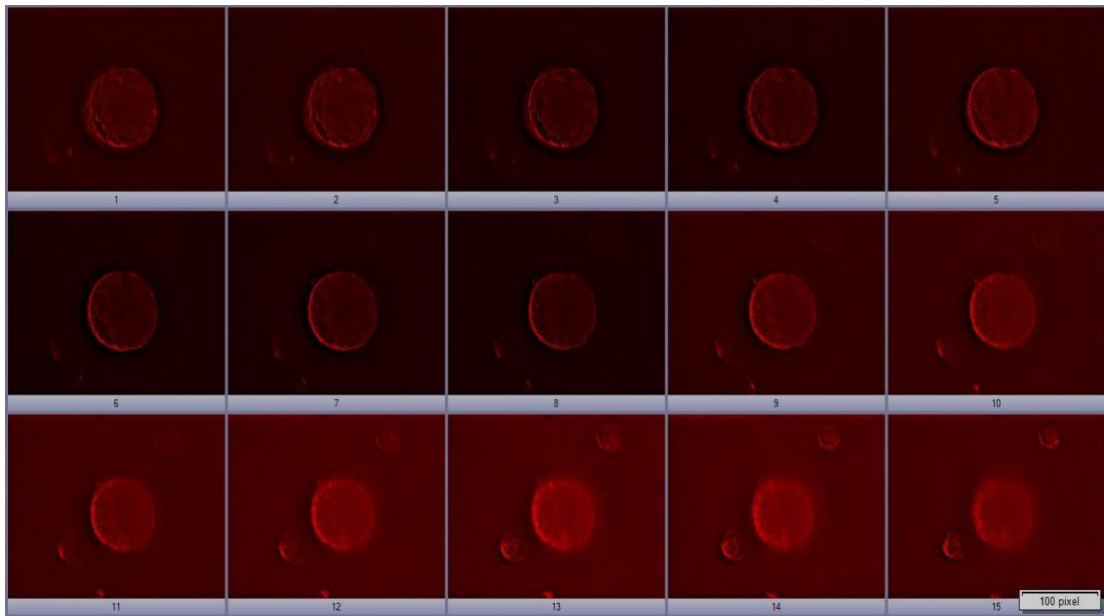
Figure 3.59: shows stacking view of the MCF7 spheroid, targeted using conjugated AuNCs. it shows uptake appears more intense on the periphery/outer boundary and bottom layer of the MCF7 spheroid. Higher level of fluorescence (from top to bottom). Using fluorescence microscopy.

CHAPTER 4

Discussion

4.   Discussion:

4.1. Basic growth characteristics of colorectal cancer cells and breast cancer cells in 2D flat cultures

2D monolayer culture studies have been proven effective at the molecular and genetic level for demonstrating cancer cell behaviour and explaining the hypothesis of the mechanisms (97). To demonstrate the effectiveness of the alamarBlue assay for measuring cell proliferation and to define initial cell density at the beginning of the experiment, cell growth was monitored for both colorectal cells (HT29) and breast cancer cells (MCF7) over time. The results showed different seeded cell density from $5x10^3$ cells/ml up to $50x10^3$ cells/ml and how these correlated with fluorescence intensity increase. Hence these results defined the linear curve graph and the window of measurements.

According to the linear alamarBlue curve $40x10^3$ cells/ml was a peak point; therefore, $40x10^3$ cells/ml was the highest optimum seeding density for HT29 and MCF7. This is in line with published reports on 2D cultures from these cell lines, where seeding densities were in the range of $3x10^3$ cells/ml to $100x10^3$ cells/ml for both HT29 and MCF7, depending on surface area seeded and time left to grow in culture before experimentation (98-100).

4.2. Metabolic activity of colorectal cancer cells and breast cancer cells in 2D and 3D (A/E & A/C)

To determine the optimum cell density in 3D for colorectal cells (HT29), cell proliferation as a direct reflection of metabolic activity was determined by alamarBlue assay. The lowest concentration of $25x10^3$ cells/ml was not the appropriate density, Although the measurements slightly increased up to day seven after this cell viability was reduced, possibly due to the small number of cells not reaching critical mass in this protocol, indicating that the cells cannot grow and become a viable mass.

There is another possible explanation for this relating to the extracellular matrix, the interaction between the cells and their surrounding environment affects their matrix attachment and survival, proliferation and differentiation; hence cells start to die if not enough such events take place (101). At $50x10^3$ cells/ml concentration, measurements slightly rose from day1 up to day10, however, due to not showing a perfect growth curve this could not be an optimum density for the experiment. $75x10^3$ cells/ml resulted in an apparent increase from day one up to day ten. However, cells still did not reach the peak point compared to the higher concentration. For both matrix conditions, of A/C and A/E, $100x10^3$ cells/ml cells/ml showed perfect growth rate and measurements dramatically increased over time points indicating that the ratio of cells to environmental cues was optimum and enabled cell growth.

For the breast cancer cells (MCF7), the cell proliferation and metabolic activity were determined by alamarBlue assay. The lowest concentration of $25x10^3$ cells/ml showed a slight increase up to day 10. Again, this indicates that cells could not provide support for their surrounding cells, in the context of a critical mass. This could be due to lack of formation of the extracellular matrix or lack of enough positive interactions with the existing matrix, which is essential for proliferation and differentiation (102). At $50x10^3$ cells/ml and $75x10^3$ cells/ml cell growth (as measured by alamarBlue) increased incrementally. However, the final concentration $100x10^3$ cells/ml showed a definite increase, perfect linear growth curve and, as was chosen as the optimum seeding density.

Colorectal (HT29) and breast (MCF7) cancer cell lines behave differently when cultured into 2D. Such as cell size, with HT29 cells smaller than MCF7 cells. The cell growth rate is size and cell cycle length dependent, therefore MCF7 grow faster than HT29 in 2D and become confluent (103). The orientation with HT29 cells forming into glandular structures more obviously than MCF7 cells. The latter characteristic may be extrapolated to their tumorigenic ability in mice, with MCF7 being rather more tumorigenic (Estrogen supplementation required) than HT29 (104). Finally, gene expression has been well characterised in these cell lines, with, for example, HT29 carrying EGFR and BRAF mutations (105) and MCF7 carrying IGBP mutations (106).

Interestingly, both HT29 and MCF7 cell lines after being seeded in 3D in vitro models, they are maintaining all transcriptional and translational levels as occurs in vivo environment (20). Such as EGFR expression increase in 3D cell culture (107).

4.3. Growth of cancer cells in different 3D matrices (tumouroids)

Well-defined in vitro 3D models of cancer which mimic tumour structures and the heterogeneity of cell populations found in human cancer tissues and which allow cell-cell and cell-matrix relationships have caused excitement to the researchers because they can be used for a broad range of diagnosis and treatment purposes (108). Many various combinations have been described, especially in the last few years.

The features of these 3D models have been studied from cell shape, cell division and multiplication, to gene and protein expression profiles of cells in 3D cell cultures (9). As collagen type-I is the most abundant extracellular matrix protein, a lot of 3D models use this as the basic protein or mix with other proteins (9) Collagen hydrogel embedded cells allow for both cell-cell and cell-matrix interactions (109) and therefore, help promote the cancer cell multiplication rate.

Some prominent examples which cover cancer and other diseases are tabulated below to demonstrate the large range of 3D models and approaches taken that can be used across different pathologies (Table 4.1).

Type	3D model and application	Cell type	Culture substrate and Matrix
Cancer Co-Culture Models	3D skin reconstruction model to study melanoma progression in human skin (110)	Keratinocytes & Melanocytes & Dermal stem cells & Melanoma Cells	Bovine Collagen I
	Organotypic skin melanoma spheroid model for in vitro drug testing (111)	Human Melanoma Cells & Keratinocytes	Collagen I
Multi-Cellular Co-Culture Models	A physiologically relevant hepatic sinusoids co-culture system (112)	Primary Rat hepatocytes & Rat Liver Endothelial cells	Collagen I
	A physiologically relevant 3D culture model to model human breast tissue (113)	Human mammary epithelial cells & human fibroblasts & adipocytes	Matrigel matrix+ Collagen I
Drug Discovery And Toxicity	Microarray for HTP toxicology assay drugs screening and their p450-generated metabolites (114)	Breast cancer cell (MCF7) & human hepatoma cell (Hep3B)	Cells compressed in Collagen I
	A plastic compression platform (RAFT) to create tumouroids (115)	Colorectal cancer cell line (HCT116 & HT29)	Cells compressed in Collagen I

Table 4.1: Examples of 3D in vitro models which mimic various pathologies, and their applications.

Although using natural hydrogels of collagen type I is an attractive proposition, since it recapitulates an essential physiological component within the 3D model, there are some disadvantages, as the matrix does not allow for quickly harvesting the cells and/or spheroids embedded in it. To do this, it is necessary to treat the collagen matrix with enzymes such as collagenase which may be too disruptive (in house experience).

Researchers even have suggested mixing two or three different gels to form composite gel matrix and to manipulate gel concentration, composition and mechanical properties for various applications (116). Therefore, two different "natural" gel forms were developed in this thesis and used to construct 3D models: The mixture of low melting point agarose with egg white (A/E) and the mixture of low melting point agarose with collagen type I (A/C).

Low melting agar was chosen, as agar has been used for decades in microbiology cultures and is known to provide a practical matrix for growth. There are reports which showed low melting agar as a potential polymer membrane to grow and transfer cells (117). Low melting point agarose modified to produce lower gelling and suitable recovery from low melting agarose gels. Therefore, this allows for ease of manipulation and help the matrix to set the gel and used in cell culture studies.

The original concentration of collagen type I was 0.25 mg/ml, and after mixing with low melted agar, as the collagen type I were diluted further (1:2 ratio) hence, the final concentration was reduced to the half about 0.12/5 mg/ml. For comparison, initial concentrations reported in a plastic compression platform model (where an absorber or weight is placed on the hydrogel to remove water and increase density) was 0.25 mg/ml (115). To manipulate gel components and increase protein available to the cells low melted agar, at the same concentration as for the A/C matrix and egg white were mixed.

There is a study that produced pre-vascular network formation by endothelial and smooth muscle cell co-culture using egg white. This matrix was appropriate for different human cell types, it is also enabled vascular and tumour cell co-culture (43).

4.4.   HT29 colorectal cancer cells in 3D matrices – morphology in tumouroid cultures

Colorectal cancer cells (HT29) were seeded at 100×10^3 cells/ml concentration in A/C matrices in 24 well plates, as described in the methodology chapter. Early on day 1 HT29 cells appeared to reside within the wells formed by the glass beads, with no sign of cell clumping or attachment. This could be due to the cancer cells needing to adapt to the new 3D environmental condition (118). Four days after cell seeding, the cells visibly started to grow/clump together in vitro, indicating they adjusted to their new surroundings. The collagen type I within the matrix is known to support 3D cell growth and differentiation, by

letting the cells to associate with one another, the ECM, and their molecular environment (31, 119). Specific interactions between cells and extracellular matrix proteins are known to drive growth and motility/migration (120). Specifically, for collagen type I, it has been reported that increase cell growth by protecting cancer cells from hypoxia and nutrient stress induced cell death that might occur in vivo-like (121). Collagen type I as a substance protein and helps the growth rate of cancer cells within A/C matrix (122). After that, cells continued to clump or aggregate and started to grow into spheroids over the timeline of the experiment, although a small number of spheroids were fully formed at day 10, with an average size range of 80 µm. This was a lesser outcome than that seen for other matrices, as reported later in this section, suggesting that the A/C matrix is not the best. This could have been due to the limited amount of protein concentration within the A/C mixture compared to the A/E mixture. The collagen type I concentration is higher in compressed gel models, whereby applying a load or an absorber, the liquid is absorbed and produced a matrix with an increase in collagen density 1.28% and protein becomes more concentrated to 120 mg/ml (212).

Colorectal cancer cells HT29 were introduced in the A/E matrix as described previously. At the early time point, day 1 HT29 cells were shown to reside within the wells formed by the glass beads. However, unlike the scenario in the A/C matrix, there were some signs of cell clumping and attachment. There were also some small spheroids already formed. The cell adaptation is essential in preserving the transcriptional and translational utilities in 3D (8). Four days after seeding, more spheroids appeared in different sizes. There were also fewer single cells observed in the A/E matrix compared to the A/C matrix. For the next time point at day, seven bigger spheroids formed and migrated outside the wells which influence tumour cell attachment and cells migratory capabilities. Although cells' migratory abilities depend on the ECM architecture, as described above (123). And eventually, at the later stages, the large spheroids were evidently formed within the tumouroid cultures, with an average size of 140 µm. There were fewer single cells in the A/E matrix compared to the A/C matrix, possibly due to the existence of ovalbumin or ovomucoid which increase the proliferation of cells in A/E condition (124) hence the spheroids formation is

much better than A/C condition. Further discussion on the egg white protein concentration is included in the next section.

4.5. MCF7 breast cancer cells in 3D matrices – morphology in tumouroid cultures

MCF7 breast cancer tumouroids were created in the A/C matrix, by the exact method described in methodology chapter, again using a concentration of 100×10^3 cells/ml. At the first-time point (Day 1) MCF7 cells appeared to reside within the wells formed by the glass beads, with no sign of cell clumping and attachment, possibly to the lag time associated with changes and adaptation to the 3D environment, of transcriptional and translational levels (8). At next time point, (Day 4) cells started to aggregate. At day 7, cells gradually began to clump and hence started to grow into spheroids. Addition at the final time point, some of the spheroids fully formed, and some spheroids completely migrated outside the wells although some cells would simply not aggregate together. This could be due to the ECM architecture which plays a pivotal role when considering cancer cell invasion (125). In some highly dense collagen type-I structures for example the breast tissue, the cancer cells depend on membrane-bound MMPs to make a path via which destruction by other MMPs and migration of cancer cells becomes conceivable (126). The average spheroid size was 60 µm.

MCF7 breast cancer tumouroids was also created in the A/E matrix, by the same method. At day 1, MCF7 cells appeared to reside within the wells formed by the glass beads, with some sign of cell clumping and attachment. At Day 4, there were some spheroids formed. This could be due to cell adaptation within the matrix, which is essential in supporting the transcriptional and translational functions in 3D (20). At day seven some spheroids and clumping cells started to migrate outside the wells. Eventually, at day ten 3D spheroids were fully formed, with only a few single cells appearing in A/E matrix when compared to the A/C matrix; also, the formation of spheroids was significantly higher than A/C matrix with a larger average size. This is possibly due to the existence of

ovalbumin or ovomucoid which increase the proliferation of cells in A/E condition (124). Hence, MCF7 spheroids formed well and more efficiently in A/E than the A/C matrix.

The MCF7 cells survived better than HT29 cells in this matrix, indicating they are more robust or more aggressive cells. This reflects their behaviour in 2D, where MCF7 cells are larger cells and have a faster growth rate (127). And their behaviour in animal models, where MCF7 cells which result in moderately differentiated tumours in vivo can be termed as more tumorigenic than HT29 cells which tend to produce well-differentiated cancers in vivo (128). HT29 have well-organized nuclei and exhibit robust cell-cell adhesion called round tumour (8). Non-invasive cells MCF7 remain as cell aggregates and do not invade into the surrounding invasion matrix, the 3D structure of MCF7 spheroids are disorganized nuclei and exhibit robust adhesion- called mass tumour (129).

Generally, the pattern of growth was accelerated in A/E compared to A/C with earlier and bigger spheroids, resulting in large spheroids at the final time point for both colorectal cancer cells and breast cancer cells. This may have been due to stability of egg white ECM which allow cells to grow and migrate and organized themselves. The egg white composition consists of protein, trace minerals, fatty material, vitamins, and glucose. The main three proteins included in egg white composition that may potentially play a role in assisting the formation of cancer cells spheroids are Ovalbumin, Ovotransferrin, and Ovomucoid (124). This matrix (A/E) also has potential for vascular and tumour cell co-culture (43). Cells grown in egg white were showed better grow, migrate, and organize themselves as pre-vascular network and significantly higher cell density than in Matrigel. 3D culture models' studies showed egg white is an alternative for Matrigel (43).

Also, as it has described earlier in this chapter, there are reports were showed low melting agar as a potential polymer membrane to grow and transfer cells (117). The report also showed the cancer cells could be grown on plastic dishes using low melt agarose with an efficiency of 80–90% (117).

For growth and expansion and movement of the cells within the matrix, a degree of breaking down of the matrix may be needed via matrix metalloproteinases, however, this line of investigation was not undertaken in this body of work. The (MMPs) enzymes that degrade ECM components and allow spheroids invasion, an upsurge in MMP production rate improves invasiveness that is independent of cell–cell adhesion. The sustenance of invasion in dense matrices requires high MMP production rates (130). And their key actions have been demonstrated in several cancer types, including breast and colorectal. The rise in ECM density and the MMP inhibition effect reduced the migration of MCF7 cells embedded in sandwich gels (131). The colon cancer cell invasion and migration showed a correlation with increased in MMP-1 gene expression, and these observations were reversed by chemical inhibitors or neutralizing antibodies against MMP-1 (132).

4.6. Propagation of cancer cells as spheroids, in 3D A/E matrix

To demonstrate whether cells could be passaged in 3D, spheroids for both HT29 and MCF7 were harvested from the tumouroid constructs by gentle centrifugation and reseeded, with a success rate. This was only attempted for the A/E matrix as this condition has more potential compared to the A/C condition due to the faster cell growth, and migration. Harvesting of spheroids and further manipulation is common for simple cancer spheroid models, such as spheroid drops. In such models, simple cancer spheroids grown in hanging drop cultures and incubated for certain time points prior to, for example, drug tests. Several interactions between cells and between cells and the matrix proteins they secrete have been described (133).

4.7. Manufacturing a novel synthetic-organic matrix for 3D tumouroids

The above technique had an excellent rate of cell/spheroid survival however the 3D matrices are mechanically weak (7). Hence, to overcome these limitations, synthetic hydrogels can be considered as potential matrices. They are created specially to copy biomolecular organisations as seen in vivo, such as polylactide (PLA), polyglycolide (PGA) (134). Synthetic-organic matrices have stronger mechanical properties than natural scaffolds. Furthermore, synthetic polymer functionalization can also be achieved by adding scaffolds to specific ECM constituents to copy structures of the biological microenvironment and therefore providing physiological prompts to the cells to enhance growth and movement (135).

Though, cell behaviour will still rely on various properties of these biomaterials including their chemistry, surface properties (hydrophobicity, hydrophilicity, topography) and structure (porosity, surface area, interconnectivity) (136). Therefore, as synthetic scaffolds are simply not made of natural components, to achieve an in vivo-like structure, with all the vital micro-environmental signs, is a complex and challenging task. Therefore, the next step was to design a new 3D model based on synthetic-organic matrices.

4.8. The physical properties of the new 3D matrix (CMC+gelatine)

Hydrogels have been the preferred matrix in establishing 3D models in cancer studies for its convenient preparation and cytocompatibility. Selecting the appropriate chemical composition of the matrix plays a significant role in the cell function control and cellular phenotype. These requirements have led to development of hydrogels derived from biological sources recently, as it closely resembles the microenvironment, suitable for 3D cultures (216).

In these studies, CMC in combination with gelatine which is normally hydrolysed collagen type 1 was selected to create 3D hydrogel cultures of

colorectal and breast cancer cells. This format was selected for its physiological significance of collagen in the growth and maintenance of the cancer molecular environment. Constructing cellular new 3D model using a CMC+gelatine combination produced a matrix with different mechanical properties and composition although it was unknown how it would influence tumour cell attachment and migratory capabilities.

Recent studies confirm the advantage of using gelatine that can promote cell proliferation (137). Due to its unique properties, gelatine is widely used in creating the gel, and in restructuring, stabilizing, emulsifying, and forming foam (138). Gelatine has also been investigated in 3D hydrogel using adipose tissue-derived stromal cells (ADSCs), and it showed that cross-linked gelatine hydrogel promoted cell adhesion, proliferation, and differentiation (137). Furthermore, hormones can be added to the polymer mixture during the preparation stage to aid in the proliferation. Cells require growth factors to proliferate and differentiate in cell culture and usually more than one growth factor is required (139). Defining the physical properties of the novel mixture was deemed essential, therefore, viscosity level and water swelling capability of the solution were analysed. To achieve high degrees of swelling, it is usual to use synthetic polymers that are water-soluble when in non-cross-linked form (140).

The combination of carboxymethyl cellulose with gelatine improved the mechanical properties of the mixture. In this study, the porous nature of the CMC/Gel hydrogels promoted the spatial structure for cell growth and proliferation, as observed by the development of 3D spheroids from the cancer cells grown within them. The spheroids generated are like those generated in standardised matrigel. Previous studies have indicated that physical properties of tissues can adopt the malignant behaviour (206, 207), by influencing cell properties, including morphology (208), proliferation (209) motility, differentiation, (210) and response to therapeutic agents (211).

The water swelling capability of the novel matrix was checked to determine the amount of water that CMC can absorb using freeze-drying which is a dehydration process. The role of water molecules in affecting the structure and

the properties of CMC+gelatine regarding swelling capability was essential because it changes the structure of the CMC+gelatine and therefore due to its high water swelling abilities the samples of CMC are suitable for biological and medical applications (141). The amount of water in CMC+gelatine affects the rheological properties. The arrangement of water molecules inside CMC+gelatine can be considered a critical point in the understanding of CMC+gelatine rheological behaviour and therefore, the amount of water in both swollen and dried forms of CMC analysed. The increase of the swelling capability of CMC+gelatine can lead to a decrease in some of the mechanical properties of the CMC+gelatine, such as tensile strength (142).

Another physical property which was investigated was the viscosity of the matrix fluid. The viscosity of solutions is indirectly related to temperature; therefore, the viscosity decreased with increases in temperature (143). A/E viscosity and A/C viscosity were higher than the novel matrix composed of CMC+gelatine, due to the existence in the natural matrices of low melting agar that helps the matrix to set the final gel (144). The results also showed CMC+gelatine viscosity was slightly higher than CMC solution alone (No gelatine) at room temperature. The viscosity level is critical, as it must not interfere with the 3D harvesting step. Here, the assumption was that the lower viscosity of the novel matrix would enable better spheroid harvesting than the natural matrices.

4.9. Metabolic activity of cancer cells in the novel 3D matrix (CMC+gelatine)

Many of cell seeding concentrations were tested over time to determine optimum conditions for growth. The lowest concentration of HT29 colorectal cancer cells 25×10^3 cells/ml showed a constant increase from day one up to day 7 and at day 10 dropped to less than 60%. Therefore, this concentration is not suitable for the experiment. The higher concentration 50×10^3 cells/ml showed solid, continuous growth curve of spheroids from day1 up to day10. The higher density 100×10^3 cells/ml of HT29 showed a similar growth curve to

50x10^3 cells/ml Both these concentrations were deemed suitable for further experiments. Eventually, at the highest density 150x10^3 cells/ml after normal increase up to day seven, the growth rate of spheroids stopped at day ten resulting in a dramatic drop in metabolic activity. This suggests that either the matrix and environment is not providing sufficient nutrients to the spheroids or that the size of the spheroids more than 250 was prohibitive and resulted in a hypoxic condition within the spheroids. The hypoxic condition is very size dependent, therefore larger spheroids are more hypoxic, as confirmed by the hypoxia studies in this report (145).

The hypoxic condition in the 3D environment it could be the possible cause of a dramatic drop in this time point. This is consistent with previous publications where in other models, for instance, different colon cancer spheroids sizes were used displayed that cell interaction, hypoxia, and drug penetration limitations are suggested as possible causes for the massive spheroids resistance to photodynamic treatment. Spheroids of over 250 sizes have been shown to be hypoxic (145).

A similar behaviour was seen for MCF7 breast cancer cells which were grown in the novel matrix., with 25x10^3 cells/ml resulting in dropped to less than 60% at day ten, therefore, this concentration is not suitable for the experiment. The higher concentrations of 50x10^3 cells/ml and 100x10^3 cells/ml resulted in an increase in metabolic activity from day one up to day 10 (with nicely formed spheroids, as described in the section below).

Finally, at the highest concentration 150x10^3 cells/ml cells in 3D showed a dramatic increase from day one up to day four, and again continues increase up to day seven, followed by a dramatic drop from day seven up to day ten spheroids attached to each other and create a massive tumour with very hypoxic condition. The potential reason is the low level of oxygen in the 3D environment and the possibility of poor penetration of nutrients through the spheroid mass which occurs in spheroids with the size of approximately 250 µm (145).

4.10. Growth and morphology of cancer cells in the novel 3D matrix CMC+gelatine matrix)

The major difference between the synthetic organic novel matrix and the natural matrices appears to be one of tissue stiffness. Stiffness for natural hydrogels is not usually reported, as hydrogels are very loose structures, with (0.2% w/v) collagen density (212). On the other hand, the stiffness of CMC matrices has been reported as (without the gelatine), which is considerably higher (146). There are studies which suggest that stiffer matrices are more beneficial for cell growth, using primary normal human lung fibroblasts to modulated cytoskeletal tension in cells propagated across a physiological assortment of matrix stiffness, this report established reducing cell tension on proliferation and matrix stiffness efficiency (147).

At day one, after seeding the colorectal HT29 and breast MCF7, small spheroids were already formed, this suggested that the cancer cells' adaptation is faster in this matrix compared to the previous natural matrices (118). Four days later spheroids size dramatically increased due to the stable 3D environment and existence of gelatine (137). At day 7 HT29 spheroids growth rate reduced possibly due to cell contact effects and hypoxia and nutrition penetration (148). Limited nutrient and metabolic waste transport are an essential concern in 3D spheroid constructs because of a bulky ECM structure (149).

At the final stage, high compact spheroids need to be harvested and transferred into the new 3D condition. It would be interesting to determine why this novel matrix appears to be more supportive of faster growth than the natural forms described above. All matrices contain varying amounts of protein, collagen, gelatine or large egg white proteins. Arguably, the egg white mixture has the highest protein content, however, this does not appear to be a determining factor in differential growth.

4.11. Growth of human umbilical vein endothelial cells in CMC+gelatine matrix.

HUVECs were seeded into the 3D CMC+gelatine matrix and tracked over different time points for ten days. HUVECs have not shown any tube formation in CMC+gelatine matrix. However, at day10 HUVECs were transferred back into the 2D condition to determine cell viability. The results were showed HUVECs kept their normal growth rate and proliferation in 2D. It has been shown in other studies that well-matched substrates can help HUVECs tubulogenesis in 3D and that substrate stiffness affects the type and technique of tube formation in 3D (150). However, since this was not the pattern found in the CMC+gelatine model described here, the question raised is whether the addition of gelatine was the determining factor in the behaviour of the HUVEC cells.

Additionally, different micro patterning methods applied to synthetic or composite matrices, growth factors, and adhesion molecules have been used to encourage HUVECs to form like tubes in vitro. Typically, there are two growth factors (BFGF, VEGF) associated with angiogenesis (151). Although, HUVECs usually make networks on compliant surfaces but not hard surfaces such as Matrigel and Egg white (43). The addition of BFGF and VEGF interrupt network formation and increase cell migration on soft surfaces (151). However, further investigation is required to determine the effect and interaction of growth factors, CMC+gelatine matrix, and cell migration and adhesions on network formation which are still uncertain.

4.12. Live/Dead Evaluation (Propidium Iodide and FDA) of cancer spheroids in CMC+gelatine matrix

The live/dead assay was used to determine spheroid viability in CMC+gelatine by tracking small spheroids from the early stage until they formed large spheroid structures. Spheroids grown in 3D CMC+gelatine model had normal

growth rate from day one up to day 5. The growth rate of spheroids from day five up to day ten was slightly reduced. As a previous cell viability studies using alamarBlue assay have exhibited that there was no significant difference in cell viability in 3D monolayers in the course of the first few days (1–5 days) compared to 2D culture (8, 152). However, the structure of spheroids was showed mostly the internal structure of the spheroids surrounded by a layer of viable cells, which may cause the lack of oxygen and nutrients and the pile up of waste at the centre of the spheroid as they grow larger (149).

There is a report that where the 3D hydrogel system made by the use of two cancer cell lines and a primary bone marrow mesenchymal stem line. And the results have shown, these 3D cell masses not only well-maintained cell viability and 3D morphology however also showed better cell function when matched to the similar 2D monolayer (153).

4.13. Levels of oxygen/ Hypoxia of cancer spheroids in CMC+gelatine matrix.

Hypoxia in spheroids grown in CMC+gelatine was measured by Hypoxia reagent at distinct time points of growth using a new automated confocal microscopy filter under development in the Department. No hypoxia was detected in matrices and spheroids for both HT29 and MCF7 at day one. There were indications that oxygen levels had started to drop to less than 5% from day four spheroids, although the latter were well formed (with average sizes around for HT29 & MCF7 respectively, 170 μm & 85 μm. This could be because HIF-1α expression had started to rise (154). There is a study were showed this overexpression is significantly related with MDR1 gene expression whose function is the ATP dependent export of substances from the inside of cells, and membranes, to the outside in colon cancer cells (213). At day 7, results have been shown to reduce spheroids growth rate with higher fluorescence intensity. Eventually, at day ten after certain time in 3D CMC+gelatine model, spheroids can develop hypoxic cores that can proceed to necrosis, closely mimicking what is seen in vivo (155)

Determining hypoxia within the spheroids is essential since it provides necessary information which underpins the growth and progression of the spheroids within any matrix, but also gives valuable information about the possible resistance of spheroids to treatment, such as, for example, photodynamic therapy and the usefulness of the spheroids as drug testing platforms. Similar hypoxic levels have been previously described with cancer spheroids of similar sizes for breast and colorectal cancer. By Validation of collagen type I 3D model using HT29 cancer cells which were used real time hypoxia measurements within a growing tumour (156) And characterise the gene expression changes linked with hypoxia in MCF7 and find a potential biomarker for hypoxia in breast cancer (157). Hypoxic regions may exist due to the difficulty of penetration of nutrients and oxygen and absence of a transport system to eliminate waste from the core of the spheroid. Its importance in response to drugs and radiation treatment has been widely described, and several attempts to increase response to treatment have involved the attempted reversal of hypoxia (158).

4.14. Propagation of cancer cells as spheroids, in 3D CMC+gelatine matrix

The isolated spheroids all showed a localised presence of calreticulin, a potential cancer marker, on their membrane surface when probed with targeted fluorescent gold nanoclusters. At day ten grown spheroids were ready to be harvested for further studies and replated within a matrix. There is a study that managed a simple microfluidic device for cell spheroid formation and spheroid harvesting (159). Harvested spheroids have high integrity (159). Hence, grown harvested spheroids are potential to be stained for targeting studies initially start with 2D fixed, and 3D fixed spheroids or eventually, for live precise targeting studies in 2D live and 3D live spheroids targeting by passing through endothelial cells. Harvested spheroids can also be exploited for more flow cytometry assays because of the sufficient cell numbers.

4.15. AuNCs

Biological imaging in vivo is faced with many more challenges than laboratory based cellular imaging. Interactions between the imaging molecule and the in vivo complex physiological environment may lead to its elimination before it reaches its target, and detection may be weak because of interference generated by the tissue components and the fact that in depth imaging is problematic with visible light (160). Therefore, new potential approaches are essential, both for molecules that can be used as imaging agents and for models which can be used to test these molecules. Several different nano scales signalling markers such as quantum dots and organic dyes have been used over the last few years for the purposes of imaging, (72) however: they often lack appropriate specificity and sensitivity and have the further disadvantages of high toxicity and low-stability (161).

Au as a new class of fluorescent metal cluster which provides some advantages for in vivo imaging compared to other nanoparticles (162). AuNCs light emission is capable of penetrating into deeper tissue and sensing stronger intensity because of weakest biological auto fluorescence. Further advantages include good water-solubility, biocompatibility, and good photostability (163) Finally, there are possible applications of such nanoparticles which can deliver both imaging and enhanced cell killing (theranostic application) which makes the use of nanoparticles in cancer very attractive (164). Hence for this part of the study, AuNCs were manufactured in the house as nanoscale signalling markers for fluorescence imaging and tested first in 2D and then in 3D cancer cell models.

4.16. Toxicity of AuNCs in 2D cultures of all cell lines.

HT29, MCF7, and HUVECs cells were exposed to both AuNCs and HAuCL4 equivalent concentrations. The results for all cell lines showed that HAuCL4 conferred a much higher level of toxicity compared to AuNCs. A Recent study

has shown AuNCs with the large photostability as well as the reduced toxicity showed their potential for uninterrupted imaging in vivo (165).

As it displayed the AuNCs fluorescence signal, the cell viability and toxicity studies reveal the nontoxic nature of AuNCs. These attractive characteristics including ultra- small size, decreased toxicity and reduced photo-bleaching make AuNCs even more appealing fluorescent probes for biological purposes. AuNCs could be simply could be detected by a fluorescent microscope (165).

4.17. Targeting cells in 2D cultures (fixed), using AuNCs-Anti-EGFR

There are several studies which describe that the epidermal growth factor receptor (EGFR) is overexpressed in different types of cancers, such as subsets of colorectal cancer and breast cancer (166). Increased EGFR expression drives increase cell replication via the MAPK signalling pathway, and it is also associated with increased motility and the metastatic phenotype (167). Generally, EGFR has been targeted in a variety of cancers, with new generation biologics (antibodies) used in the clinic, including for colorectal and breast cancer (168). Therefore, overexpression of EGFR, detected by AuNCs conjugated to anti-EGFR antibodies was studied here, in both colorectal and breast cancer cells in 2D fixed cell cultures, to determine the suitability of the whole concept. The validation of the conjugation between nanoclusters and antibody was carried out by a colleague in blotting experiments and were not presented in this thesis.

2D cultures of HT29 colorectal cancer cells were fixed and exposed to AuNCs conjugated to anti-EGFR antibodies (AuNCs-Anti-EGFR) or unconjugated AuNCs, with only the former cultures showing fluorescence and therefore uptake of the AuNCs-Anti-EGFR, this is consistent with previous work, which demonstrated that HT29 cells express EGFR (115, 169) and overexpression of EGFR in colorectal cancer cells could be a potential reason for that. 2D cultures of MCF7 breast cancer cells were fixed and exposed to AuNCs conjugated to

anti-EGFR antibodies (AuNCs-Anti-EGFR) or unconjugated AuNCs, with only the former cultures showing fluorescence and therefore uptake of the AuNCs-Anti-EGFR. Other studies were showed that MCF7 cells express EGFR (170, 171) Overexpression of EGFR in breast cancer cells could be a potential reason for that.

Clinically, EGFR is targeted using the monoclonal antibody Cetuximab (172). This is often used for EGFR positive colorectal cancer patients. Some clinical trials in breast cancer have revealed that targeting EGFR increases the chemosensitivity of breast cancer cells (173). Therefore, more widespread EGFR-targeting could have a promising therapeutic role in breast cancer. Therefore, it is quite important to continue exploring ways of increasing and improving the targeting of such a promising biomarker.

4.18. Targeting cells in 2D cultures (fixed), using AuNCs-Anti-CRT

The second biomarker investigated for targeting using AuNCs was Calreticulin (CRT), a cytoplasmic calcium-binding protein (174). CRT is a multifunctional protein predominantly found in endoplasmic reticulum (ER) (175). Usually, the protein appears to act as control chaperone by stopping the proteins that are misfolded from progressing to the Golgi apparatus [21]. CRT also acts as Ca2+ storage protein, therefore playing an essential role in the intracellular signal transduction systems and therefore in tasks such as cellular proliferation and cell death. It also acts as a nuclear hormone receptor gene transcription modulator (176).

The results showed that CRT exists on the surface of cancer cells; its original labelling on cancer cell surface by anti-CRT conjugated AuNCs indicates that CRT translocates to the cell surface during carcinogenesis, perhaps causing immunotolerance of the malignant cells between other functions. There have been previous studies associating CRT to various cancers (177). AuNCs functioned as fluorescent bio-probes accurately identifying surface-bound CRT (178) Validation of the conjugation between the AuNCs and the anti-CRT antibody was carried out via dot blots, using increasing concentrations of "cold"

antibody. Experiments to determine the expression of CRT were conducted in both cancer cell lines, HT29 and MCF7 and in the endothelial cell line HUVEC.

2D cultures of HT29 colorectal cancer cells and MCF7 breast cancer cells were fixed and exposed AuNCs to conjugated to anti-CRT antibodies (AuNCs-Anti-CRT) or to unconjugated AuNCs, with only the former cultures showing fluorescence and therefore uptake of the AuNCs-Anti-CRT. This strongly suggests that HT29 cells overexpress CRT, as it described earlier in our previous report were indicated that CRT is present on the surface of cancer cells (176) and there is a study were showed that the calreticulin gene was over expressed in MCF7 human breast cancer cell lines (170).

2D cultures of HUVECs endothelial cells were fixed and exposed to AuNCs conjugated to anti-CRT antibodies (AuNCs-Anti-CRT) or to unconjugated AuNCs, however, both conditions not showing any sign of fluorescence. This could be due to CRT has not expressed on the surface of HUVECs endothelial cells (176). The CRT is expressed on the surface of a tumour derived cells of the solid cancers investigated, in the absence of any form of induction (176). Other studies were showed that CRT expression levels in tumour tissues significantly higher than CRT levels compared to normal tissues (179). CRT has also shown to be an essential biomarker for bladder urothelial cancer detection (180).

4.19. Targeting cells in 2D (live), using AuNCs-Anti-CRT and AuNCs

The next stage was to target CRT in live cancer cells. The impact of CRT expression on cell proliferation depends on cancer cell types. Live 2D cultures of HT29 colorectal cancer cells and MCF7 breast cancer cells were exposed to AuNCs conjugated to anti-CRT antibodies (AuNCs-Anti-CRT) or to unconjugated AuNCs, with only the former cultures showing fluorescence and therefore uptake of the AuNCs-Anti-CRT.

The imaging of targeted HT29 cancer cells using fluorescence microscopy revealed that AuNCs-Anti-CRT could identify and trace the CRT on live cells (176). Increasing the exposure time of AuNCs-Anti-CRT and AuNCs may eventually increase the uptake in live cells. The imaging of targeted MCF7 cancer cells using fluorescence microscopy revealed that AuNCs-Anti-CRT could detect and trace the CRT mostly on the membrane surface of breast cancer cells (176) Although, this should be considered that if exposure time increase this may lead to uptake of AuNCs-Anti-CRT and AuNCs in live cells.

The route of focus is imaging fluorescence and then at the same setting for light transmission images. However this is only true for the cells that bound the AuNCs-Anti-CRT (top row). As the fluorescence was evident in the cells below focusing took place under light transmission. Therefore the field of focus and penetration under light transmission different for the top row.

In effective drug development understanding of drug uptake and diffusion within tissues is an essential feature (181). Previous studies were exposed spheroids more precisely replicate in vivo barriers to drug uptake and diffusion than 2D cell culture system. The 3D models may be useful for the drug toxicity assays as well as a model for drug development (182).

4.20. Targeting 3D fixed spheroids using AuNCs-Anti-CRT and AuNCs

The effectiveness of AuNCs-Anti-CRT targeting in 2D cancer cells was examined under both live and fixed conditions. The results showed the specificity of targeting cancer cells using AuNCs-Anti-CRT. However, using 3D models could be a complementary, more powerful option which may give results closer to the in vivo scenario (9). The 3D culture systems not only keep the 3D cell to cell associations and cell to ECM interactions in monoculture for studying cell behaviour that mimics in vivo conditions, but 3D models also provide an opportunity for the co-culture of multiple types of cells to more closely mimic the in vivo conditions (31). The goal of using 3D models is to

develop and design, fast, precise, and reproducible high-content imaging techniques to examine the properties and fate of AuNCs-Anti-CRT within a 3D tissue mimic and their effect on the morphology and viability of 3D spheroids which are closer to cancer islands and glands observed in human cancer tissues (183).

At day10 HT29 spheroids grown in CMC+gelatine matrix was harvested and fixed and incubated with AuNCs-Anti-CRT. This showed uptake of the targeted AuNCs-Anti-CRT, as demonstrated by the NIR fluorescent (false red colour) images. Uptake appeared more intense on the periphery/outer boundary of the spheroids consistent with CRT overexpression. At the same time, control experiments where fixed HT29 spheroids were incubated with AuNCs showed a reduced uptake of the AuNCs, as demonstrated by the red fluorescent compared to spheroids incubated with targeted AuNCs-Anti-CRT. This distinct labelling on the spheroid surface by anti-CRT conjugated AuNCs suggests that CRT translocates to the cell surface during carcinogenesis (176). DAPI fluorescence was used to identify of cell nuclei and describe well-populated spheroids. The results also indicated more cells towards the periphery of the spheroid, and fewer cells at the core of the spheroid.

At day10 MCF7 spheroids grown in CMC+gelatine matrix was harvested and fixed and incubated with AuNCs-Anti-CRT. This showed uptake of the targeted AuNCs-Anti-CRT, as demonstrated by the NIR fluorescent (false red colour) images. Uptake appeared more intense on the periphery/outer boundary of the spheroids consistent with CRT overexpression. At the same time, control experiments where fixed MCF7 spheroids were incubated with AuNCs showed a reduced uptake of the AuNCs, as demonstrated by the red fluorescent compared to spheroids incubated with targeted AuNCs-Anti-CRT. This distinct labelling on the spheroid surface by anti-CRT conjugated AuNCs suggests that CRT translocates to the cell surface during carcinogenesis (176). DAPI fluorescence was used to identify of cell nuclei and describe well-populated spheroids. The results also indicated more cells towards the periphery of the spheroid, and fewer cells at the core of the spheroid.

Well-populated spheroids and all cell nuclei were identified based on DAPI fluorescence, with probably more cells towards the periphery of the spheroid, and fewer cells at the core of the spheroid, which determines to target, displayed by red fluorescence. There are studies where nanoparticles were used specially to target the cancer cells. To regulate gene expression, in MCF7 cancer cells, the nanoparticle-conjugated TFO were delivered directly into the nucleus of MCF7 cancer cells using ultra-small gold nanoparticles (184). Another report has shown the direct visualization of interactions between drug-loaded nanoparticles and the cancer cell nucleus (185).

Studying of gold nanoparticles in two-dimensional (2D) and three-dimensional (3D) cell cultures have shown HT29 cancer cells taken up most of the nanoparticles with FA and the targeting nanoparticles have more correspondence to cancer cells than the pure drugs and untreated nanoparticles (186). These new approaches revealed that increased therapeutic effectiveness could provide new plans were provided to choose appropriate nano-carriers for targeted therapy. The penetration of gold nanomaterials is essential in molecular level, current studies revealed that penetration of gold nanomaterials through the membrane is size dependent hence, if gold nanomaterials is smaller than 3 nm, the AuNCs have great properties because of their ultrafine dimension and unique form The AuNCs light emitting is efficient to penetrate within tissue and shows stronger intensity detection (214), which directly affects the uptake time in targeted therapy (187).

4.21. Targeting live cancer spheroids through an endothelial cell barrier in a complex tumouroid construct, using AUNCs-anti-CRT

Having shown appropriate targeting capabilities of the AUNCs-Anti-CRT molecules, using variously fixed and live cell cultures, the purpose of this section was to investigate whether targeted AuNCs would differentiate their targets within a more complex 3D construct, which incorporates an endothelial barrier. Both HT29 and MCF7 live spheroids were grown as above and placed

in a new matrix, with a filter insert on top seeded with a monolayer of HUVECs. The cancer spheroids were targeted using conjugated AuNCs-Anti-CRT which had to traverse the filter. Control groups included filter barriers with no endothelial cells on them. Imaging was carried out 2 h later, using fluorescence microscopy. Comparisons focused on the effect of the endothelial cell populated filter barrier.

The cancer spheroids targeted by passing through HUVECs seeded filter inserts, showed higher fluorescence intensity compared to the empty filter insert condition. This shows the appropriate regulation of HUVECs as an endothelial barrier, which selectively absorbs fluid and solutes (188). Fluid, solutes, and even circulating cells can cross the basement membrane through two different routes, the transcellular pathway (cell body) and paracellular pathway (between the cells). Naturally, HUVECs grown on a 2D surface such as a filter insert, tend to form cord-like structures (189).

Several pathways allow AuNCs-Anti-CRT to pass through an endothelial barrier to target spheroids within the matrix. The transcellular is one of the potential pathways. The mechanism includes vesicle-mediated endocytosis at the endothelial luminal membrane, followed by transcytosis across the cell, and exocytosis at the basolateral membrane (190, 191). There is also another possible reason for the higher fluorescence intensity of targeted spheroids as follows; Aquaporins are membrane proteins expressed in endothelial cells (192). They are important for the control of water homeostasis by providing selective passage for the rapid movement of water, and other uncharged solutes such as AuNCs, across diverse cell membranes (193).

The blood-brain boundary prohibits the passage of most treatment agents into the brain (194). The studies have shown that the gold nanoparticles are potential to pass through human brain endothelium and then to enter astrocytes. The nanoparticles have the correct properties for effective and particular therapeutic agent's carriers within the blood-brain barrier (195). This could be further investigated in vivo as a platform for targeted cancer therapies.

4.22. Monitoring and localizing of AuNCs-Anti-CRT within spheroids

Following the above experiments, HT29 and MCF7 spheroids were targeted using AuNCs-Anti-CR and then removed from the matrix and the filter and fixed to allow for further investigations of how the AuNCs-Anti-CRT interacted within the spheroids. After imaging using fluorescence microscopy, both cancer cell spheroids showed similar results with the AuNCs-Anti-CRT mostly on the outer edges and bottom of the spheroids.

Further consideration needs to compare targeting studies in 2D cultures and 3D spheroids. CRT expressed on the cell surface, in other words non-ER CRT is considered as a signal for cancer cells by anti-phagocytic signal CD47 (196). It has been previously described that an antiphagocytic signal CD47 was increased with high amounts of CRT on cancer cell surfaces to avoid phagocytosis by the immune system (196). Therefore, the ability of the CD47 by anti-CD47 antibodies might be therapeutic to the cell phagocytic uptake (197). The results are an indication that CRT mediated immune responses is an important link to the development of new anticancer therapy.

The expression of CRT in 2D appears uniform, while in 3D it appears on the outer boundary of the spheroid (198).The targeting 3D view and Z stacking view of both HT29 and MCF7 spheroids confirm the difference with 2D cultures, to determine whether the latter is a true picture, that the outer surface expression of CRT in spheroids is a true phenotype, other investigations must take place, such as immunohistochemistry and immunofluorescence using different antibodies to verify the present findings. Unfortunately, this was not carried out due to time constraints. In another study, it was showed that powerful prognostic biomarkers were a constituent of CRT expression and were responsible for the enhanced local anti-tumour immune response in the lungs (199).

Overall, overexpression of non-ER CRT and the attachment efficiency of AuNCs-Anti-CRT to this CRT may be different in 3D and 2D cultures due to differences in phenotype of cancer cells while as a monolayer, or as a spheroid.

Further study has also shown the influence of the ECM on cancer growth where EGFR used colorectal cancer cells and gene expression were different in 2D and 3D cultures (107). This demonstrates strongly that using 3D models is different than using 2D models and may be a truer representation of the in vivo situation. The further investigation also confirmed CRT expression in human colorectal cancer cells which is associated with infiltration of T-cells (200).

CHAPTER 5

Future prospective and conclusion

5. Future prospective and conclusion:

To date, most methods describing 3D cell culture systems for diagnostic or drug testing have been mainly recognised as a proof-of-concept approach. Majority of the knowledge obtained so far are the advantages over other types of 3D construction, potential anti-cancer drug evaluation compared to 2D systems. The use of 3D cell culture systems for diagnostic characterisation and evaluating novel anti-cancer drugs has yet to be translated to the mainstream. However, with the popularity amongst researchers in 3D systems and numerous availability of 3D matrices, data obtained will almost incorporate with 2D and animal studies.

While different types of 3D matrices are widely accessible to most researchers, standardisation and a universal system is needed whereby data are reproducible and reliable. Majority of the 3D systems are rigid and are difficult in the quantification of drugs or imaging due to the presence of the matrices. Pharmaceutical and clinical biopsies could benefit immensely using universal 3D matrices to screen novel therapeutics for anti-cancer activities. Drug efficacy data obtained would be more physiologically relevant than data obtained from 2D monolayer culture system.

Additionally, the 3D cell culture system is inexpensive and robust compared to animal trials. Weakly adherent cells can sometimes be rescued in 3D systems and qualify for drug screenings without loss of cells as would in 2D monolayer system. Currently, improved development in cultured liver cells (hepatocytes) in 3D to test the liver toxicity of novel therapeutics have been established. It is known that hepatocytes rapidly halt synthesising drug metabolising enzymes when cultured on 2D monolayer, however, in 3D format, these cells retain these function (217, 218).

Another potential application of 3D drug sensitivity study is in the expanding field of personalised medicine. The treatment and prevention of cancer has greatly benefitted from introduction of personalised medicine, with genetic evaluation of genes, such as breast cancer (BRACA) 1 and 2 mutations, the

detection of the expression of certain proteins that can tailor effective therapies such as human epidermal growth factor receptor 2 (HER2) expression. The application of 3D matrices for the future could include tumour biopsies directly transferred, cultured and treated with and array of anti-cancer drugs. With universal standardisation and replicable matrices, 3D drug selection and imaging can be a potential solution to cancer therapy.

For any type of cancer, cancer theranostics is an important field. There have been many advances in this field. The current cancer therapeutics procedures for cancer patients' and supportive care, makes cancer therapeutics procedures a vital tool for oncologists and all professionals involved in cancer treatment. For the scientists one of the most potential method is using nanoparticles in cancer theranostics, hence, the use of nanoparticles become a priority in cancer theranostics.

The latest studies show that the 3D cell culture models in vitro are potentially the strong tool for the early stage of cancer theranostics, before in vivo studies and eventually clinical trials. During this research study, the hydrogel culture matrix was made of CMC+gelatine as a 3D model for studying the growth and potential drug targeting of cancer cells. The use of carboxymethylcellulose (CMC) porous as a component in a binary system was successfully prepared by an aqueous system. The porous structure was fine-tuned by altering the composition of the CMC and gelatine in water. When polymerised under heating it could be saturated with growth medium for 3D culture growth. On top of that, it produced excellent thermal and swelling because the liquid medium is well retained in the CMC polymer matrix because of the presence of -OH and -COOH groups.

Once tuned, the chemical and physical properties of the hydrogels give a basis for the analysis of the native cancer cell molecular environment. The main characteristics of breast and colorectal cancer cells grown in the matrix were compared with 2D monolayer cultures. For the first time, it has been shown that 3D spheroids can be harvested and isolated from the matrix for evaluation of cancer markers by targeting with fluorescent gold nanoclusters. In the future two possible ways

1. Use this novel 3D matrix but change the biological material

- Collected ex-vivo biopsies could be transferred directly into matrix and grown in the laboratory.
- Diagnose and further culture and then treat with various anti-cancer drugs to determine response.
- Evaluate the current status of the disease progression using the underlying mechanisms.

This would be an approach to personalized medicine.

2. To increase the complexity of the existing model to be able to investigate interactions and cross-talk with immune derived cells such as Monocytes This model is flexible and components and cells can be separated for molecular investigation. Such an immunocompetent model would be invaluable for testing action of immune therapies.

CHAPTER 6

References

6. References

1.   Chinen AB, Guan CM, Ferrer JR, Barnaby SN, Merkel TJ, Mirkin CA. Nanoparticle Probes for the Detection of Cancer Biomarkers, Cells, and Tissues by Fluorescence. Chem Rev. 2015;115(19):10530-74.

2.   Lane LA, Qian X, Nie S. SERS Nanoparticles in Medicine: From Label-Free Detection to Spectroscopic Tagging. Chem Rev. 2015;115(19):10489-529.

3.   Menon JU, Jadeja P, Tambe P, Vu K, Yuan B, Nguyen KT. Nanomaterials for photo-based diagnostic and therapeutic applications. Theranostics. 2013;3(3):152-66.

4.   Chwalek K, Bray LJ, Werner C. Tissue-engineered 3D tumor angiogenesis models: potential technologies for anti-cancer drug discovery. Adv Drug Deliv Rev. 2014;79-80:30-9.

5.   Breslin S, O'Driscoll L. Three-dimensional cell culture: the missing link in drug discovery. Drug Discov Today. 2013;18(5-6):240-9.

6.   Basavaraj S, Betageri GV. Can formulation and drug delivery reduce attrition during drug discovery and development-review of feasibility, benefits and challenges. Acta Pharm Sin B. 2014;4(1):3-17.

7.   Tibbitt MW, Anseth KS. Hydrogels as extracellular matrix mimics for 3D cell culture. Biotechnol Bioeng. 2009;103(4):655-63.

8.   Edmondson R, Broglie JJ, Adcock AF, Yang L. Three-dimensional cell culture systems and their applications in drug discovery and cell-based biosensors. Assay Drug Dev Technol. 2014;12(4):207-18.

9.   Antoni D, Burckel H, Josset E, Noel G. Three-dimensional cell culture: a breakthrough in vivo. Int J Mol Sci. 2015;16(3):5517-27.

10.   Khaitan D, Chandna S, Arya MB, Dwarakanath BS. Establishment and characterization of multicellular spheroids from a human glioma cell line; Implications for tumor therapy. J Transl Med. 2006;4:12.

11.   Ivanov DP, Parker TL, Walker DA, Alexander C, Ashford MB, Gellert PR, et al. Multiplexing spheroid volume, resazurin and acid phosphatase viability assays for high-throughput screening of tumour spheroids and stem cell neurospheres. PLoS One. 2014;9(8):e103817.

12.   Weiswald LB, Bellet D, Dangles-Marie V. Spherical cancer models in tumor biology. Neoplasia. 2015;17(1):1-15.

13.   Chitcholtan K, Sykes PH, Evans JJ. The resistance of intracellular mediators to doxorubicin and cisplatin are distinct in 3D and 2D endometrial cancer. J Transl Med. 2012;10:38.

14.   Luca AC, Mersch S, Deenen R, Schmidt S, Messner I, Schafer KL, et al. Impact of the 3D microenvironment on phenotype, gene expression, and EGFR inhibition of colorectal cancer cell lines. PLoS One. 2013;8(3):e59689.

15.   Bielecka ZF, Maliszewska-Olejniczak K, Safir IJ, Szczylik C, Czarnecka AM. Three-dimensional cell culture model utilization in cancer stem cell research. Biol Rev Camb Philos Soc. 2017;92(3):1505-20.

16.   Price KJ, Tsykin A, Giles KM, Sladic RT, Epis MR, Ganss R, et al. Matrigel basement membrane matrix influences expression of microRNAs in cancer cell lines. Biochem Biophys Res Commun. 2012;427(2):343-8.

17.   Sung KE, Su X, Berthier E, Pehlke C, Friedl A, Beebe DJ. Understanding the impact of 2D and 3D fibroblast cultures on in vitro breast cancer models. PLoS One. 2013;8(10):e76373.

18.   Ross DT, Scherf U, Eisen MB, Perou CM, Rees C, Spellman P, et al. Systematic variation in gene expression patterns in human cancer cell lines. Nat Genet. 2000;24(3):227-35.

19.   Birgersdotter A, Sandberg R, Ernberg I. Gene expression perturbation in vitro--a growing case for three-dimensional (3D) culture systems. Semin Cancer Biol. 2005;15(5):405-12.

20.   Cao J, Luo Z, Cheng Q, Xu Q, Zhang Y, Wang F, et al. Three-dimensional regulation of transcription. Protein Cell. 2015;6(4):241-53.

21.   Li H, Fan X, Houghton J. Tumor microenvironment: the role of the tumor stroma in cancer. J Cell Biochem. 2007;101(4):805-15.

22.   Fang Y, Eglen RM. Three-Dimensional Cell Cultures in Drug Discovery and Development. SLAS Discov. 2017;22(5):456-72.

23.   Lovitt CJ, Shelper TB, Avery VM. Advanced cell culture techniques for cancer drug discovery. Biology (Basel). 2014;3(2):345-67.

24.   Walker DM, Boey G, McDonald LA. The pathology of oral cancer. Pathology. 2003;35(5):376-83.

25.   Riffle S, Hegde RS. Modeling tumor cell adaptations to hypoxia in multicellular tumor spheroids. J Exp Clin Cancer Res. 2017;36(1):102.

26.   Loh QL, Choong C. Three-dimensional scaffolds for tissue engineering applications: role of porosity and pore size. Tissue Eng Part B Rev. 2013;19(6):485-502.

27.   Li J, Chen M, Fan X, Zhou H. Recent advances in bioprinting techniques: approaches, applications and future prospects. J Transl Med. 2016;14:271.

28.   Dai R, Wang Z, Samanipour R, Koo KI, Kim K. Adipose-Derived Stem Cells for Tissue Engineering and Regenerative Medicine Applications. Stem Cells Int. 2016;2016:6737345.

29.   Zhu J, Marchant RE. Design properties of hydrogel tissue-engineering scaffolds. Expert Rev Med Devices. 2011;8(5):607-26.

30.   Cheema U, Yang SY, Mudera V, Goldspink GG, Brown RA. 3-D in vitro model of early skeletal muscle development. Cell Motil Cytoskeleton. 2003;54(3):226-36.

31.   Xu X, Farach-Carson MC, Jia X. Three-dimensional in vitro tumor models for cancer research and drug evaluation. Biotechnol Adv. 2014;32(7):1256-68.

32.   Ulery BD, Nair LS, Laurencin CT. Biomedical Applications of Biodegradable Polymers. J Polym Sci B Polym Phys. 2011;49(12):832-64.

33.   van Tienen TG, Heijkants RG, Buma P, de Groot JH, Pennings AJ, Veth RP. Tissue ingrowth and degradation of two biodegradable porous polymers with different porosities and pore sizes. Biomaterials. 2002;23(8):1731-8.

34.   Zeng J, Xu X, Chen X, Liang Q, Bian X, Yang L, et al. Biodegradable electrospun fibers for drug delivery. J Control Release. 2003;92(3):227-31.

35.   Chan BP, Leong KW. Scaffolding in tissue engineering: general approaches and tissue-specific considerations. Eur Spine J. 2008;17 Suppl 4:467-79.

36.   Do AV, Khorsand B, Geary SM, Salem AK. 3D Printing of Scaffolds for Tissue Regeneration Applications. Adv Healthc Mater. 2015;4(12):1742-62.

37.   Millerot-Serrurot E, Guilbert M, Fourre N, Witkowski W, Said G, Van Gulick L, et al. 3D collagen type I matrix inhibits the antimigratory effect of doxorubicin. Cancer Cell Int. 2010;10:26.

38.   Staton CA, Stribbling SM, Tazzyman S, Hughes R, Brown NJ, Lewis CE. Current methods for assaying angiogenesis in vitro and in vivo. Int J Exp Pathol. 2004;85(5):233-48.

39.   Modulevsky DJ, Lefebvre C, Haase K, Al-Rekabi Z, Pelling AE. Apple derived cellulose scaffolds for 3D mammalian cell culture. PLoS One. 2014;9(5):e97835.

40.   Szot CS, Buchanan CF, Freeman JW, Rylander MN. 3D in vitro bioengineered tumors based on collagen I hydrogels. Biomaterials. 2011;32(31):7905-12.

41.   Minchinton AI, Tannock IF. Drug penetration in solid tumours. Nat Rev Cancer. 2006;6(8):583-92.

42.   Bonnans C, Chou J, Werb Z. Remodelling the extracellular matrix in development and disease. Nat Rev Mol Cell Biol. 2014;15(12):786-801.

43.   Mousseau Y, Mollard S, Qiu H, Richard L, Cazal R, Nizou A, et al. In vitro 3D angiogenesis assay in egg white matrix: comparison to Matrigel, compatibility to various species, and suitability for drug testing. Lab Invest. 2014;94(3):340-9.

44.   Kaipparettu BA, Kuiatse I, Tak-Yee Chan B, Benny Kaipparettu M, Lee AV, Oesterreich S. Novel egg white-based 3-D cell culture system. Biotechniques. 2008;45(2):165-8, 70-1.

45.   Brunner CA, Groner RW. Carboxy-methyl-cellulose hydrogel-filled breast implants - an ideal alternative? A report of five years' experience with this device. Can J Plast Surg. 2006;14(3):151-4.

46.   DiMasi JA, Hansen RW, Grabowski HG. The price of innovation: new estimates of drug development costs. J Health Econ. 2003;22(2):151-85.

47.   Shield K, Ackland ML, Ahmed N, Rice GE. Multicellular spheroids in ovarian cancer metastases: Biology and pathology. Gynecol Oncol. 2009;113(1):143-8.

48.   Shroff K, Pearce TR, Kokkoli E. Enhanced integrin mediated signaling and cell cycle progression on fibronectin mimetic peptide amphiphile monolayers. Langmuir. 2012;28(3):1858-65.

49.   Vinci M, Gowan S, Boxall F, Patterson L, Zimmermann M, Court W, et al. Advances in establishment and analysis of three-dimensional tumor spheroid-based functional assays for target validation and drug evaluation. BMC Biol. 2012;10:29.

50.   Horvath P, Aulner N, Bickle M, Davies AM, Nery ED, Ebner D, et al. Screening out irrelevant cell-based models of disease. Nat Rev Drug Discov. 2016;15(11):751-69.

51.   Dudley AC. Tumor endothelial cells. Cold Spring Harb Perspect Med. 2012;2(3):a006536.

52.   Szabo A, Merks RMH. Blood vessel tortuosity selects against evolution of aggressive tumor cells in confined tissue environments: A modeling approach. PLoS Comput Biol. 2017;13(7):e1005635.

53.   Eales KL, Hollinshead KE, Tennant DA. Hypoxia and metabolic adaptation of cancer cells. Oncogenesis. 2016;5:e190.

54.   Rajabi M, Mousa SA. The Role of Angiogenesis in Cancer Treatment. Biomedicines. 2017;5(2).

55.   Ucuzian AA, Gassman AA, East AT, Greisler HP. Molecular mediators of angiogenesis. J Burn Care Res. 2010;31(1):158-75.

56.   Mendichovszky I, Jackson A. Imaging hypoxia in gliomas. Br J Radiol. 2011;84 Spec No 2:S145-58.

57.   Walsh JC, Lebedev A, Aten E, Madsen K, Marciano L, Kolb HC. The clinical importance of assessing tumor hypoxia: relationship of tumor hypoxia to prognosis and therapeutic opportunities. Antioxid Redox Signal. 2014;21(10):1516-54.

58.   Brown JM, Wilson WR. Exploiting tumour hypoxia in cancer treatment. Nat Rev Cancer. 2004;4(6):437-47.

59.   Kraft JC, Freeling JP, Wang Z, Ho RJ. Emerging research and clinical development trends of liposome and lipid nanoparticle drug delivery systems. J Pharm Sci. 2014;103(1):29-52.

60.   In: Levit L, Balogh E, Nass S, Ganz PA, editors. Delivering High-Quality Cancer Care: Charting a New Course for a System in Crisis. Washington (DC)2013.

61.   Housman G, Byler S, Heerboth S, Lapinska K, Longacre M, Snyder N, et al. Drug resistance in cancer: an overview. Cancers (Basel). 2014;6(3):1769-92.

62.   In: Hewitt M, Herdman R, Holland J, editors. Meeting Psychosocial Needs of Women with Breast Cancer. Washington (DC)2004.

63.   Farkona S, Diamandis EP, Blasutig IM. Cancer immunotherapy: the beginning of the end of cancer? BMC Med. 2016;14:73.

64.   Yingchoncharoen P, Kalinowski DS, Richardson DR. Lipid-Based Drug Delivery Systems in Cancer Therapy: What Is Available and What Is Yet to Come. Pharmacol Rev. 2016;68(3):701-87.

65.   Albanese A, Tang PS, Chan WC. The effect of nanoparticle size, shape, and surface chemistry on biological systems. Annu Rev Biomed Eng. 2012;14:1-16.

66.   Singh R, Lillard JW, Jr. Nanoparticle-based targeted drug delivery. Exp Mol Pathol. 2009;86(3):215-23.

67.   Florence AT. "Targeting" nanoparticles: the constraints of physical laws and physical barriers. J Control Release. 2012;164(2):115-24.

68.   Dawidczyk CM, Kim C, Park JH, Russell LM, Lee KH, Pomper MG, et al. State-of-the-art in design rules for drug delivery platforms: lessons learned from FDA-approved nanomedicines. J Control Release. 2014;187:133-44.

69.   Zheng J, Nicovich PR, Dickson RM. Highly fluorescent noble-metal quantum dots. Annu Rev Phys Chem. 2007;58:409-31.

70.   Riehemann K, Schneider SW, Luger TA, Godin B, Ferrari M, Fuchs H. Nanomedicine--challenge and perspectives. Angew Chem Int Ed Engl. 2009;48(5):872-97.

71.   Arvizo R, Bhattacharya R, Mukherjee P. Gold nanoparticles: opportunities and challenges in nanomedicine. Expert Opin Drug Deliv. 2010;7(6):753-63.

72.   Zhu Y, Hong H, Xu ZP, Li Z, Cai W. Quantum dot-based nanoprobes for in vivo targeted imaging. Curr Mol Med. 2013;13(10):1549-67.

73.   Jung D, Min K, Jung J, Jang W, Kwon Y. Chemical biology-based approaches on fluorescent labeling of proteins in live cells. Mol Biosyst. 2013;9(5):862-72.

74.   Narvekar M, Xue HY, Eoh JY, Wong HL. Nanocarrier for poorly water-soluble anticancer drugs--barriers of translation and solutions. AAPS PharmSciTech. 2014;15(4):822-33.

75.   Upadhyay RK. Drug delivery systems, CNS protection, and the blood brain barrier. Biomed Res Int. 2014;2014:869269.

76.   Kim EG, Kim KM. Strategies and Advancement in Antibody-Drug Conjugate Optimization for Targeted Cancer Therapeutics. Biomol Ther (Seoul). 2015;23(6):493-509.

77.   Smaglo BG, Aldeghaither D, Weiner LM. The development of immunoconjugates for targeted cancer therapy. Nat Rev Clin Oncol. 2014;11(11):637-48.

78.   Sajja HK, East MP, Mao H, Wang YA, Nie S, Yang L. Development of multifunctional nanoparticles for targeted drug delivery and noninvasive imaging of therapeutic effect. Curr Drug Discov Technol. 2009;6(1):43-51.

79.   Baskar S, Muthusamy N. Antibody-based therapeutics for the treatment of human B cell malignancies. Curr Allergy Asthma Rep. 2013;13(1):33-43.

80.   Marschall AL, Frenzel A, Schirrmann T, Schungel M, Dubel S. Targeting antibodies to the cytoplasm. MAbs. 2011;3(1):3-16.

81.   Saper CB. A guide to the perplexed on the specificity of antibodies. J Histochem Cytochem. 2009;57(1):1-5.

82.   Descotes J. Immunotoxicity of monoclonal antibodies. MAbs. 2009;1(2):104-11.

83.   Fontanges Q, De Mendonca R, Salmon I, Le Mercier M, D'Haene N. Clinical Application of Targeted Next Generation Sequencing for Colorectal Cancers. Int J Mol Sci. 2016;17(12).

84.   Vanneman M, Dranoff G. Combining immunotherapy and targeted therapies in cancer treatment. Nat Rev Cancer. 2012;12(4):237-51.

85.   Scott AM, Allison JP, Wolchok JD. Monoclonal antibodies in cancer therapy. Cancer Immun. 2012;12:14.

86.   Lu YC, Weng WC, Lee H. Functional roles of calreticulin in cancer biology. Biomed Res Int. 2015;2015:526524.

87.   Afshar N, Black BE, Paschal BM. Retrotranslocation of the chaperone calreticulin from the endoplasmic reticulum lumen to the cytosol. Mol Cell Biol. 2005;25(20):8844-53.

88.   Park BJ, Lee DG, Yu JR, Jung SK, Choi K, Lee J, et al. Calreticulin, a calcium-binding molecular chaperone, is required for stress response and fertility in Caenorhabditis elegans. Mol Biol Cell. 2001;12(9):2835-45.

89.   Zamanian M, Veerakumarasivam A, Abdullah S, Rosli R. Calreticulin and cancer. Pathol Oncol Res. 2013;19(2):149-54.

90.   Hsu WM, Hsieh FJ, Jeng YM, Kuo ML, Chen CN, Lai DM, et al. Calreticulin expression in neuroblastoma--a novel independent prognostic factor. Ann Oncol. 2005;16(2):314-21.

91.   Weber GF, Bjerke MA, DeSimone DW. Integrins and cadherins join forces to form adhesive networks. J Cell Sci. 2011;124(Pt 8):1183-93.

92.   Sirenko O, Mitlo T, Hesley J, Luke S, Owens W, Cromwell EF. High-content assays for characterizing the viability and morphology of 3D cancer spheroid cultures. Assay Drug Dev Technol. 2015;13(7):402-14.

93.   Kunz-Schughart LA, Freyer JP, Hofstaedter F, Ebner R. The use of 3-D cultures for high-throughput screening: the multicellular spheroid model. J Biomol Screen. 2004;9(4):273-85.

94.   Krausz E, de Hoogt R, Gustin E, Cornelissen F, Grand-Perret T, Janssen L, et al. Translation of a tumor microenvironment mimicking 3D tumor growth co-culture assay platform to high-content screening. J Biomol Screen. 2013;18(1):54-66.

95.   Pelletier MJ. Control of out-of-focus light intensity in confocal raman microscopy using optical preprocessing. Appl Spectrosc. 2009;63(6):591-6.

96.   Griffiths G, Lucocq JM. Antibodies for immunolabeling by light and electron microscopy: not for the faint hearted. Histochem Cell Biol. 2014;142(4):347-60.

97.   Cortese B, Palama IE, D'Amone S, Gigli G. Influence of electrotaxis on cell behaviour. Integr Biol (Camb). 2014;6(9):817-30.

98.   Palanisamy SK, Trisciuoglio D, Zwergel C, Del Bufalo D, Mai A. Metabolite profiling of ascidian Styela plicata using LC-MS with multivariate statistical analysis and their antitumor activity. J Enzyme Inhib Med Chem. 2017;32(1):614-23.

99.   Pavlovich E, Volkova N, Yakymchuk E, Perepelitsyna O, Sydorenko M, Goltsev A. In Vitro Study of Influence of Au Nanoparticles on HT29 and SPEV Cell Lines. Nanoscale Res Lett. 2017;12(1):494.

.100   Greish K, Taha S, Jasim A, Elghany SA, Sultan A, AlKhateeb A, et al. Styrene maleic acid encapsulated raloxifene micelles for management of inflammatory bowel disease. Clin Transl Med. 2017;6(1):28.

.101   Barthes J, Ozcelik H, Hindie M, Ndreu-Halili A, Hasan A, Vrana NE. Cell microenvironment engineering and monitoring for tissue engineering and regenerative medicine: the recent advances. Biomed Res Int. 2014;2014:921905.

.102   Humphrey JD, Dufresne ER, Schwartz MA. Mechanotransduction and extracellular matrix homeostasis. Nat Rev Mol Cell Biol. 2.12-802:(12)15;014

.103   Ginzberg MB, Kafri R, Kirschner M. Cell biology. On being the right (cell) size. Science. 2015;348(6236):1245075.

.104   Benz CC, Scott GK, Sarup JC, Johnson RM, Tripathy D, Coronado E, et al. Estrogen-dependent, tamoxifen-resistant tumorigenic growth of MCF-7 cells transfected with HER2/neu. Breast Cancer Res Treat. 1992;24(2):85-95.

.105   Benlloch S, Paya A, Alenda C, Bessa X, Andreu M, Jover R, et al. Detection of BRAF V600E mutation in colorectal cancer: comparison of automatic sequencing and real-time chemistry methodology. J Mol Diagn. 2006;8(5):540-3.

.106   Soh CL, McNeil K, Owczarek CM, Hardy MP, Fabri LJ, Pearse M, et al. Exogenous administration of protease-resistant, non-matrix-binding IGFBP-2 inhibits tumour growth in a murine model of breast cancer. Br J Cancer. 2014;110(12):2855-64.

.107   Breslin S, O'Driscoll L. The relevance of using 3D cell cultures, in addition to 2D monolayer cultures, when evaluating breast cancer drug sensitivity and resistance. Oncotarget. 2016;7(2.56-45745:(9

.108   Wang C, Tang Z, Zhao Y, Yao R, Li L, Sun W. Three-dimensional in vitro cancer models: a short review. Biofabrication. 2014;6(2):022001.

.109   Ahearne M. Introduction to cell-hydrogel mechanosensing. Interface Focus. 2014;4(2):20130038.

.110   Li L, Fukunaga-Kalabis M, Herlyn M. The three-dimensional human skin reconstruct model: a tool to study normal skin and melanoma progression. J Vis Exp. 2011(54).

.111   Vorsmann H, Groeber F, Walles H, Busch S, Beissert S, Walczak H, et al. Development of a human three-dimensional organotypic skin-melanoma spheroid model for in vitro drug testing. Cell Death Dis. 2013;4:e719.

.112   Xiao W, Perry G, Komori K, Sakai Y. New physiologically-relevant liver tissue model based on hierarchically cocultured primary rat hepatocytes with liver endothelial cells. Integr Biol (Camb). 2015;7(11):1412-22.

.113   Vidi PA, Bissell MJ, Lelievre SA. Three-dimensional culture of human breast epithelial cells: the how and the why. Methods Mol Biol. 2013;945:193-219.

.114   Lee MY, Kumar RA, Sukumaran SM, Hogg MG, Clark DS, Dordick JS. Three-dimensional cellular microarray for high-throughput toxicology assays. Proc Natl Acad Sci U S A. 2008;105(1):59-63.

.115   Magdeldin T, Lopez-Davila V, Villemant C, Cameron G, Drake R, Cheema U ,et al. The efficacy of cetuximab in a tissue-engineered three-dimensional in vitro model of colorectal cancer. J Tissue Eng. 2014;5:2041731414544183.

.116   Wozniak MA, Keely PJ. Use of three-dimensional collagen gels to study mechanotransduction in T47D breast epithelial cells. Biol Proced Online. 2005;7:144-61.

.117   Natarajan S, Chow TT, Shay JW, Wright WE. Replica plating of mammalian cells using low melt agarose. Cytotechnology. 2007;54(3):145-7.

.118   Justice BA, Badr NA, Felder RA. 3D cell culture opens new dimensions in cell-based assays. Drug Discov Today. 2009;14(1-2):102-7.

.119   Somaiah C, Kumar A, Mawrie D, Sharma A, Patil SD, Bhattacharyya J, et al. Collagen Promotes Higher Adhesion, Survival and Proliferation of Mesenchymal Stem Cells. PLoS One. 2015;10(12):e0145068.

.120   Kurosaka S, Kashina A. Cell biology of embryonic migration. Birth Defects Res C Embryo Today. 2008;84(2):102-22.

.121   Rodrigo R, Libuy M, Feliu F, Hasson D. Oxidative stress-related biomarkers in essential hypertension and ischemia-reperfusion myocardial damage. Dis Markers. 2013;35(6):773-90.

.122   Li J, Li X, Lan T, Qi C, He X, Yang H, et al. [Type I collagen secreted by lung cancer cells promotes cancer cell growth in a three- dimensional culture system]. Nan Fang Yi Ke Da Xue Xue Bao. 2014;34(8):1129-34.

.123   Lu P, Takai K, Weaver VM, Werb Z. Extracellular matrix degradation and remodeling in development and disease. Cold Spring Harb Perspect Biol. 2011;3(12).

.124   Mizunoya W, Tashima A, Sato Y, Tatsumi R, Ikeuchi Y. The growth-promoting activity of egg white proteins in the C2C12 myoblast cell line. Anim Sci J. 2015;86(2):194-9.

.125   Li XY, Ota I, Yana I, Sabeh F, Weiss SJ. Molecular dissection of the structural machinery underlying the tissue-invasive activity of membrane type-1 matrix metalloproteinase. Mol Biol Cell. 2008;19(8):3221-33.

.126   Deakin NE, Chaplain MA. Mathematical modeling of cancer invasion: the role of membrane-bound matrix metalloproteinases. Front Oncol. 2013;3:70.

.127   Yang J, Dungrawala H, Hua H, Manukyan A, Abraham L, Lane W, et al. Cell size and growth rate are major determinants of replicative lifespan. Cell Cycle. 2011;10(1):144-55.

.128   Riedl A, Schlederer M, Pudelko K, Stadler M, Walter S, Unterleuthner D, et al. Comparison of cancer cells in 2D vs 3D culture reveals differences in AKT-mTOR-S6K signaling and drug responses. J Cell Sci. 2017;130(1):203-18.

.129   Kenny PA, Lee GY, Myers CA, Neve RM, Semeiks JR, Spellman PT, et al. The morphologies of breast cancer cell lines in three-dimensional assays correlate with their profiles of gene expression. Mol Oncol. 2007;1(1):84-96.

.130   Kumar S, Kapoor A, Desai S, Inamdar MM, Sen S. Proteolytic and non-proteolytic regulation of collective cell invasion: tuning by ECM density and organization. Sci Rep. 2016;6:19905.

.131   Lee MH, Wu PH, Staunton JR, Ros R, Longmore GD, Wirtz D. Mismatch in mechanical and adhesive properties induces pulsating cancer cell migration in epithelial monolayer. Biophys J. 2012;102(12):2731-41.

.132   Raufman JP, Cheng K, Saxena N, Chahdi A, Belo A, Khurana S, et al. Muscarinic receptor agonists stimulate matrix metalloproteinase 1-dependent invasion of human colon cancer cells. Biochem Biophys Res Commun. 2011;415(2):319-24.

.133   Foty R. A simple hanging drop cell culture protocol for generation of 3D spheroids. J Vis Exp. 2011(51).

.134   Kim EJ, Yoon SJ, Yeo GD, Pai CM, Kang IK. Preparation of biodegradable PLA/PLGA membranes with PGA mesh and their application for periodontal guided tissue regeneration. Biomed Mater. 2009;4(5.055001:(

.135   Nakayama KH, Hou L, Huang NF. Role of extracellular matrix signaling cues in modulating cell fate commitment for cardiovascular tissue engineering. Adv Healthc Mater. 2014;3(5):628-41.

.136   Gunatillake P, Mayadunne R, Adhikari R. Recent developments in biodegradable synthetic polymers. Biotechnol Annu Rev. 2006;12:301-47.

.137   Yang G, Xiao Z, Ren X, Long H, Qian H, Ma K, et al. Enzymatically crosslinked gelatin hydrogel promotes the proliferation of adipose tissue-derived stromal cells. PeerJ. 2016;4:e2497.

.138   Tabari M. Investigation of Carboxymethyl Cellulose (CMC) on Mechanical Properties of Cold Water Fish Gelatin Biodegradable Edible Films. Foods. 2017;6(6).

.139   Goustin AS, Leof EB, Shipley GD, Moses HL. Growth factors and cancer. Cancer Res. 1986;46(3):1015-29.

.140   Ahmed EM. Hydrogel: Preparation, characterization, and applications: A review. J Adv Res. 2015;6(2):105-21.

.141   Shah R, Saha N, Saha P. Influence of temperature, pH and simulated biological solutions on swelling and structural properties of biomineralized (CaCO3) PVP-CMC hydrogel. Prog Biomater. 2015;4(2-4):123-36.

.142   Tongdeesoontorn W, Mauer LJ, Wongruong S, Sriburi P, Rachtanapun P. Effect of carboxymethyl cellulose concentration on physical properties of biodegradable cassava starch-based films. Chem Cent J. 2011;5(1):6.

.143   Romano MR, Romano V, Mauro A, Angi M, Costagliola C, Ambrosone L. The Effect of Temperature Changes in Vitreoretinal Surgery. Transl Vis Sci Technol. 2016;5(1):4.

.144   Lee PY, Costumbrado J, Hsu CY, Kim YH. Agarose gel electrophoresis for the separation of DNA fragments. J Vis Exp. 2012(62).

.145   West CM. Size-dependent resistance of human tumour spheroids to photodynamic treatment. Br J Cancer. 1989;59(4):510-4.

.146   Jeong JY, Chung PK, Yoo JC. Effect of sodium hyaluronate/carboxymethyl cellulose (Guardix-sol) on retear rate and postoperative stiffness in arthroscopic rotator cuff repair patients: A prospective cohort study. J Orthop Surg (Hong Kong). 2017;25(2):2309499017718908.

.147   Mih JD, Marinkovic A, Liu F, Sharif AS, Tschumperlin DJ. Matrix stiffness reverses the effect of actomyosin tension on cell proliferation. J Cell Sci. 2012;125(Pt 24):5974-83.

.148   Mehta G, Hsiao AY, Ingram M, Luker GD, Takayama S. Opportunities and challenges for use of tumor spheroids as models to test drug delivery and efficacy. J Control Release. 2012;164(2):192-204.

.149   Nam KH, Smith AS, Lone S, Kwon S, Kim DH. Biomimetic 3D Tissue Models for Advanced High-Throughput Drug Screening. J Lab Autom. 2015;20(3).15-201:

.150   Saunders RL, Hammer DA. Assembly of Human Umbilical Vein Endothelial Cells on Compliant Hydrogels. Cell Mol Bioeng. 2010;3(1):60-7.

.151   Lee SH, Jeong D, Han YS, Baek MJ. Pivotal role of vascular endothelial growth factor pathway in tumor angiogenesis. Ann Surg Treat Res. 2015;89(1):1-8.

.152   Gurski LA, Jha AK, Zhang C, Jia X, Farach-Carson MC. Hyaluronic acid-based hydrogels as 3D matrices for in vitro evaluation of chemotherapeutic drugs using poorly adherent prostate cancer cells. Biomaterials. 2009;30(30):6076-85.

.153   Ben-Yoav H, Melamed S, Freeman A, Shacham-Diamand Y, Belkin S. Whole-cell biochips for bio-sensing: integration of live cells and inanimate surfaces. Crit Rev Biotechnol. 2011;31(4):337-53.

.154   Ding Z, Yang L, Xie X, Xie F, Pan F, Li J, et al. Expression and significance of hypoxia-inducible factor-1 alpha and MDR1/P-glycoprotein in human colon carcinoma tissue and cells. J Cancer Res Clin Oncol. 2010;136(11):1697-707.

.155   Vinnitsky V. The development of a malignant tumor is due to a desperate asexual self-cloning process in which cancer stem cells develop the ability to mimic the genetic program of germline cells. Intrinsically Disord Proteins. 2014;2(1):e29997.

.156   Nyga A, Loizidou M, Emberton M, Cheema U. A novel tissue engineered three-dimensional in vitro colorectal cancer model. Acta Biomater. 2013;9(8):7917-26.

.157   Hamdan FH, Zihlif MA. Gene expression alterations in chronic hypoxic MCF7 breast cancer cell line. Genomics. 2014;104(6 Pt B):477-81.

.158   Ayuso JM, Virumbrales-Munoz M, Lacueva A, Lanuza PM, Checa-Chavarria E, Botella P, et al. Development and characterization of a microfluidic model of the tumour microenvironment. Sci Rep. 2016;6:36086.

.159   Patra B, Chen YH, Peng CC, Lin SC, Lee CH, Tung YC. A microfluidic device for uniform-sized cell spheroids formation, culture, harvesting and flow cytometry analysis. Biomicrofluidics. 2013;7(5):54114.

.160   Richardson DS, Lichtman JW. Clarifying Tissue Clearing. Cell. 2015;162(2):246-57.

.161   Parikh R, Mathai A, Parikh S, Chandra Sekhar G, Thomas R. Understanding and using sensitivity, specificity and predictive values. Indian J Ophthalmol. 2008;56(1):45-50.

.162   Sun HT, Sakka Y. Luminescent metal nanoclusters: controlled synthesis and functional applications. Sci Technol Adv Mater. 2014;15(1):014205.

.163   Zou C, Wu B, Dong Y, Song Z, Zhao Y, Ni X, et al. Biomedical photoacoustics: fundamentals, instrumentation and perspectives on nanomedicine. Int J Nanomedicine. 2017;12:179-95.

.164   Fernandez-Fernandez A, Manchanda R, McGoron AJ. Theranostic applications of nanomaterials in cancer: drug delivery, image-guided therapy, and multifunctional platforms. Appl Biochem Biotechnol. 2011;165(7-8):1628-51.

.165   Shang L, Nienhaus GU. Gold nanoclusters as novel optical probes for in vitro and in vivo fluorescence imaging. Biophys Rev. 2012;4(4):313-22.

.166   Hatanpaa KJ, Burma S, Zhao D, Habib AA. Epidermal growth factor receptor in glioma: signal transduction, neuropathology, imaging, and radioresistance. Neoplasia. 2010;1.84-675:(9)2

.167   Freudenberg JA, Wang Q, Katsumata M, Drebin J, Nagatomo I, Greene MI. The role of HER2 in early breast cancer metastasis and the origins of resistance to HER2-targeted therapies. Exp Mol Pathol. 2009;87(1):1-11.

.168   Scott AM, Allison JP ,Wolchok JD. Monoclonal antibodies in cancer therapy. Cancer Immun. 2012;12:14.

.169   Xu H, Yu Y, Marciniak D, Rishi AK, Sarkar FH, Kucuk O, et al. Epidermal growth factor receptor (EGFR)-related protein inhibits multiple members of the EGFR family in colon and breast cancer cells. Mol Cancer Ther. 2005;4(3):435-42.

.170   Subik K, Lee JF, Baxter L, Strzepek T, Costello D, Crowley P, et al. The Expression Patterns of ER, PR, HER2, CK5/6, EGFR, Ki-67 and AR by Immunohistochemical Analysis in Breast Cancer Cell Lines. Breast Cancer (Auckl). 2010;4:35-41.

.171   Moerkens M, Zhang Y, Wester L, van de Water B, Meerman JH. Epidermal growth factor receptor signalling in human breast cancer cells operates parallel to estrogen receptor alpha signalling and results in tamoxifen insensitive proliferation. BMC Cancer. 2014;14:283.

.172   Martinelli E, De Palma R, Orditura M, De Vita F, Ciardiello F. Anti-epidermal growth factor receptor monoclonal antibodies in cancer therapy. Clin Exp Immunol. 2009;158(1):1-9.

.173   Nakai K, Hung MC, Yamaguchi H. A perspective on anti-EGFR therapies targeting triple-negative breast cancer. Am J Cancer Res. 2016;6(8):1609-23.

.174   Michalak M, Robert Parker JM, Opas M. Ca2+ signaling and calcium binding chaperones of the endoplasmic reticulum. Cell Calcium. 2002;32(5-6):269-78.

.175   Lu YC, Weng WC, Lee H. Functional roles of calreticulin in cancer biology. Biomed Res Int. 2015;2015:526524.

.176   Ramesh BS, Giorgakis E, Lopez-Davila V, Dashtarzheneha AK, Loizidou M. Detection of cell surface calreticulin as a potential cancer biomarker using near-infrared emitting gold nanoclusters. Nanotechnology. 2016;27(28):285101.

.177   Pan Z, Lu YY, Liu F. Sunlight-activated long-persistent luminescence in the near-infrared from Cr(3+)-doped zinc gallogermanates. Nat Mater. 2011;11(1):58-63.

.178   Cheng Z, Wu Y, Xiong Z, Gambhir SS, Chen X. Near-infrared fluorescent RGD peptides for optical imaging of integrin alphavbeta3 expression in living mice. Bioconjug Chem. 2005;16(6):1433-41.

.179   Vaksman O, Davidson B, Trope C, Reich R. Calreticulin expression is reduced in high-grade ovarian serous carcinoma effusions compared with primary tumors and solid metastases. Hum Pathol. 2013;44(12):2677-83.

.180   Kageyama S, Isono T, Iwaki H, Wakabayashi Y, Okada Y, Kontani K, et al. Identification by proteomic analysis of calreticulin as a marker for bladder cancer and evaluation of the diagnostic accuracy of its detection in urine. Clin Chem. 2004;50(5):857-66.

.181   Jang SH, Wientjes MG, Lu D, Au JL. Drug delivery and transport to solid tumors. Pharm Res. 2003;20(9):1337-50.

.182   Achilli TM, McCalla S, Meyer J, Tripathi A, Morgan JR. Multilayer spheroids to quantify drug uptake and diffusion in 3D. Mol Pharm. 2014;11(7):2071-81.

.183   Sirenko O, Mitlo T, Hesley J, Luke S ,Owens W, Cromwell EF. High-content assays for characterizing the viability and morphology of 3D cancer spheroid cultures. Assay Drug Dev Technol. 2015;13(7):402-14.

.184   Huo S, Jin S, Ma X, Xue X, Yang K, Kumar A, et al. Ultrasmall gold nanoparticles as carriers for nucleus-based gene therapy due to size-dependent nuclear entry. ACS Nano. 2014;8(6):5852-62.

.185   Dam DH, Lee JH, Sisco PN, Co DT, Zhang M, Wasielewski MR, et al. Direct observation of nanoparticle-cancer cell nucleus interactions. ACS Nano. .26-3318:(4)6;2012

.186   Xie X, Liao J, Shao X, Li Q, Lin Y. The Effect of shape on Cellular Uptake of Gold Nanoparticles in the forms of Stars, Rods, and Triangles. Sci Rep. 2017;7(1):3827.

.187   Li Z, Chen HY, Schouteden K, Picot T, Houben K, Liao TW, et al. Size-Dependent Penetration of Gold Nanoclusters through a Defect-Free, Nonporous NaCl Membrane. Nano Lett. 2016;16(5):3063-70.

.188   Simoneau B, Houle F, Huot J. Regulation of endothelial permeability and transendothelial migration of cancer cells by tropomyosin-1 phosphorylation. Vasc Cell. 2012;4(1):18.

.189   Zhang AP, Qu X, Soman P, Hribar KC, Lee JW, Chen S, et al. Rapid fabrication of complex 3D extracellular microenvironments by dynamic optical projection stereolithography. Adv Mater. 2012;24(31).70-4266:

.190   Chidlow JH, Jr., Sessa WC. Caveolae, caveolins, and cavins: complex control of cellular signalling and inflammation. Cardiovasc Res. 2010;86(2):219-25.

.191   Kohn S, Nagy JA, Dvorak HF, Dvorak AM. Pathways of macromolecular tracer transport across venules and small veins. Structural basis for the hyperpermeability of tumor blood vessels. Lab Invest. 1992;67(5):596-607.

.192   Verkman AS. Aquaporins. Curr Biol. 2013;23(2):R52-5.

.193   Day RE, Kitchen P, Owen DS, Bland C, Marshall L, Conner AC, et al. Human aquaporins: regulators of transcellular water flow. Biochim Biophys Acta. 2014;1840(5):1492-506.

.194   Upadhyay RK. Drug delivery systems, CNS protection, and the blood brain barrier. Biomed Res Int. 2014;2014:869269.

.195   Gromnicova R, Davies HA, Sreekanthreddy P, Romero IA, Lund T, Roitt IM, et al. Glucose-coated gold nanoparticles transfer across human brain endothelium and enter astrocytes in vitro. PLoS One. 2013;8(12):e81043.

.196   Chao MP, Jaiswal S, Weissman-Tsukamoto R, Alizadeh AA, Gentles AJ, Volkmer J, et al. Calreticulin is the dominant pro-phagocytic signal on multiple human cancers and is counterbalanced by CD47. Sci Transl Med. 2010;2(63):63ra94.

.197   Raghavan M, Wijeyesakere SJ, Peters LR, Del Cid N. Calreticulin in the immune system: ins and outs. Trends Immunol. 2013;34(1):13-21.

.198   Toma-Dasu I, Dasu A. Modelling tumour oxygenation, reoxygenation and implications on treatment outcome. Comput Math Methods Med. 2013;2013:141087.

.199   Fucikova J, Becht E, Iribarren K, Goc J, Remark R, Damotte D, et al. Calreticulin Expression in Human Non-Small Cell Lung Cancers Correlates with Increased Accumulation of Antitumor Immune Cells and Favorable Prognosis. Cancer Res. 2016;76(7):1746-56.

.200   Peng RQ, Chen YB, Ding Y, Zhang R, Zhang X, Yu XJ, et al. Expression of calreticulin is associated with infiltration of T-cells in stage IIIB colon cancer. World J Gastroenterol. 2010;16(19):2428-34.

201.   Loessner D, Stok KS, Lutolf MP, Hutmacher DW, Clements JA, Rizzi SC. Bioengineered 3D platform to explore cell-ECM interactions and drug resistance of epithelial ovarian cancer cells. Biomaterials. 2010;31(32):8494-506.

202.   Hakkinen KM, Harunaga JS, Doyle AD, Yamada KM. Direct comparisons of the morphology, migration, cell adhesions, and actin cytoskeleton of fibroblasts in four different three-dimensional extracellular matrices. Tissue Eng Part A. 2011;17(5-6):713-24.

203.   Yu M, Lin G, Arshadi N, Kalatskaya I, Xue B, Haider S, et al. Expression profiling during mammary epithelial cell three-dimensional morphogenesis identifies PTPRO as a novel regulator of morphogenesis and ErbB2-mediated transformation. Mol Cell Biol. 2012;32(19):3913-24.

204.   Breslin S, O'Driscoll L. The relevance of using 3D cell cultures, in addition to 2D monolayer cultures, when evaluating breast cancer drug sensitivity and resistance. Oncotarget. 2016;7(29):45745-56.

205. Gehlsen KR, Dickerson K, Argraves WS, Engvall E, Ruoslahti E. Subunit structure of a laminin-binding integrin and localization of its binding site on laminin. J Biol Chem. 1989;264(32):19034-8.

206. Samani A, Plewes D. An inverse problem solution for measuring the elastic modulus of intact ex vivo breast tissue tumours. Phys Med Biol. 2007;52(5):1247-60.

207. Krouskop TA, Wheeler TM, Kallel F, Garra BS, Hall T. Elastic moduli of breast and prostate tissues under compression. Ultrason Imaging. 1998;20(4):260-74.

208. Isenberg BC, Dimilla PA, Walker M, Kim S, Wong JY. Vascular smooth muscle cell durotaxis depends on substrate stiffness gradient strength. Biophys J. 2009;97(5):1313-22.

209. Hadjipanayi E, Mudera V, Brown RA. Close dependence of fibroblast proliferation on collagen scaffold matrix stiffness. J Tissue Eng Regen Med. 2009;3(2):77-84.

210. Kloxin AM, Benton JA, Anseth KS. In situ elasticity modulation with dynamic substrates to direct cell phenotype. Biomaterials. 2010;31(1):1-8.

211. McKee CT, Wood JA, Shah NM, Fischer ME, Reilly CM, Murphy CJ, et al. The effect of biophysical attributes of the ocular trabecular meshwork associated with glaucoma on the cell response to therapeutic agents. Biomaterials. 2011;32(9):2417-23.

212. Magdeldin T, Lopez-Davila V, Pape J, Cameron GW, Emberton M, Loizidou M, et al. Engineering a vascularised 3D in vitro model of cancer progression. Sci Rep. 2017;7:44045.

213. Brinkmann U. Functional polymorphisms of the human multidrug resistance (MDR1) gene: correlation with P glycoprotein expression and activity in vivo. Novartis Found Symp. 2002;243:207-10; discussion 10-2, 31-5.

214. Chen LY, Wang CW, Yuan Z, Chang HT. Fluorescent gold nanoclusters: recent advances in sensing and imaging. Anal Chem. 2015;87(1):216-29.

215. Govindaraju S, Ankireddy SR, Viswanath B, Kim J, Yun K. Fluorescent Gold Nanoclusters for Selective Detection of Dopamine in Cerebrospinal fluid. Sci Rep. 2017;7:40298.

216. Ingber DE, Mow VC, Butler D, Niklason L, Huard J, Mao J, et al. Tissue engineering and developmental biology: going biomimetic. Tissue Eng. 2006;12(12):3265-83.

217. Gomez-Lechon MJ, Donato MT, Castell JV, Jover R. Human hepatocytes as a tool for studying toxicity and drug metabolism. Curr Drug Metab. 2003;4(4):292-312.

218. Daly AK. Individualized drug therapy. Curr Opin Drug Discov Devel. 2007;10(1):29-36.

219. Yeh YC, Creran B, Rotello VM. Gold nanoparticles: preparation, properties, and applications in bionanotechnology. Nanoscale. 2012;4(6):1871-80.

Figure 1.4: Tumour development from Stage 0 until stage IV
http://www.onlinecancerguide.com/colon-cancer/4-stages-of-colorectal-cancer/

All other images are property of the author.